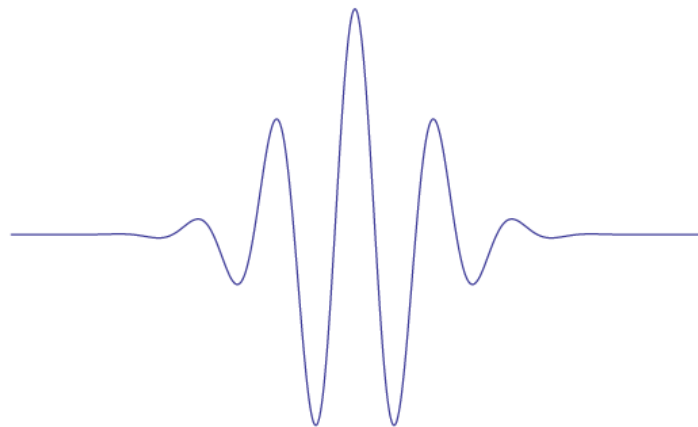




ΕΘΝΙΚΟ ΜΕΤΣΟΒΙΟ ΠΟΛΥΤΕΧΝΕΙΟ  
Σχολή Πολιτικών Μηχανικών  
Εργαστήριο Αντισεισμικής Τεχνολογίας

# ΕΛΕΓΧΟΣ ΔΟΜΙΚΗΣ ΑΚΕΡΑΙΟΤΗΤΑΣ ΚΑΤΑΣΚΕΥΩΝ ΥΠΟ ΣΕΙΣΜΙΚΗ ΦΟΡΤΙΣΗ ΜΕ ΤΗΝ ΜΕΘΟΔΟ ΣΥΝΕΧΩΝ ΚΥΜΑΤΟΜΟΡΦΩΝ



Διπλωματική Εργασία  
Αναστάσιος Στάμου

Επιβλέπων: Αν. Καθηγητής Μιχαήλ Φραγκιαδάκης

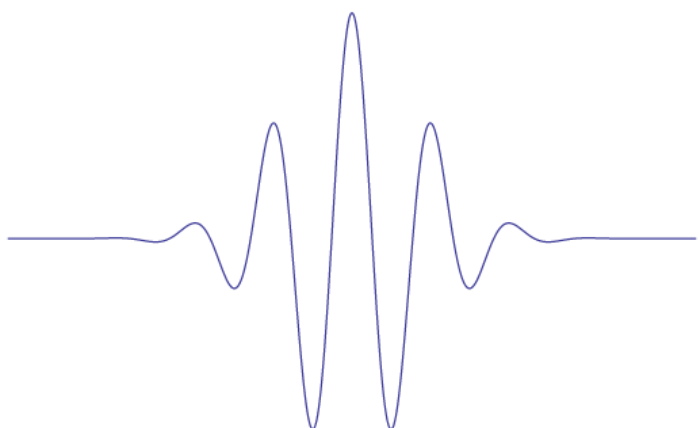
Αθήνα, Οκτώβριος 2021





ΕΘΝΙΚΟ ΜΕΤΣΟΒΙΟ ΠΟΛΥΤΕΧΝΕΙΟ  
Σχολή Πολιτικών Μηχανικών  
Εργαστήριο Αντισεισμικής Τεχνολογίας.

# ΕΛΕΓΧΟΣ ΔΟΜΙΚΗΣ ΑΚΕΡΑΙΟΤΗΤΑΣ ΚΑΤΑΣΚΕΥΩΝ ΥΠΟ ΣΕΙΣΜΙΚΗ ΦΟΡΤΙΣΗ ΜΕ ΤΗΝ ΜΕΘΟΔΟ ΣΥΝΕΧΩΝ ΚΥΜΑΤΟΜΟΡΦΩΝ



Διπλωματική Εργασία  
Στάμου Αναστάσιος

Επιβλέπων: Αν. Καθηγητής Μιχαήλ Φραγκιαδάκης

Αθήνα, Οκτώβριος 2021



Copyright © Αναστάσιος Στάμου, 2021

Με επιφύλαξη παντός δικαιώματος

Απαγορεύεται η αντιγραφή, αποθήκευση σε αρχείο πληροφοριών, διανομή, αναπαραγωγή, μετάφραση ή μετάδοση της παρούσας εργασίας, εξ ολοκλήρου ή τμήματος αυτής, για εμπορικό σκοπό, υπό οποιαδήποτε μορφή και με οποιοδήποτε μέσο επικοινωνίας, ηλεκτρονικό ή μηχανικό, χωρίς την προηγούμενη έγγραφη άδεια του συγγραφέα. Επιτρέπεται η αναπαραγωγή, αποθήκευση και διανομή για σκοπό μη κερδοσκοπικό, εκπαιδευτικής ή ερευνητικής φύσης, υπό την προϋπόθεση να αναφέρεται η πηγή προέλευσης και να διατηρείται το παρόν μήνυμα. Ερωτήματα που αφορούν στη χρήση της εργασίας για κερδοσκοπικό σκοπό πρέπει να απευθύνονται προς τον συγγραφέα.

Η έγκριση της διπλωματικής εργασίας από τη Σχολή Πολιτικών Μηχανικών του Εθνικού Μετσόβιου Πολυτεχνείου δεν υποδηλώνει αποδοχή των απόψεων του συγγραφέα (Ν. 5343/1932, Άρθρο 202).

Copyright © Anastasios Stamou, 2021

All Rights Reserved

Neither the whole nor any part of this diploma thesis may be copied, stored in a retrieval system, distributed, reproduced, translated, or transmitted for commercial purposes, in any form or by any means now or hereafter known, electronic or mechanical, without the written permission from the author. Reproducing, storing and distributing this thesis for non-profitable, educational or research purposes is allowed, without prejudice to reference to its source and to inclusion of the present text. Any queries in relation to the use of the present thesis for commercial purposes must be addressed to its author.

Approval of this diploma thesis by the School of Civil Engineering of the National Technical University of Athens (NTUA) does not constitute in any way an acceptance of the views of the author contained herein by the said academic organisation (L. 5343/1932, art. 202).

Αναστάσιος Στάμου (2021)  
Διπλωματική εργασία  
Έλεγχος δομικής ακεραιότητας κατασκευών υπό σεισμική φόρτιση με την χρήση συνεχών  
κυματομορφών  
Εργαστήριο Αντισεισμικής Τεχνολογίας, Εθνικό Μετσόβιο Πολυτεχνείο, Αθήνα.

Anastasios Stamou (2021)  
Diploma Thesis  
Structural Health Monitoring under earthquake excitation with the use of Wavelets  
Laboratory of Earthquake Engineering, National Technical University of Athens, Greece

## Ευχαριστίες

Πρώτα από όλους θα ήθελα να ευχαριστήσω τον κ. Φραγκιαδάκη που δέχτηκε να συνεργαστεί μαζί μου και για την παραπάνω από άψογη συνεργασία και καθοδήγηση. Τέλος θα ήθελα να ευχαριστήσω την οικογένεια και τους φίλους μου για την συνεχή υποστήριξη σε όλη την διάρκεια των σπουδών μου.





## Αφιέρωση

Στους γονείς μου που ποτέ δεν σταμάτησαν να πιστεύουν σε εμένα.





ΕΘΝΙΚΟ ΜΕΤΣΟΒΙΟ ΠΟΛΥΤΕΧΝΕΙΟ  
ΣΧΟΛΗ ΠΟΛΙΤΙΚΩΝ ΜΗΧΑΝΙΚΩΝ  
ΕΡΓΑΣΤΗΡΙΟ ΑΝΤΙΣΕΙΣΜΙΚΗΣ ΤΕΧΝΟΛΟΓΙΑΣ

ΔΙΠΛΩΜΑΤΙΚΗ ΕΡΓΑΣΙΑ

## **Έλεγχος δομικής ακεραιότητας κατασκευών υπό σεισμική φόρτιση με την μέθοδο συνεχών κυματομορφών**

**Αναστάσιος Στάμου**

Επιβλέπων: Αν. Καθηγητής Μιχαήλ Φραγκιαδάκης  
Αθήνα, Οκτώβριος 2021

### **ΠΕΡΙΛΗΨΗ**

Η δυναμική ανάλυση μια κατασκευής αποτελεί ένα πολύπλοκο και θεμελιώδες πρόβλημα πολιτικού μηχανικού. Συχνά η επίλυση του προβλήματος ιδιοτιμών ενός στατικού προσομοιώματος απέχει αρκετά από την πραγματικότητα για λόγους στατιστικής, εφαρμογής συντελεστών ασφαλείας ή αλλαγών κατά την υλοποίηση του έργου. Η γνώση των πραγματικών ιδιοτήτων της κατασκευής είναι απαραίτητη για την σωστή προσομοίωση και την εκτίμηση της συμπεριφοράς του υπό μια δυναμική φόρτιση (σεισμός, αέρας κ.λπ.)

Αυτή η διπλωματική εργασία πραγματεύεται την λειτουργική ιδιομορφική ανάλυση και αποτίμηση μιας υπάρχουσας κατασκευής με την χρήση συνεχών κυματομορφών (Wavelets). Μέσω της ανάλυσης με Wavelets είναι δυνατός ο υπολογισμός των φυσικών συχνοτήτων ταλάντωσης, των ιδιοσχημάτων, της απόσβεσης καθώς και τον εντοπισμό ζημιών σε μια κατασκευή κατά την διάρκεια μιας δυναμικής φόρτισης.

Δύο τύποι μετασχηματισμού με την χρήση Wavelets μελετήθηκαν. Ο συνεχής και ο διακριτός. Οι μετασχηματισμοί αυτοί εφαρμόστηκαν σε προσομοιώματα δισδιάστατων και τρισδιάστατων πλαισίων και κτιρίων καθώς και σε μετρήσεις από πραγματικά κτίρια. Τα αποτελέσματα αυτά σχολιάζονται και συγκρίνονται, ενώ επισημαίνονται πιθανά προβλήματα που προκύπτουν κατά την διάρκεια των αναλύσεων που επηρεάζουν τα αποτελέσματα και γίνονται προτάσεις για την αντιμετώπιση τους.

Στόχος της εργασίας αυτής είναι μέσα από την κατανόηση του θεωρητικού υπόβαθρου της λειτουργικής ιδιομορφικής ανάλυσης και των Wavelets να γίνει ένα βήμα προς την ζωντανή παρακολούθηση της κατάστασης μια κατασκευής ενώ είναι σε λειτουργία και η έγκαιρη και βέλτιστη οικονομικά αντιμετώπιση βλαβών.





NATIONAL TECHNICAL UNIVERSITY OF ATHENS  
SCHOOL OF CIVIL ENGINEERING  
LABORATORY OF EARTHQUAKE ENGINEERING

DIPLOMA THESIS

## **Structural Health Monitoring under earthquake excitation with the use of Wavelets.**

**Anastasios Stamou**

Supervisor: Assistant Professor Michail Fragiadakis  
October 2021

### **ABSTRACT**

Dynamic analysis of a structure is complicated and common problem for a civil engineer. Often solving the eigenvalue problem of a structural model differs from the actual building because of statistics, safety factors or small changes during the construction phase. Knowing the real structural characteristics is a necessity to be able to correctly simulate the buildings response under a dynamic load (earthquake, wind etc.)

The present diploma thesis studies Operational Modal Analysis and evaluation of the damage of an existing structure with the use of Wavelet analysis. Through wavelet analysis it is possible to calculate the natural frequencies, mode shapes, damping ratio as well as locate damages on a building during an excitation from a dynamic load.

2 types of Wavelet transforms were studied. Continuous and Discrete. These transforms were applied on 2d, 3d models and recordings from real buildings. The results are discussed and compared while difficulties from applying the methods are highlighted. Few ways to overcome those difficulties are also suggested.

Goal of this thesis is through the understanding of the theoretical background behind operational modal analysis and wavelets to move a step closer towards live structural health monitoring of an existing building as well as monitor system performance and make corresponding maintenance decisions.



## Contents

<b>1</b>	<b>INTRODUCTION .....</b>	<b>1</b>
1.1	Introduction to Structural Health Monitoring.....	1
1.2	About this Thesis Structure .....	2
<b>2</b>	<b>ANALYSIS IN THE FREQUENCY DOMAIN .....</b>	<b>3</b>
2.1	Fourier Series and Fourier Integral .....	3
2.2	Fourier Transform .....	4
2.3	Properties of the Fourier Transform .....	5
2.3.1	Linearity property of the Fourier Transform .....	5
2.3.2	Time reversal property of the Fourier Transform .....	5
2.3.3	Time shift property of the Fourier Transform .....	6
2.3.4	The differentiation and integration properties .....	6
2.4	Discrete Fourier Transform.....	6
2.5	The Fast Fourier Transform (FFT).....	6
<b>3</b>	<b>TIME-FREQUENCY ANALYSIS.....</b>	<b>9</b>
3.1	The Short Time Fourier Transform and the Spectrogram.....	9
3.2	Continuous Wavelet Transform (CWT) .....	10
3.3	Discrete Wavelet Transform (DWT) .....	12
3.4	Mother Wavelet Choice .....	12
3.4.1	Continuous Wavelet Transform.....	12
3.4.3	Discrete Wavelet Transform.....	16
3.5	MATLAB Wavelet Toolbox Function.....	17
<b>4</b>	<b>DYNAMIC LOADS USED .....</b>	<b>19</b>
4.1	Kobe Earthquake .....	19
4.2	MATLAB generated low amplitude ambient vibration (White-Noise) .....	22
<b>5</b>	<b>DISCRETE WAVELET TRANSFORM (DWT) APPLICATIONS .....</b>	<b>23</b>
5.1	Automatization of the method .....	23
5.2	1 Story 2D Seismostruct model.....	24
5.3	10 Story 2D Seismostruct model.....	28
5.4	6 Story 3D Seismostruct model.....	32
5.5	10 Story 2D Seismostruct model using Menegotto – Pinto steel model .....	39
5.6	Sherman Oaks – 13 Story commercial building, .....	43
<b>6</b>	<b>CONTINUOUS WAVELET TRANSFORM (CWT) APPLICATIONS.....</b>	<b>47</b>
6.1	Estimation of Damping Ratio and Mode shapes using wavelet transform.....	47
6.2	Random Decrement (RD) Method .....	48

6.3	1 Story 2D Seismostruct model. ....	48
6.4	10 Story 2D Seismostruct model. ....	52
6.5	6 Story 3D Seismostruct model. ....	59
6.6	Modal Assurance Distribution (MAD) .....	68
6.7	Europroteas.....	70
6.8	Sherman Oaks – 13 Story commercial building. ....	78
<b>7</b>	<b>CONCLUSIONS.....</b>	<b>85</b>
<b>8</b>	<b>REFERENCES .....</b>	<b>87</b>



# 1 INTRODUCTION

## 1.1 Introduction to Structural Health Monitoring

During the lifespan of a building very often damage is observed. The cause might be excessive earthquake excitation, severe environmental conditions, degradation of the material's properties, fatigue and numerous other reasons. This damage usually is observed by visual inspection of the building elements from experienced civil engineers. Most of the times, if the damage is severe, it is easy to observe. But there are also cases that the damage cannot be observed.

Structural health monitoring ensures that every bit of damage is located and dealt with so structural safety can be ensured with the lowest possible maintenance cost. In the latest years structural health monitoring is becoming more and more popular as an effective way to monitor the health of a building in real time.

Damage detection includes finding out if damage exists, where, and how severe it is. One of the main group of methods for damage detection is modal analysis methods. The idea is that damage alters the modal parameters of the building (natural frequencies, damping ratios and mode shapes).

There are two different types of modal analysis methods.

Experimental modal analysis methods, also going by the name of forced vibration methods, are conducted with carefully controlled excitations. They are input-output methods which means that both the system's input and output are known. This reduces randomness and allows for better understanding of the structure's characteristics.

Operational modal analysis methods, also going by the name of ambient vibration methods, on the other hand, do not control the excitation on the structure. They are output-only methods, since the system's input is unknown. These methods do not require extra equipment and can be conducted without performing an evacuation prior to them. The disadvantage of OMA methods is, since the ambient vibration is random, there is a chance that some periodicity is present to it, which can produce false results. Thus, the methods should be able to distinguish the system's eigenfrequencies from excitation frequencies through stochastic procedures.

In this thesis only OMA was studied. Specifically, OMA through the use of wavelets. In the last years wavelets have gained popularity as one of the tools for OMA. Through Discrete and Continuous wavelet transform buildings' modal properties are calculated through analysis of recordings from accelerometers placed in different places around an existing building.

## 1.2 About this Thesis Structure

The thesis contains 8 chapters.

- Introduction
- Analysis in the Frequency domain: Theoretical basis of Fourier Series, Integral, Series, Continuous and Discrete Transform.
- Time-Frequency Analysis: Short-time Fourier transform, Continuous and Discrete Wavelet transform, Mother wavelet Choice, MATLAB's wavelet toolbox.
- Dynamic Loads used: Kobe Earthquake – low amplitude ambient vibration, their Fourier transform and their Welch Power Spectrum.
- Discret Wavelet Transform applications: Single degree of freedom model, multiple degrees of freedom model, Sherman Oaks – 13 story commercial building.
- Continuous Wavelet Transform applications: Single degree of freedom model, multiple degrees of freedom model, Europroteas, Sherman Oaks – 13 story commercial building, Modal assurance distribution, Improving the method.
- Conclusions
- References

## 2 ANALYSIS IN THE FREQUENCY DOMAIN

Transforms change one function into another, according to some fixed set of rules. The transformed function is often easier to handle and provides us with additional information. They are extensively used in structural dynamics, signal processing and in OMA.

The family of Fourier transforms consists of four transforms. These are shown in Figure 2-1. They all decompose a function into sinusoids. They are the four possible combinations of continuous/discrete and periodic/aperiodic. Since we are going to apply the transform on discrete signals, the Fourier Transform and Fourier series are not usable. Still, since they are the theoretical basis for the discrete transforms, they will be discussed. Our signals are also finite in length. However, all four transforms are defined from  $-\infty$  to  $+\infty$ , which means that we would have to act like our signal is infinite in length. This can be done either by extending the signal with zeros to create an aperiodic discrete signal, or by duplicates of it to create a periodic discrete signal. In the first case we would use the Discrete Time Fourier Transform, while in the latter we would use the Discrete Fourier Transform. It turns out that an infinite number of sinusoids are required to synthesize a signal that is aperiodic, making it impossible to calculate the Discrete Time Fourier Transform using the computer. We are only left to use the Discrete Fourier Transform in signal processing.





Type of Transform	Example Signal
Fourier Transform <i>signals that are continuous and aperiodic</i>	
Fourier Series <i>signals that are continuous and periodic</i>	
Discrete Time Fourier Transform <i>signals that are discrete and aperiodic</i>	
Discrete Fourier Transform <i>signals that are discrete and periodic</i>	

Figure 2-1: The Fourier transforms, [12]

### 2.1 Fourier Series and Fourier Integral

A continuous periodic function  $x(t)$  with period  $T$ , can be represented as an infinite series of harmonic (sines and cosines) components of different periods. The variable  $t$  can be anything, but since in our applications we use time, it can be assumed that in everything that follows it represents time, while  $\omega$  the cyclic frequency. The series is called Fourier series and has the form of:

$$x(t) = a_0 + \sum_{k=1}^{\infty} \left( a_k \cos\left(\frac{2\pi k t}{T}\right) + b_k \sin\left(\frac{2\pi k t}{T}\right) \right) \quad (2-1)$$

where

$$a_0 = \frac{1}{T} \int_{-T/2}^{T/2} x(t) dt \quad (2-2)$$

$$a_k = \frac{2}{T} \int_{-T/2}^{T/2} x(t) \cos\left(\frac{2\pi k t}{T}\right) dt, k \geq 1 \quad (2-3)$$

$$b_k = \frac{2}{T} \int_{-T/2}^{T/2} x(t) \sin\left(\frac{2\pi k t}{T}\right) dt, k \geq 1 \quad (2-4)$$

The cyclic frequency of the  $k$ -th harmonics is  $\omega_k = 2\pi/T$ . The increment of cyclic frequency from one harmonic to the next is constant and equal to  $\Delta\omega = 2\pi/T$ . This means that the periodicity of the continuous signal makes its harmonic series representation discrete. In the case of an aperiodic function ( $T \rightarrow \infty$ ), from the last expression we get that  $\Delta\omega \rightarrow 0$ , thus the representation tends to become continuous. Doing so causes the series to become a definite integral with limit  $\omega = 0$ s to  $\omega = \infty$  allowing us to represent any continuous function, periodic or aperiodic, in harmonic terms of every real frequency  $\omega$ . This integral is called Fourier integral and has the form of:

$$x(t) = 2 \int_0^{+\infty} A(\omega) \cos\omega t d\omega + 2 \int_0^{+\infty} B(\omega) \sin\omega t d\omega \quad (2-5)$$

where

$$A(\omega) = \frac{1}{2\pi} \int_0^{+\infty} x(t) \cos\omega t dt \quad (2-6)$$

$$B(\omega) = \frac{1}{2\pi} \int_0^{+\infty} x(t) \sin\omega t dt \quad (2-7)$$

Equation is the representation of the Fourier Transform by the Fourier integral, or the inverse Fourier Transform. The integral indicates the frequency composition of an aperiodic function.

## 2.2 Fourier Transform

We can put equations (2-6) and (2-7) together and define a complex function of  $\omega$  (or  $f = \omega/2\pi$ ). This complex number has a real part of  $A(\omega)$  and an imaginary part of  $-B(\omega)$ . as in (2-8). This is how the Fourier transform  $X(\omega)$  is defined. By using Euler's formula (2-9), we can bring (2-8) in the form of (2-10), called the complex form of the Fourier Transform (FT). The functions  $x(t)$  and  $X(\omega)$  are called transform pairs. We write  $F\{x\} = X$ .

$$X(\omega) = A(\omega) - iB(\omega) \quad (2-8)$$

$$e^{i\theta} = \cos\theta + i\sin\theta \quad (2-9)$$

$$X(\omega) = \frac{1}{2\pi} \int_{-\infty}^{+\infty} x(t) e^{-i\omega t} dt \quad (2-10)$$

Notice that  $X(\omega)$  is a complex function of  $\omega$ , while  $x(t)$  is a real function of  $t$ . This is why we say that the transformation  $x(t)$  is transferred from the time to the frequency domain. Both  $x(t)$  and  $X(\omega)$  are continuous and describe the same thing, but in a different way. By looking at definitions of mean value, cross correlation and the real and imaginary part of  $X(\omega)$ , (2-6) and (2-7), we conclude that  $A(\omega)$  and  $B(\omega)$  are the cross correlations of cosines and sines, respectively, of all possible frequencies, scaled with the factor of  $1/2\pi$ . The complex form of  $X(\omega)$  just packs these two correlations together in one function. Also (2-5) states that we need both parts to return to the time domain. In the end,  $A(\omega)$  and  $B(\omega)$  tell us how close to a cosine or sine of frequency  $\omega$  is our function  $x(t)$ . This is the in the polar notation. We graph the magnitude  $|X(\omega)|$  and angle  $\arg(X(\omega))$ , to get the Fourier magnitude and Fourier phase respectively. The magnitude and phase are a pair-to-pair replacement for the real and imaginary part of  $X(\omega)$ . The two notations are equivalent and related by using the property of the trigonometric functions (2-11) by setting  $M = X(\omega)$  and  $\theta = \arg(X(\omega))$ :

$$A\cos(x) + B\sin(x) = M\cos(x + \theta) \quad (2-11)$$

$$\arg(X(\omega)) = \arctan\left(\frac{\text{Im}X(\omega)}{\text{Re}X(\omega)}\right) \quad (2-12)$$

$$|X(\omega)| = \left(\text{Re}(X(\omega))^2 + \text{Im}(X(\omega))^2\right)^{1/2} \quad (2-13)$$

$$\text{Re}(X(\omega)) = |X(\omega)|\cos(\arg(X(\omega))) \quad (2-14)$$

$$\text{Im}(X(\omega)) = |X(\omega)|\sin(\arg(X(\omega))) \quad (2-15)$$

## 2.3 Properties of the Fourier Transform

### 2.3.1 Linearity property of the Fourier Transform

The FT is linear, as it possesses the properties of homogeneity and additivity. Homogeneity means that scaling a function with a complex number in the time domain will result in an identical scaling in the frequency domain. Additivity means that adding two functions in the time domain will result in an addition in the frequency domain. With the FTs  $X_1(t)$  and  $X_2(t)$  of two functions  $x_1(t)$  and  $x_2(t)$  known, we can directly calculate their linear combination by:

$$F\{c_1x_1(t) + c_2x_2(t)\} = c_1X_1(\omega) + c_2X_2(\omega) \quad (2-16)$$

Example 1:

$$\begin{aligned} F\{2e^{-t}u(t) + 3e^{-2t}u(t)\} &= F\{2e^{-t}u(t)\} + F\{3e^{-2t}u(t)\} \\ &= 2F\{e^{-t}u(t)\} + 3F\{e^{-2t}u(t)\} = \frac{2}{1+i\omega} + \frac{3}{2+i\omega} \end{aligned} \quad (2-17)$$

### 2.3.2 Time reversal property of the Fourier Transform

Reversing the time domain of a function  $x(t)$  that is replacing  $t$  with  $-t$ , will result in the reversal of  $X(\omega)$  in the frequency domain, replacing  $\omega$  with  $-\omega$ . It is expressed by:

$$F\{x(-t)\} = X(-\omega) \quad (2-18)$$

### 2.3.3 Time shift property of the Fourier Transform

Shifting a function  $x(t)$  in the time domain by  $t_0$ , causes its FT to be multiplied by a complex exponential  $e^{-i\omega kt_0}$ .

$$F\{x(t - t_0)\} = X(\omega)e^{-i\omega kt_0} \quad (2-19)$$

Example 2:  $g(t)$  is a pulse of width 2 and we want to calculate the Fourier Transform

$$g(t) = \begin{cases} 1 & 3 \leq t \leq 5 \\ 0 & \text{otherwise} \end{cases}$$

$$G(\omega) = \int_3^5 1e^{-i\omega t} dt = \left[ \frac{e^{-i\omega t}}{-i\omega} \right]_3^5 = \frac{e^{-5i\omega} - e^{-3i\omega}}{-i\omega} = \frac{e^{-4i\omega}(e^{i\omega} - e^{-i\omega})}{i\omega} = e^{-4i\omega} 2 \left( \frac{\sin\omega}{\omega} \right)$$

### 2.3.4 The differentiation and integration properties

The FT of the derivative and integral of  $x(t)$  is calculated easily if  $X(\omega)$  is known:

$$F\{\dot{x}(t)\} = X(\omega)i\omega_k \quad (2-20)$$

$$F\left\{ \int x(t) dt \right\} = \frac{X(\omega)}{i\omega_k} \quad (2-21)$$

## 2.4 Discrete Fourier Transform

The Discrete Fourier Transform (DFT) takes a periodic discrete function and turns it into a discrete function in the frequency domain. The discrete nature of both domains makes it the only transform that can be used with computers and one of the primary tools in signal processing. By transforming a discrete function  $x_k$ , with step  $\Delta t = 1/f_s$  between the function's values, size  $N$ , total length  $T$ , we end up with a discrete function  $X_k$ . Its real part is symmetric while its imaginary party is antisymmetric inside the frequency domain  $[-N/2, N/2 - 1]$ , if  $N$  is even or  $[-(N - 1)/2, (N - 1)/2]$  if  $N$  is odd. The frequency step is  $\Delta f = f_s/N$ . This means we only need to plot half the frequency domain. The count  $k$  of the frequency step is called bin number. The DFT is performed by using the equation (2-22), which we get from (2-10) if we discretize both domains:

$$X_k = F\{x_k\} = \sum_{k=0}^{N-1} x_k e^{-\frac{2\pi kni}{N}} \quad (2-22)$$

$$Re(X_k) = \sum_{k=0}^{N-1} x_k \cos\left(\frac{2\pi kni}{N}\right) \quad (2-23)$$

$$Im(X_k) = - \sum_{k=0}^{N-1} x_k \sin\left(\frac{2\pi kni}{N}\right) \quad (2-24)$$

The real and imaginary part of  $X_k$ , are the cross correlation of  $x_k$  with cosines and sines of discrete frequencies  $k/N$ .

## 2.5 The Fast Fourier Transform (FFT)

One of the most useful algorithms to calculate the DFT is the Fast Fourier Transform (FFT). Discovered by J. W. Cooley and J. W. Tukey in 1965 and since then has been used in most applications. It has high

computational efficiency. This means it can reduce the computation time by hundreds while producing the same result as any other algorithm, as even for a small sample size as seen in Figure. The algorithm's code itself is small but understanding the internal workings is much more complicating. It can still be used to the fullest assuming one has knowledge of the DFT. This algorithm is present in most programming packages, such as MATLAB and Python.





## 3 TIME-FREQUENCY ANALYSIS.

### 3.1 The Short Time Fourier Transform and the Spectrogram.

The short time Fourier transform and the spectrogram are used to analyse the frequency content of signals when the frequency content varies with time. This is achieved through the application of DFT. Segments of the original signal are windowed out from the rest of the signal and then DFT is applied to each segment. The segments can also be overlapping. We can display the DFT coefficients as a function of both time and frequency on 2 axis. This way we can have a better insight on the time varying frequency characteristics of the signal.

$$X[n, \lambda] = \sum_{m=-\infty}^{+\infty} x[n + m]w[m]e^{-j\lambda m} \quad (3-1)$$

where

$$\lambda = \frac{2\pi}{N}k \quad (3-2)$$

and length of the signal  $N$  is bigger than the length of the window  $L$ . This gives us the final short time Fourier transform

$$X[n, k] = \sum_{m=0}^{L-1} x[n + m]w[m]e^{-jk\left(\frac{2\pi}{N}\right)m} \quad (3-3)$$

where  $n$  is the reference time,  $k$  is the frequency,  $x(t)$  is the signal,  $w[m]$  is the time window.  $L$  trades temporal resolution for frequency resolution, as  $L$  increases details that change in time are lost but better resolution in the frequency domain is achieved.

The spectrogram is defined as the magnitude squared of the short time Fourier Transform.

$$|X[n, k]|^2 \quad (3-4)$$

The short time Fourier transform is invertible

$$x[n + m] = \frac{1}{Nw[m]} \sum_{k=0}^{N-1} X[n, k]e^{j\left(\frac{2\pi}{N}\right)km} \quad (3-5)$$

but once the spectrogram is computed, magnitude squared is throwing away phase or sine information so the spectrogram is not invertible.

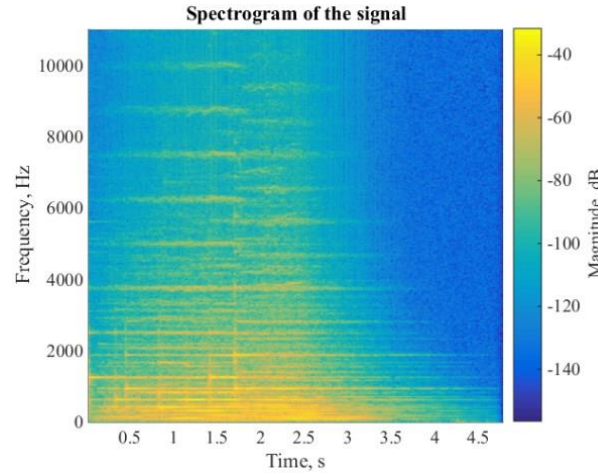


Figure 3-1: Short-Time Fourier Transform Spectrogram [26]

### 3.2 Continuous Wavelet Transform (CWT)

Wavelet analysis provides a powerful tool to characterize local features of a signal. Unlike the Fourier transform, where the function used as the basis of decomposition is always a sinusoidal wave, other basis functions can be selected for the wavelet shape according to the features of the signal. The basis function in wavelet analysis is defined by two parameters: scale and translation. These properties lead to a multi-resolution representation for non-stationary signals.

The Continuous wavelets transform of a signal  $f(t)$  is defined as:

$$T_{\psi}[u](b, a) = \frac{1}{a} \int_{-\infty}^{+\infty} u(t) \bar{\psi}\left(\frac{t-b}{a}\right) dt \quad (3-6)$$

where  $\psi(\cdot)$  is a square integrable and piece-wise continuous function called the mother or analyzing wavelet, and  $\bar{\psi}(\cdot)$  is its complex conjugate. The pair  $(b, a)$  is called the time-scale variable of the analysis, where  $a$  ( $a > 0$ ) is a scale parameter that plays the role of the inverse of frequency, and  $b$  is a translation parameter related to time. (3-6) can be viewed as either the inner product between the signal  $u(t)$  and the shifted and scaled copies of  $\psi(t)$ :  $\psi_{b,a}(t) = \left(\frac{1}{a}\right) \psi\left(\frac{t-b}{a}\right)$ , or as the convolution product between  $u(t)$  and  $\frac{1}{a} \bar{\psi}\left(-\frac{\cdot}{a}\right)$ . The function  $\psi(t)$  is an admissible mother wavelet when  $C_{\psi}$ , defined by

$$C_{\psi} = \int_0^{+\infty} |\hat{\psi}(\alpha\omega)|^2 \left(\frac{d\alpha}{\alpha}\right), \quad (3-7)$$

is finite, non-zero and independent of the real number  $\omega$ . In Eq. (3-7),  $\hat{\psi}(\omega)$  is the Fourier transform (FT) of  $\psi(t)$ :  $\hat{\psi}(\omega) = \int_{-\infty}^{+\infty} \psi(t) e^{-\omega t} dt$ . When admissibility condition is verified, the signal  $u(t)$  can be reconstructed by

$$u(t) = \frac{1}{C_{\psi}} \int_{-\infty}^{+\infty} \int_0^{+\infty} T_{\psi}[u](b, a) \psi\left(\frac{t-b}{a}\right) \left(\frac{da}{a}\right) db. \quad (3-8)$$

Moreover, Parseval's theorem applied to (3-6) gives the following expression in frequency domain:

$$T_{\psi}[u](b, a) = \frac{1}{2\pi} \int_{-\infty}^{+\infty} \hat{u} \bar{\hat{\psi}}(\alpha\omega) e^{i\omega b} d\omega \quad (3-9)$$

The local resolution of the CWT in time and in frequency depends on the dilation parameter  $a$  and is determined, respectively, by the duration  $\Delta t_{\psi}$  and bandwidth  $\Delta\omega_{\psi}$  of the mother wavelet:

$$\Delta t = \alpha \Delta t_\psi, \quad \Delta \omega = \frac{\Delta \omega_\psi}{\alpha} \quad (3-10)$$

Here,  $\Delta t_\psi$  and  $\Delta \omega_\psi$  are stated in terms of root mean squares which are equivalent to standard deviation in statistics

$$\Delta t_\psi = \frac{1}{\|\psi\|_2} \sqrt{\int_{-\infty}^{+\infty} (t - t_\psi)^2 |\psi(t)|^2 dt}. \quad (3-11)$$

$$\Delta \omega_\psi = \frac{1}{\|\hat{\psi}\|_2} \sqrt{\int_{-\infty}^{+\infty} (\omega - \omega_\psi)^2 |\hat{\psi}(\omega)|^2 d\omega} \quad (3-12)$$

where  $t_\psi$  and  $\omega_\psi$  are the center of  $\psi(t)$  and  $\hat{\psi}(\omega)$ , respectively,

$$t_\psi = \int_{-\infty}^{+\infty} t \frac{|\psi(t)|^2}{\|\psi\|_2^2} dt \quad \omega_\psi = \int_{-\infty}^{+\infty} \omega \frac{|\hat{\psi}|^2}{\|\hat{\psi}\|_2^2} dt \quad (3-13)$$

$\|\cdot\|_2$  denotes the classical norm in the space of square integrable functions. The function  $\psi$  is said to be localized about the phase point  $(t_\psi, \omega_\psi)$  with uncertainty  $\mu(\psi) = \Delta t_\psi \Delta \omega_\psi$ . It can be seen from Equation (3-10) that  $\mu(\psi_{b,a}) = \Delta t \Delta \omega = \mu(\psi)$ . The Heisenberg uncertainty principle states that  $\mu(\psi) \geq \frac{1}{2}$ , thus an improvement of the time localization (i.e., an increase of  $\Delta \omega$ ). If  $\omega_\psi/\alpha$  is considered to be the frequency variable  $\omega$ , then the  $t\omega$  plane can be viewed as the time-frequency plane. The localization domain for the CWT at point  $(b, \omega = \omega_\psi/\alpha)$  becomes

$$[b + at_\psi - \alpha \Delta t_\psi, b + at_\psi + \alpha \Delta t_\psi] \times \left[ \frac{\omega_\psi/\alpha}{2(\Delta \omega_\psi/\alpha)} - \frac{\Delta \omega_\psi}{\alpha}, \frac{\omega_\psi}{\alpha} + \frac{\Delta \omega_\psi}{\alpha} \right]. \quad (3-14)$$

Referring to the conventional frequency analysis of constant-Q filters, the Q factor is introduced as the ratio of the centre-frequency to the frequency bandwidth

$$Q = \frac{\omega_\psi/\alpha}{2(\Delta \omega_\psi/\alpha)} = \frac{\omega_\psi}{2\Delta \omega_\psi} \quad (3-15)$$

$Q$  is independent of  $\alpha$ . Gram-Hansen and Dorize [24] associate this  $Q$  value to the filter bank of a  $(1/N)$ th octave that is a classical notion in acoustics: a  $(1/N)$ th octave band of center frequency  $\omega_\psi$  is a band  $[\omega_1, \omega_2]$  with  $\omega_1 = 2^{-1/2N} \omega_\psi$  and  $\omega_2 = 2^{1/2N} \omega_\psi$ , hence  $Q = 1/2^{1/2N} - 2^{-1/2N}$ .

Due to the linearity property of the CWT, the signal of multi-components can be processed as

$$T_\psi \left[ \sum_{j=1}^N u_j \right] (b, a) = \sum_{j=1}^N T_\psi [u_j] (b, a). \quad (3-16)$$

Using localization properties of the mother wavelets, in both time and frequency domains a particular component  $u_j$  can be extracted from multi-component signals. If  $\psi$  and  $u$  are continuous and piecewise differentiable, the integration by parts theorem allows relation (3-6) to be rewritten as

$$T_\psi [\dot{u}] (b, a) = \frac{1}{a} [u(t) \bar{\psi} \left( \frac{t-b}{a} \right)] \Big|_{-\infty}^{+\infty} - \frac{1}{a} \int_{-\infty}^{+\infty} u(t) \bar{\psi} \left( \frac{t-b}{a} \right) dt \quad (3-17)$$

Moreover, when  $\psi$  is square and absolutely integrable and  $\dot{u}$  is of finite energy, the CWT of  $\dot{u}$  with  $\psi$  is then related to the CWT of  $u$  with  $\dot{\psi}$ :

$$T_\psi [\dot{u}] (b, a) = -\frac{1}{a} T_{\dot{\psi}} [u] (b, a). \quad (3-18)$$

This relation can be easily extended to the finite energy signal  $\ddot{u}$  when  $\ddot{\psi}$  is square and absolutely integrable:

$$T_{\ddot{\psi}}[\ddot{u}](b, a) = -\frac{1}{a} T_{\dot{\psi}}[\dot{u}](b, a) = \frac{1}{a^2} T_{\psi}[u](b, a). \quad (3-19)$$

It should be also noted that for the expression of  $T_{\dot{\psi}}[\dot{u}]$  and of  $T_{\ddot{\psi}}[\ddot{u}]$  in the frequency domain [see (3-9)],  $\hat{\psi}$  and  $\hat{\ddot{\psi}}$  can be substituted by  $-i\omega\hat{\psi}(\omega)$  and  $-i\omega^2\hat{\psi}(\omega)$  respectively.

### 3.3 Discrete Wavelet Transform (DWT)

By discretizing the parameters,  $a$  and  $b$ , a discrete version of the wavelet transform. (DWT) is obtained (Newland (1993)). The procedure becomes more efficient if dyadic values of  $a$  and  $b$  are used, i.e.

$$a = 2^j \quad b = 2^k \quad j, k \in Z \quad (3-20)$$

where  $Z$  is a set of positive integers. The corresponding discretized wavelets  $\Psi_{j,k}$  are defined as

$$\Psi_{j,k}(t) = 2^{-\frac{j}{2}} \Psi(2^{-j}t - k) \quad (3-21)$$

where  $\Psi_{j,k}$  forms an orthonormal base. In the discrete wavelet analysis, the signal can be represented by its approximations and details. The signal is passed through a series of high pass filters, which relate to details, to analyze the high frequencies and through a series of low-pass filters, which relate to approximations, in order to analyze the low frequencies. The detail at level  $j$  is defined as

$$D_j = \sum_{k \in Z} a_{j,k} \Psi_{j,k}(t) \quad (3-22)$$

where  $a_{j,k}$  is defined as

$$a_{j,k} = \int_{-\infty}^{+\infty} f(t) \bar{\Psi}_{j,k}(t) dt \quad (3-23)$$

and the approximation at level  $J$  is defined as

$$A_j = \sum_{j > J} D_j \quad (3-24)$$

Finally, the signal  $f(t)$  can be represented by

$$f(t) = A_j + \sum_{j \leq J} D_j \quad (3-25)$$

### 3.4 Mother Wavelet Choice

#### 3.4.1 Continuous Wavelet Transform.

The optimal mother wavelet  $\Psi$  for modal identification purposes using the free responses of a m.d.o.f system should satisfy the following conditions:

- $\psi$  is admissible (3-7)
- $\psi$  is progressive.
- $\psi$  has good time and frequency localization properties
- The first and the second derivatives of  $\psi$  satisfy the three previous conditions and thus Eq. (3-19) can be used.

The first condition is obvious. Several reasons suggest the use of progressive wavelets instead of real ones for the analysis of real signals: It allows the direct connection between a real signal and its associated analytic signal. The wavelet transform of real signals using real wavelets yields real wavelet coefficients and there is no natural way of making a connection with some "local spectrum" which one would like associate with a given signal. The third condition is very important in the context of time-frequency analysis and the final condition makes the processing by CWT of displacement, velocity and acceleration easier without differential and integral operations.

Three complex-valued mother wavelets are compared. One or two parameters appear in the definition of each mother wavelet and strongly influence the localization properties. The first one is the Morlet wavelet, Figure 3-2: Real-valued Morlet wavelet [17], Figure 3-3: Complex-Valued Morlet wavelet [17]. The second is the Cauchy wavelet of order  $n$ , intensively used in quantum mechanics when  $n = 1$  and also by Argoul et al when  $n > 1$ , Figure 3-4: The Cauchy wavelet [18]. Finally, the third one is the harmonic wavelet recently proposed by Newland, Figure 3-5: The Harmonic wavelet [20].

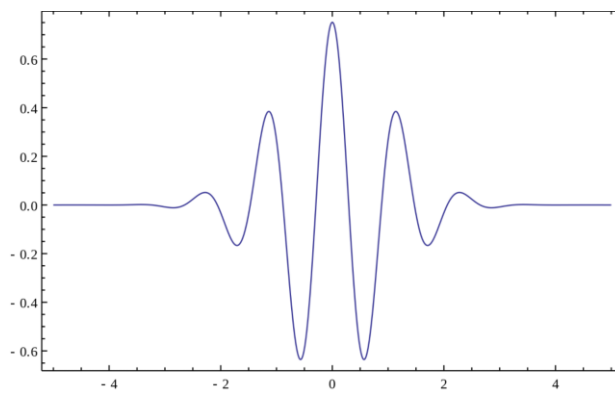


Figure 3-2: Real-valued Morlet wavelet [17]



Figure 3-3: Complex-Valued Morlet wavelet [17]

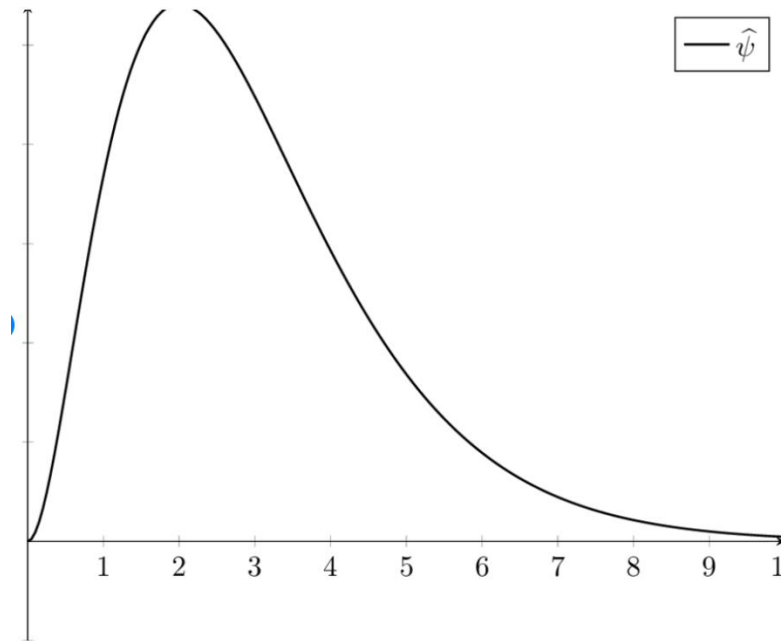


Figure 3-4: The Cauchy wavelet [18]

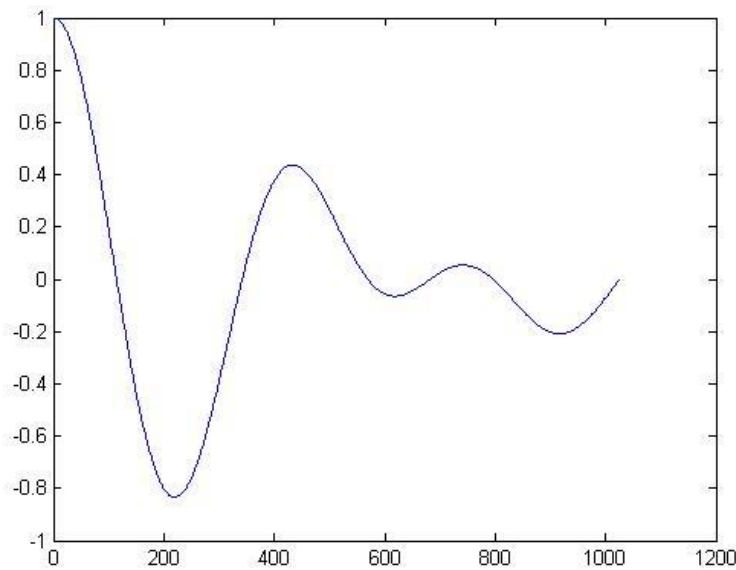


Figure 3-5: The Harmonic wavelet [20]

The formulae of  $\psi(t)$ ,  $\hat{\psi}(\omega)$ ,  $C_\psi$ ,  $t_\psi$ ,  $\omega_\psi$ ,  $\Delta t_\psi$ ,  $\Delta \omega_\psi$ ,  $\mu_\psi$  and  $Q$  are given in Table 3-1 for the three wavelets. The first and the second condition are verified by both Cauchy and harmonic wavelets. The Morlet wavelet is only numerically admissible and progressive when the product of the two parameters  $\beta\delta$  is large enough ( $\beta\delta \geq 5$  in practice). According to the third condition the Morlet wavelet has its time-frequency window with the smallest area allowable ( $\frac{1}{2}$ ) by the Heisenberg inequality. The uncertainty  $\mu_\psi$  of the Cauchy wavelet behaves asymptotically with this threshold when its order parameter  $n$  tends towards infinity. The harmonic wavelet has infinite uncertainty but its support in frequency domain is compact. This property allows the isolation of components with close frequencies. Newland improves time localization by windowing the spectrum of wavelets, but it is more complicated. The last condition is easily verified by the definition of the Cauchy wavelet given in Table 3-1: Definition of the main

characteristics of the three mother wavelets.. The first and the second derivatives of  $\psi_n$  are also the Cauchy wavelets since

$$\dot{\psi}_n(t) = i(n+1)\psi_{n+1}(t) \text{ and } \ddot{\psi}_n(t) = -(n+1)(n+2)\psi_{n+2}(t) \quad (3-26)$$

and the identification procedure with  $\dot{u}$  and  $\ddot{u}$  by the aid of Eq (3-19) is limited.

The properties of the mother wavelet can be referred to the parameter Q defined in relation (3-15).

Table 3-1: Definition of the main characteristics of the three mother wavelets.

	<i>Morlet Wavelet</i>	<i>Cauchy Wavelet</i>	<i>Harmonic Wavelet</i>
$\psi(t)$	$e^{-t^2/(2\delta^2)} e^{i\beta t}$	$\left(\frac{i}{t+i}\right)^{n+1}$	$\frac{e^{i2n\pi t} - e^{i2m\pi t}}{i2\pi(n-m)t}$
$\hat{\psi}(\omega)$	$\delta\sqrt{2\pi} e^{-(\omega-\beta)^2\delta^2/2}$	$\frac{2\pi\omega^n e^{-\omega}}{n!} \theta(\omega)$	$\frac{\theta[(\omega-m2\pi)(n2\pi-\omega)]}{(n-m)2\pi}$
$C_\psi$	$\infty$	$4\pi^2 \left(\frac{1}{2^{2n}}\right) \left(\frac{(2n-1)!}{(n!)^2}\right)$	$\frac{1}{4\pi^2(n-m)^2} \ln\left(\frac{n}{m}\right)$
$t_\psi$	0	0	0
$\omega_\psi$	$\beta$	$n + \frac{1}{2}$	$(n+m)\pi$
$\Delta\omega_\psi$	$\frac{1}{\delta\sqrt{2}}$	$\frac{\sqrt{2n+1}}{2}$	$(n-m)\pi$
$\Delta t_\psi$	$\frac{\delta}{\sqrt{2}}$	$\frac{1}{\sqrt{2n-1}}$	$\infty$
$\mu_\psi$	$\frac{1}{2}$	$\frac{1}{2} \sqrt{1 + \frac{2}{2n-1}}$	$\infty$
Q	$\frac{\beta\delta}{\sqrt{2}}$	$\frac{n + \frac{1}{2}}{\sqrt{2n+1}}$	$\frac{n+m}{2(n-m)}$

### 3.4.3 Discrete Wavelet Transform.

A wavelet is virtually any waveform that has limited duration and zero average. It is important to notice that the results of wavelet transformation depend on the choice of the wavelet selected. There are several wavelet families that can be selected.

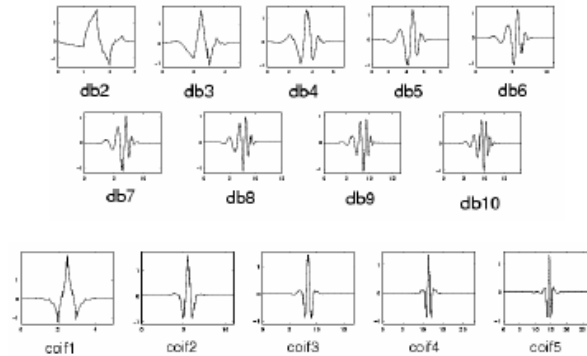


Figure 3-6: Families of Daubechie (DB) and Coiflet (Coif) Wavelets [8]

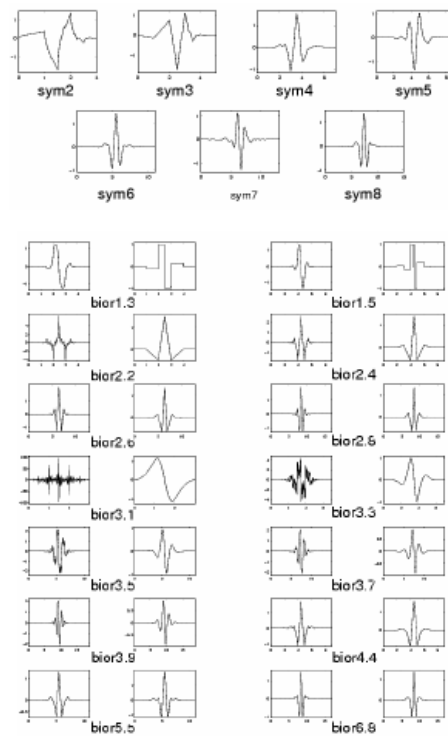


Figure 3-7: Families of Symlet (Sym) and Biorthogonal (Bior) Wavelets [8]

The results of wavelet transform, both discrete and continuous, strongly depend on the choice of wavelet selected. In earthquake engineering the most common wavelets are Daubechies and Biorthogonals. Both bior 6.8 and DB4 were used during this thesis and the results were always similar.



### 3.5 MATLAB Wavelet Toolbox Function

MATLAB's CWT toolbox is using a function based on expansion of the integral for a discrete time interval  $k$  and  $k+1$

$$WT(a, b) = \frac{1}{\sqrt{a}} \sum_k x(k) \left( \int_{-\infty}^{k+1} \psi\left(\frac{t-b}{a}\right) dt - \int_{-\infty}^k \psi\left(\frac{t-b}{a}\right) dt \right) \quad (3-27)$$

The interval subtraction is calculated through finite differences. In MATLAB the numerical integral of  $\psi(t)$  is calculated only once, instead of each dilated and shifted wavelet, and the values of the integral are dilated to obtain the integral of  $\psi_{(\alpha,b)}(t)$ . The discrete number of points of the mother wavelet integral depends on a precision parameter  $p$ , which can take positive integer values, with higher values meaning better discretization of the wavelet. This procedure is improving the processing time and memory limits used by the program because the integral of the mother wavelet is computed only once and has a fixed length of discrete points. This means it doesn't depend on the length of the signal. This means that the results obtained from MATLAB are only an **approximation** of the CWT and considerable numerical pitfalls can be introduced in some cases.

Another thing that needs to be addressed is the **edge effect**. While wavelet is shifted along the beginning and the end of the signal, a part of it falls outside the signal. This has a result the generation of useless coefficients in that region that are causing the **edge effect**. This means every CWT analysis needs to start after a certain time period.

$$\Delta T = \beta \Delta t_f = \frac{\beta f_c \sqrt{f_b}}{2f}$$

where  $f_b$  is the bandwidth parameter and  $f_c$  is the mother wavelet central frequency and  $\beta$  equals to 4.

MATLAB is generating a cone of influence that marks the territory on the scalogram affected by the edge effect automatically. The `cwtfilerbank` and `cwt` functions use an approximation to the  $1/e$  rule to delineate the COI. The approximation involves adding one time-domain standard deviation at each scale to the beginning of the observation interval and subtracting one time-domain standard deviation at each scale from the end of the interval.

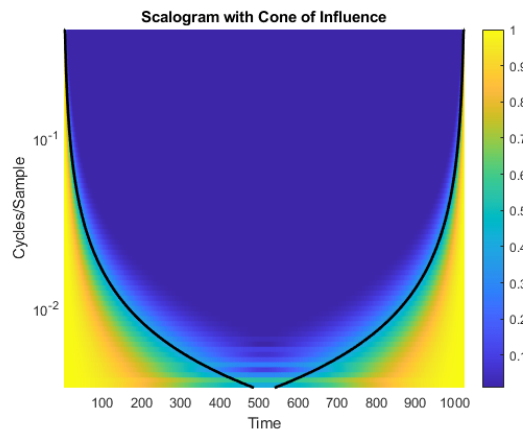


Figure 3-8: MATLAB generated Cone of influence



## 4 DYNAMIC LOADS USED

### 4.1 Kobe Earthquake

Kobe earthquake, also known as The Great Hanshin earthquake, occurred on January 17, 1995 in Japan. The tremors lasted approximately 20 seconds. Recordings used are from Fukushima sensors downloaded from PeerNGA [21]. Response Spectra and Welch Power Spectrum from SeismoLee.eu [23].

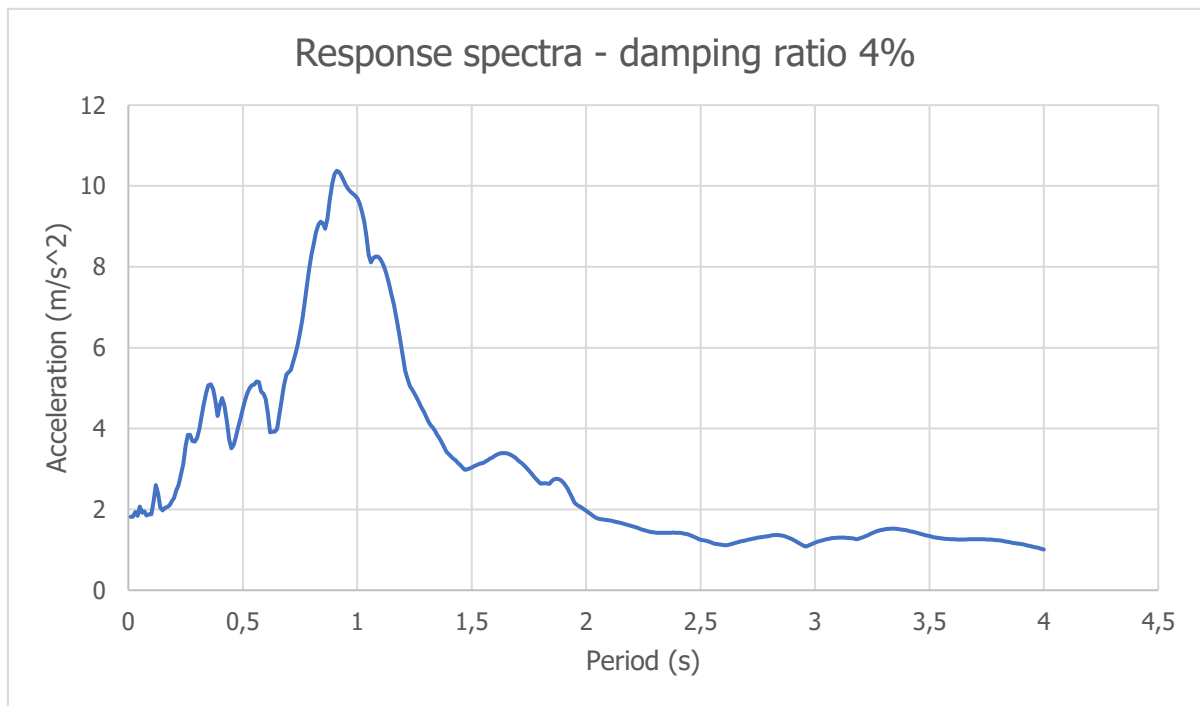


Figure 4-1: X Axis Response Spectra

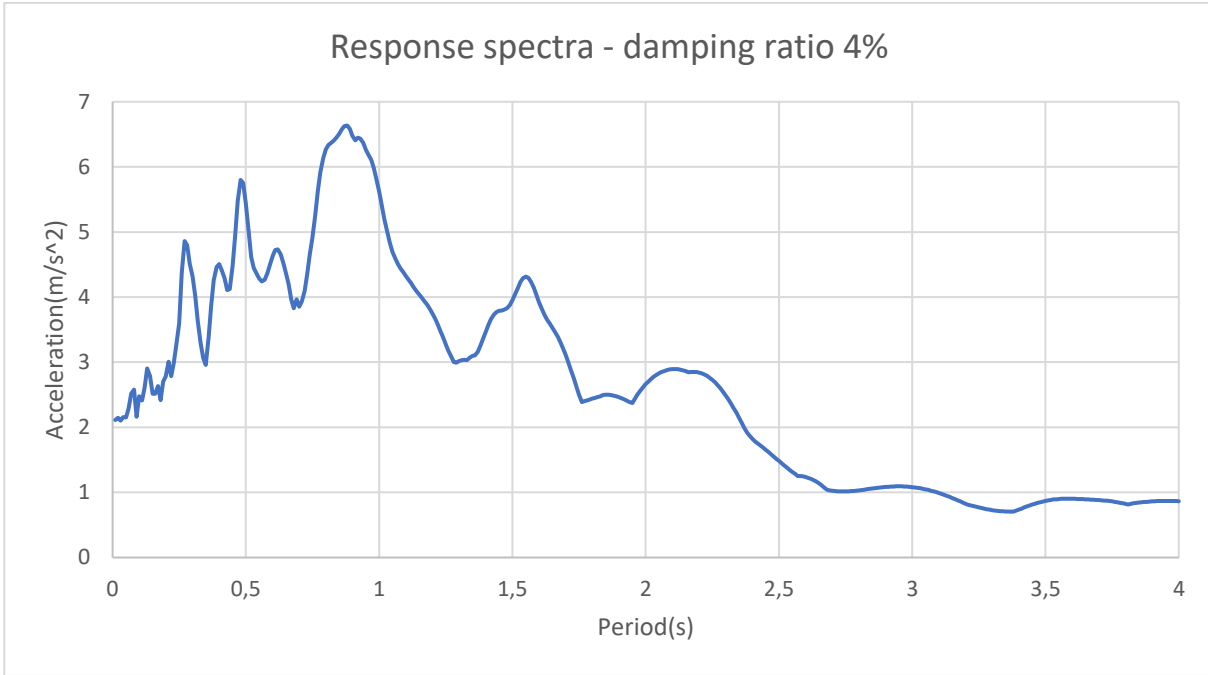


Figure 4-2: X Axis Response Spectra

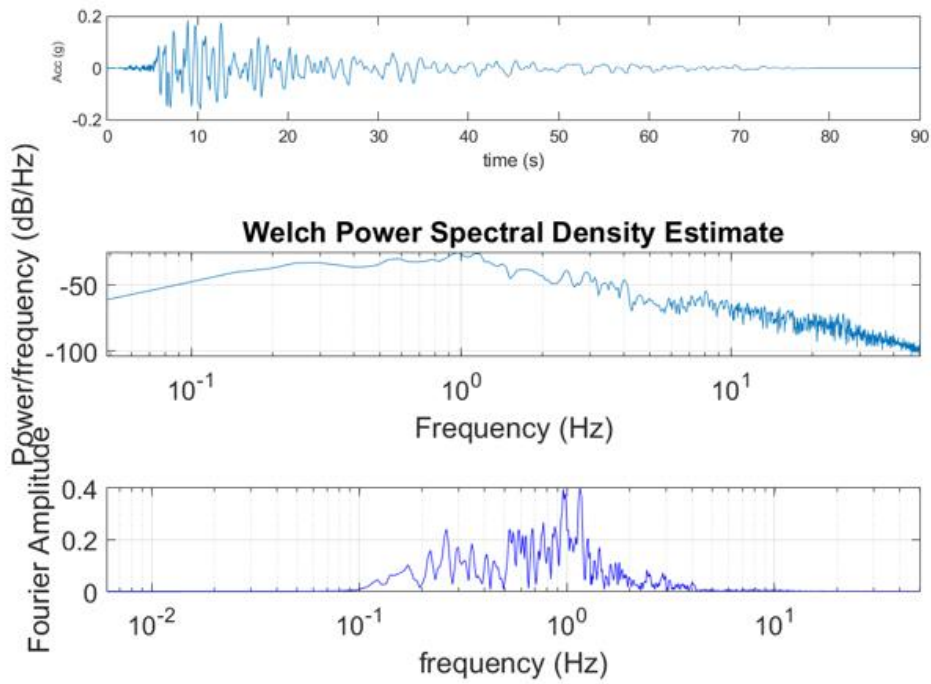


Figure 4-3: X-Axis Accelerations signal – Welch Power Spectral Density Estimate – Fourier transform

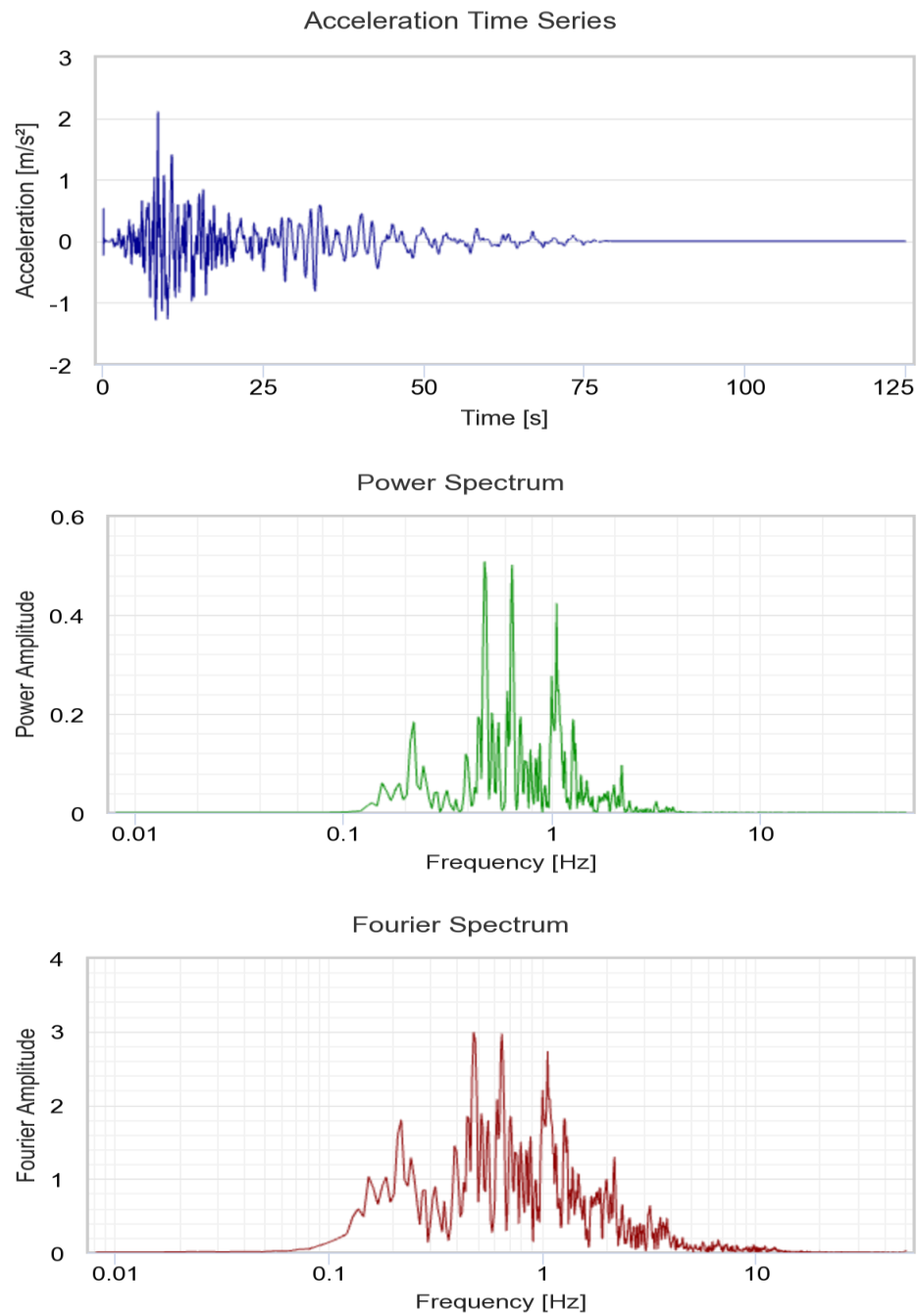


Figure 4-4: Y-Axis Accelerations signal – Welch Power Spectral Density Estimate – Fourier transform

## 4.2 MATLAB generated low amplitude ambient vibration (White-Noise)

White noise is a random signal that has equal amplitude at different frequencies. Such signal is easy to make in MATLAB with the following code.

```
N=8000  
ao = 0.1;  
A= ao.*randn(1,N);
```

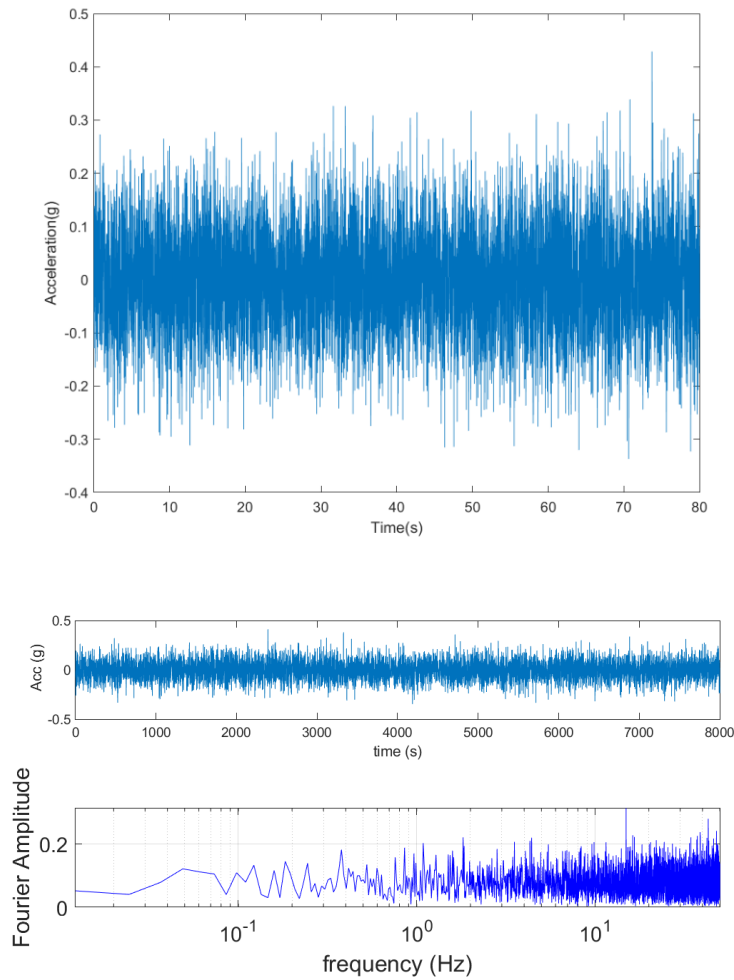


Figure 4-5: White Noise Accelerations signal — Fourier transform

## 5 DISCRETE WAVELET TRANSFORM (DWT) APPLICATIONS

When a structure is subjected to earthquake excitation, if the excitation is strong enough some of the structural members will yield. Furthermore, if the excitation is strong enough to push the member deep into the anelastic section, there will be visible damage that can be observed with visual inspection. If the excitation is just strong enough to make the member yield without visible damage, there is no way to visually tell that a member has been damaged. Especially if it's covered. Wavelet analysis can help detect this kind of damage. When a member yields, there is degradation of its stiffness which affects the frequency the building is oscillating. This change is imprinted in the form of spikes in details diagram of its wavelet transform.

Discrete wavelet analysis was tested on 4 different recordings

1. 1 Story 2D frame simulated with Seismostruct 2020
2. 10 Story 2d frame simulated with Seismostruct 2020
3. 6 Story 3d building simulated with Seismostruct 2020
4. Sherman Oaks – 13 Story Commercial Building (recordings from StrongMotion.org)

### 5.1 Automatization of the method

The above method is dependent on manual observation on the wavelet detail signal. For this reason, there is need for a more robust and automated numerical procedure. For this reason, for every details signal, the absolute maximum value of the signal,  $\max D$ , will be calculated. A portion of that value will be compared to the rest absolute values of the signal. With trial and error, the most efficient value is  $p = 0.25 * \max D$ . After that the parameter  $R$  is calculated.  $R$  is the percentage of how many times the absolute values of the details signal exceed  $p$ . If the calculated  $R$  is small enough, usually  $< 1\%$ , it is an indicator that spikes exist in that detail signal. Otherwise, if  $R > 1\%$  then no spikes exist, and consequently no damage has occurred.

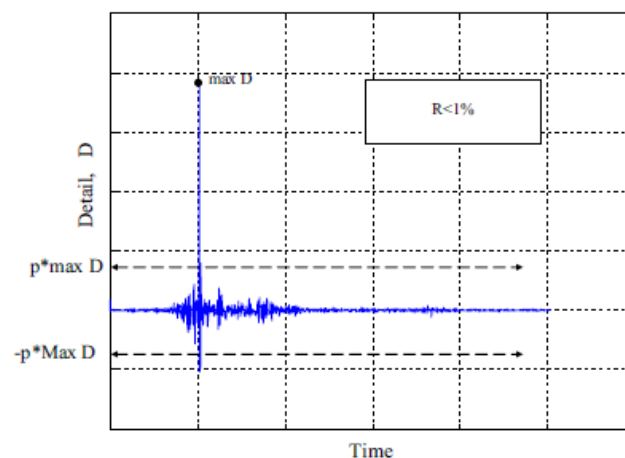


Figure 5-1: Representative picture correlating the limits of  $R$  value with spikes of wavelet details signal for  $R < 1\%$  [1]

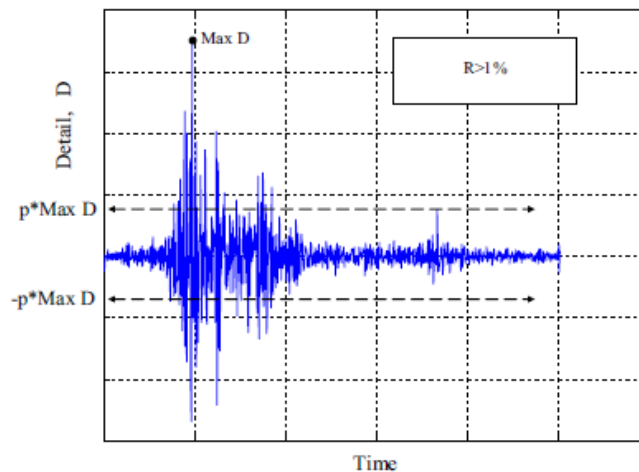


Figure 5-2: Representative picture correlating the limits of R value with spikes of wavelet details signal for  $R > 1\%$  [1]

## 5.2 1 Story 2D Seismostruct model.

SeismoStruct is a Finite Elements package capable of predicting the large displacement behavior of space frames under static or dynamic loading, taking into account both geometric nonlinearities and material inelasticity.

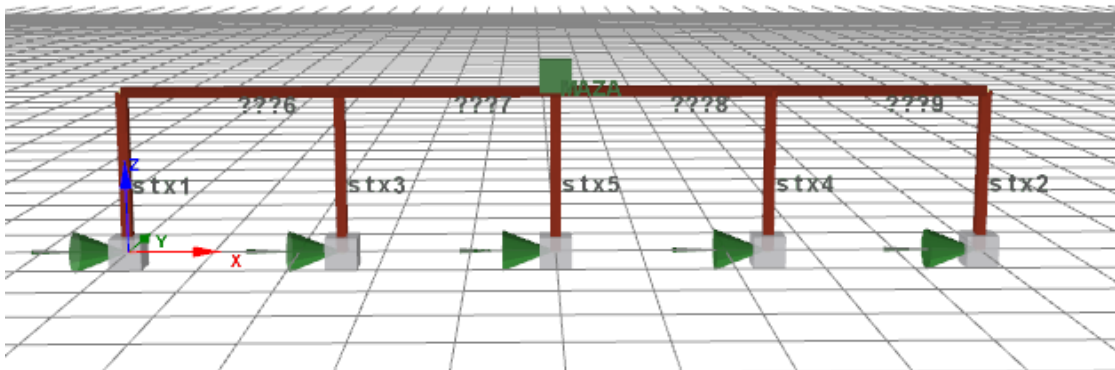


Figure 5-3: Seismostruct model.

The present system was modelled as 1 Story single degree of freedom 2D steel frame. The height of the story is 3m. Mass of 350MGr was concentrated on the middle of the beam. There are 5 columns with different elastic modulus and yield strength of 270Mpa. The columns and the beam are 0.2x0.2m. The steel is following the bilinear model. Elastic Modulus of Column1 and Column2 is  $1.5 \cdot 10^8$ Kpa. Elastic Modulus of Column 3 and Column 4 is  $2 \cdot 10^8$ Kpa. Elastic Modulus of Column 5 is  $4 \cdot 10^8$ Kpa. Elastic Modulus of the beam is  $2 \cdot 10^{10}$ Kpa and it is behaving only linear elastic. The acting load is Kobe's earthquake. Newmark's method was used to solve the differential equation.  $\lambda$  scaling factor of 0.1 and 1.5 was applied to the load for the 2 simulations.

For scaling factor of 0.1 maximum displacement of the top was 0.002m.



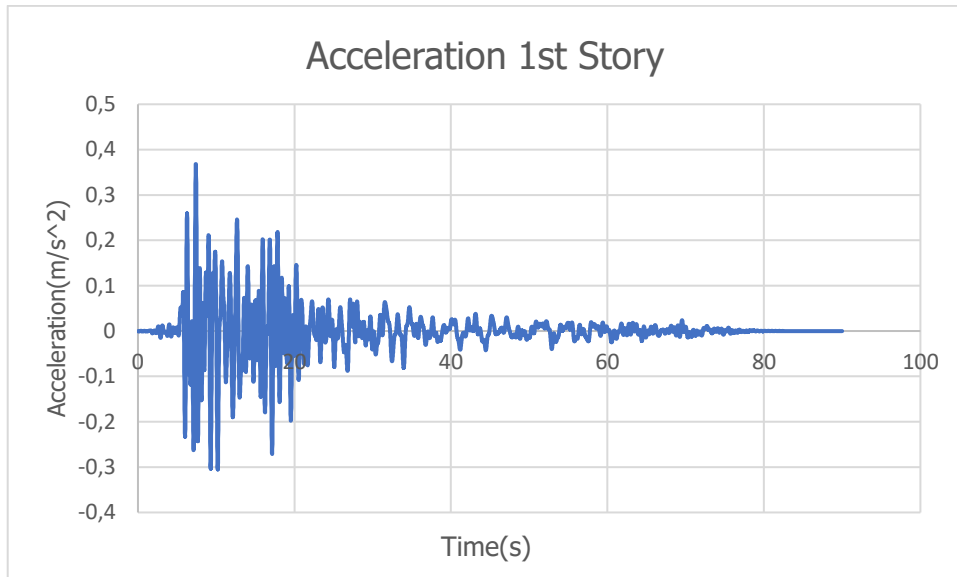


Figure 5-4: Accelerations diagram of the first story center of mass.

After applying the first level discrete wavelet transform using Daubechies 4 wavelet we are getting the following 1<sup>st</sup> level details diagram.

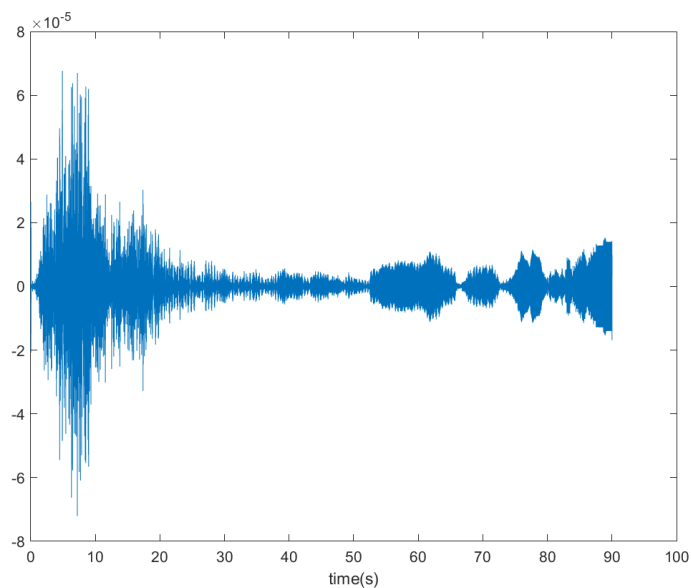


Figure 5-5: 1<sup>st</sup> level Details diagram

There are no spikes. The R Value is equal to 4.4% which means that there is no damage present. The results are confirmed from SeismoStruct where it's observed that all the columns did not reach their yielding point.

For  $\lambda$  scaling factor of 1.5 maximum displacement of the top was 0.034m

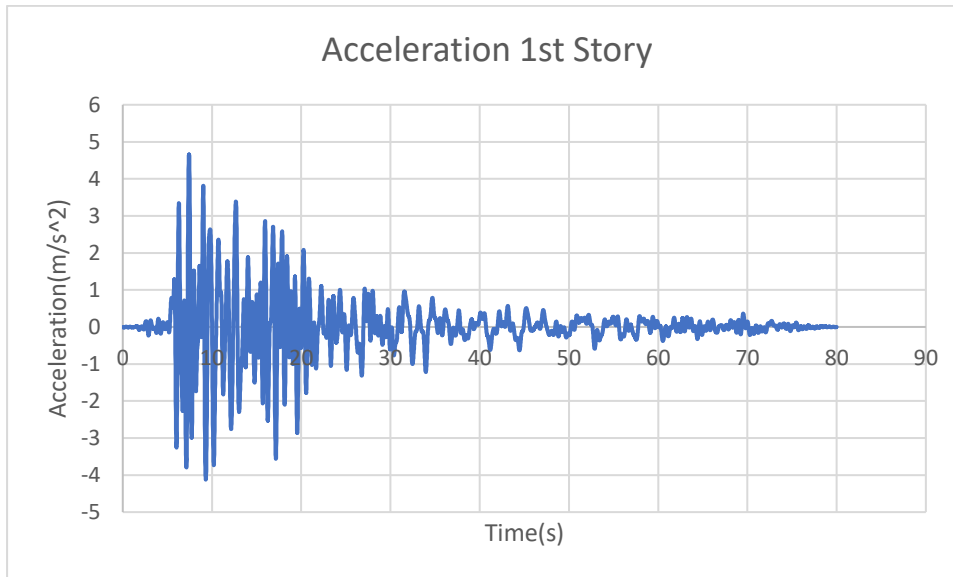


Figure 5-6: Accelerations' diagram of the first story center of mass

After applying the first level discrete wavelet transform using Daubechies 4 wavelet we are getting the following details diagram.

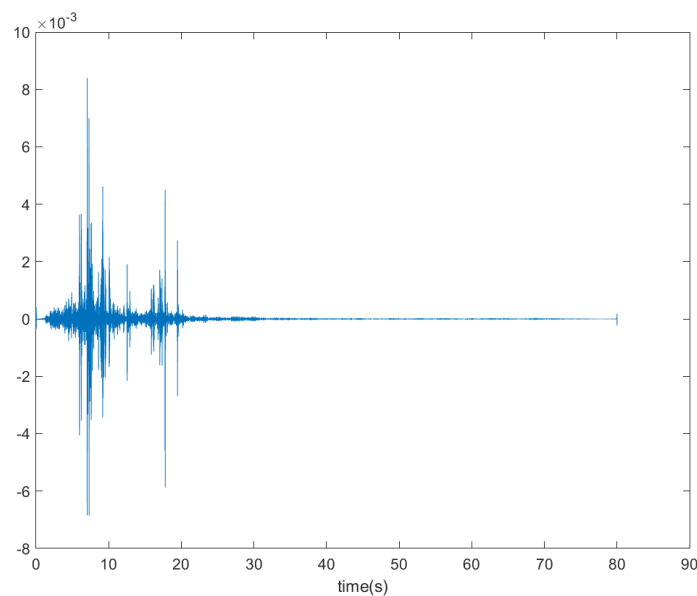
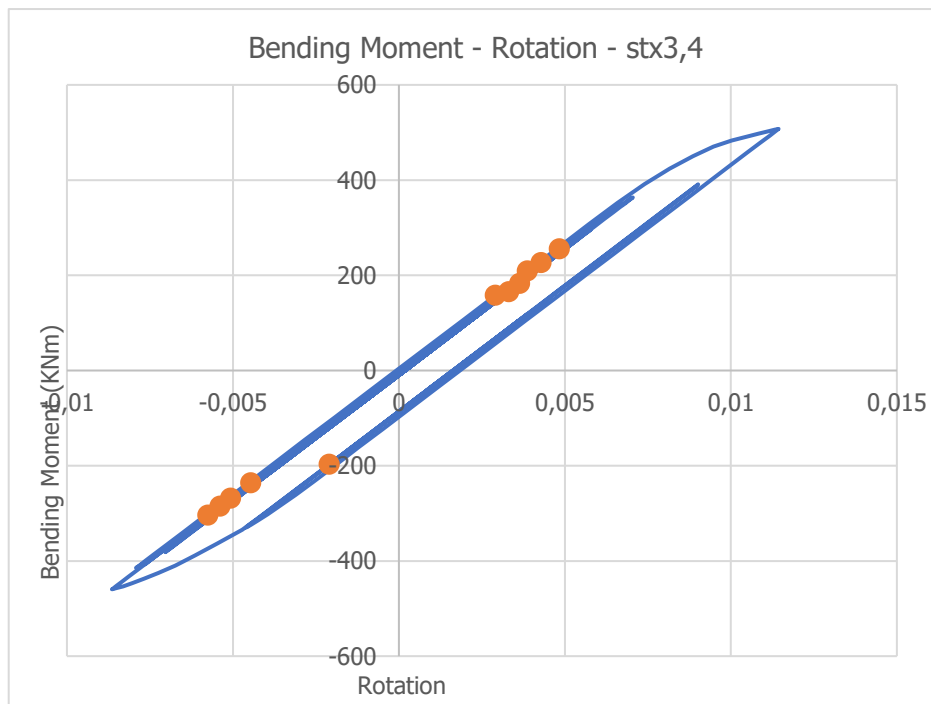
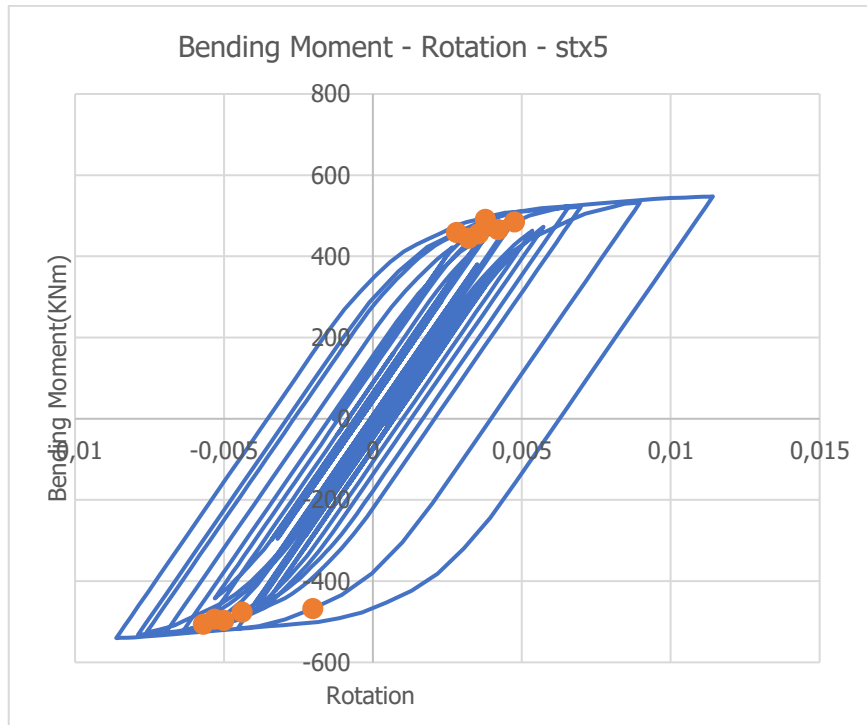


Figure 5-7: 1<sup>st</sup> level Details Diagram

There are big spikes that match with the yielding moments given from Seismostruct. R value is equal to 0.43% which confirms that there are spikes and that indicates that there is damage.

This is also confirmed from SeismoStruct that all the columns reached and surpassed their yielding point multiple times during the excitation as seen on Figure 5-8. Bending Moment and Rotation values for each spike time moment are marked with orange.



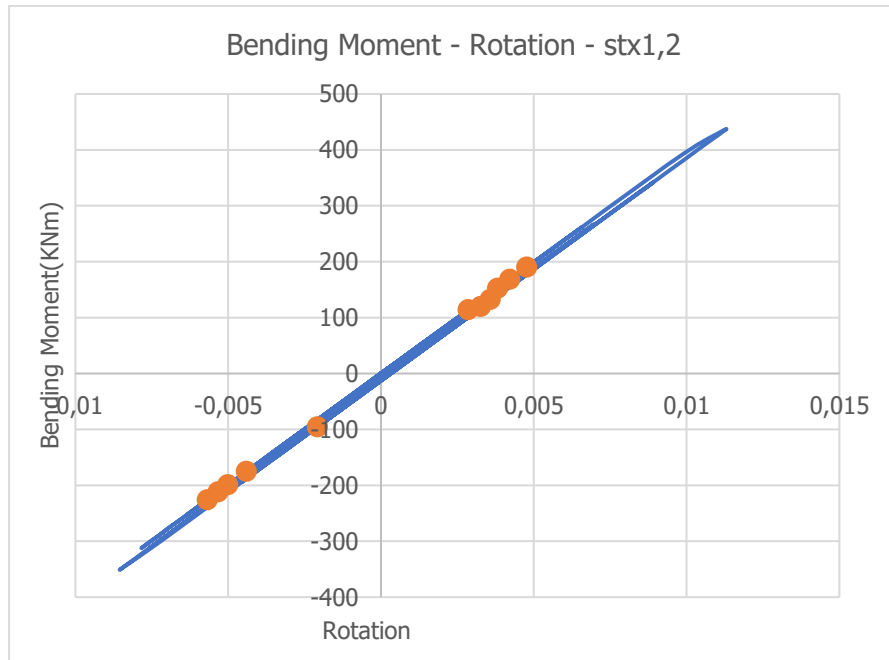


Figure 5-8: Bending Moment – Rotation Diagrams

### 5.3 10 Story 2D Seismostruct model.

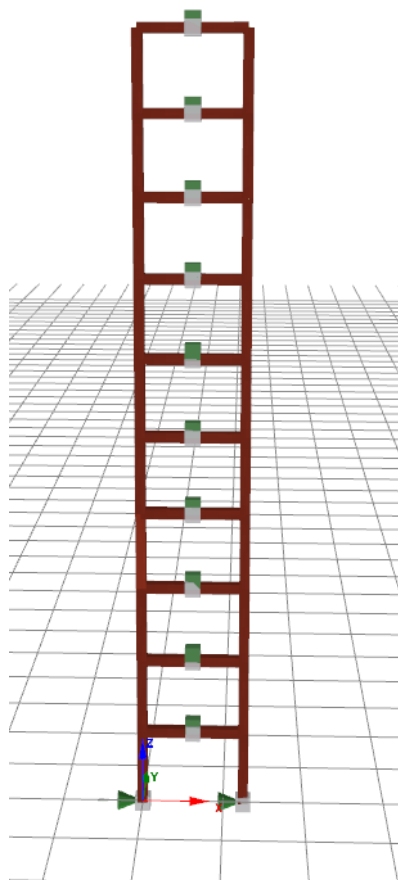


Figure 5-9: Seismostruct model

The present system was modelled as 10 Story 2D steel frame. The height of each story is 3m. Mass of 150MGr was concentrated on the middle of each beam. Columns and beams are 0.4x0.4m. Elastic modulus of each column is  $1.5 \cdot 10^8$ Kpa and the yield stress  $\sigma_y$  is 135Mpa, steel is following the bilinear model.. Elastic modulus for the beams is  $2 \cdot 10^{10}$ KPa. For this model all elements except the ones between the 1<sup>st</sup> and the 2<sup>nd</sup> story are always moving linearly.

First for  $\lambda$  scaling factor of 0.1 there is no damage on any of the elements.

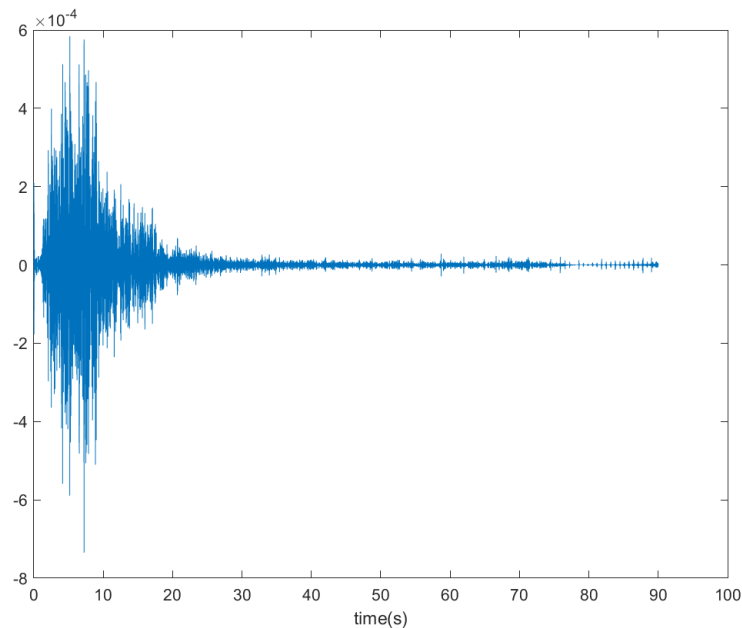


Figure 5-10:1<sup>st</sup> level Details diagram

All 1<sup>st</sup> level details diagrams follow the same pattern.

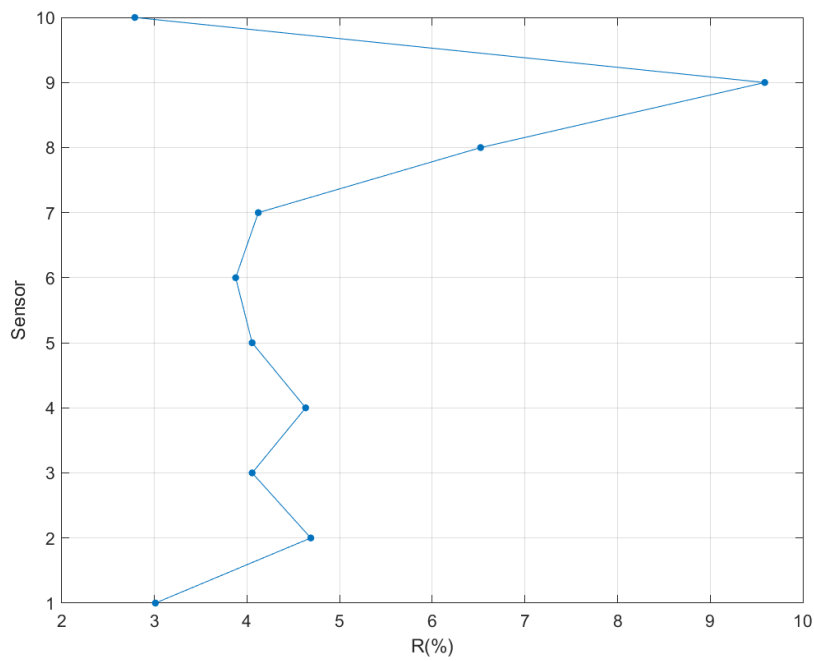
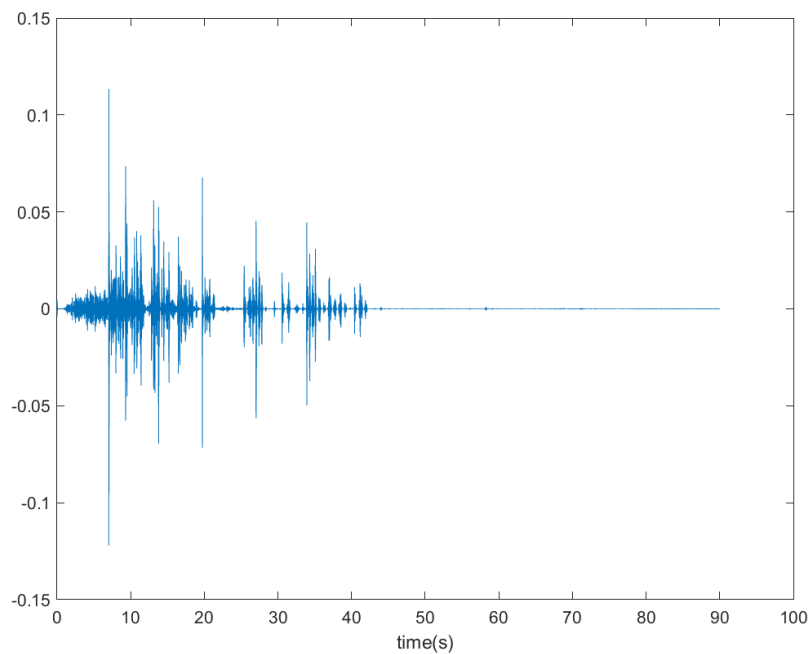


Figure 5-11: R Values for each story

From the R values calculated there is no damage indicated which is also confirmed from the results of the Seismostruct analysis.

For  $\lambda$  scaling factor of 2 the columns between the 1<sup>st</sup> and the 2<sup>nd</sup> story are past their yielding point.



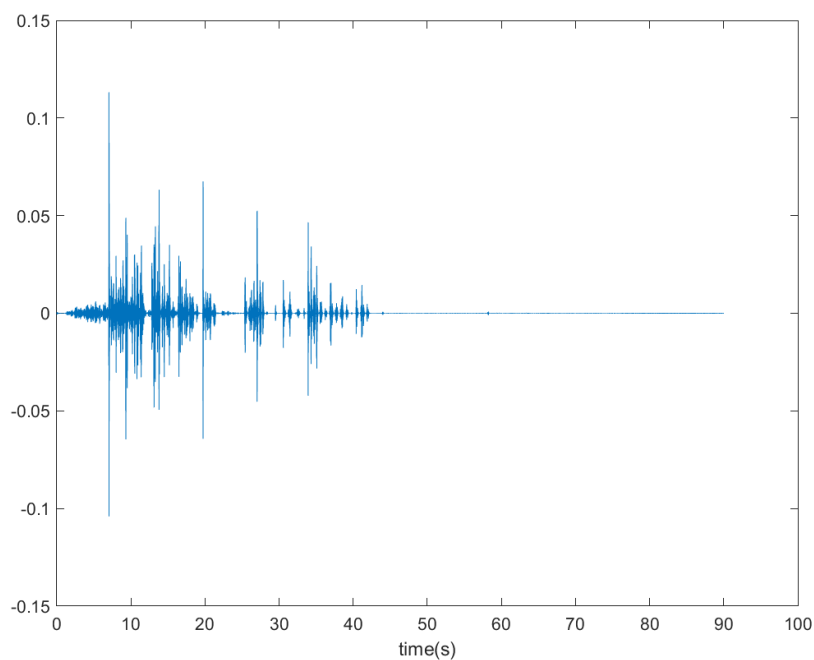


Figure 5-12: 1<sup>st</sup> level Details diagram of the accelerations of the first 2 floors.

There are obvious spikes which are also confirmed by the R values

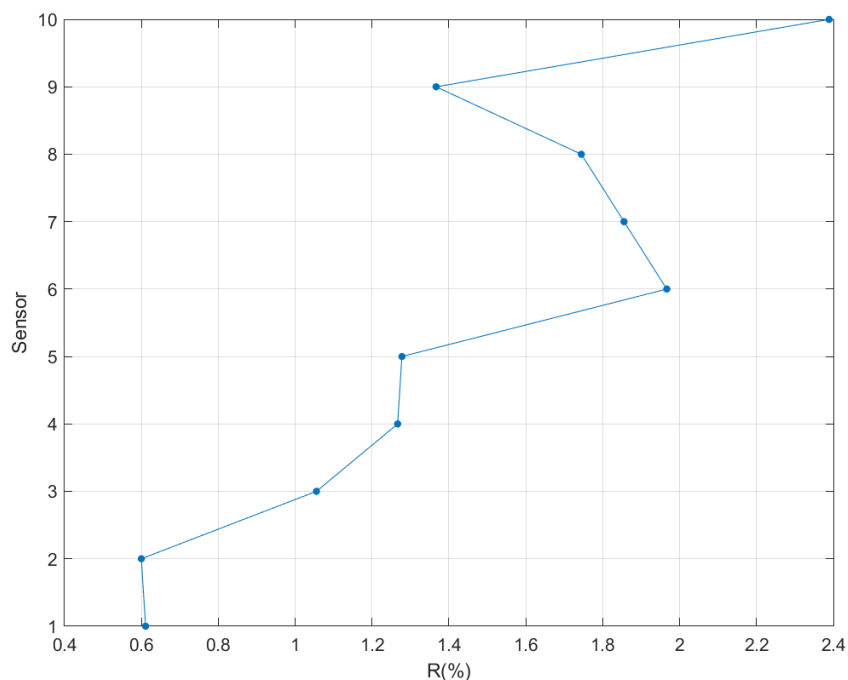


Figure 5-13: R Values

Close to the damage R values are below 1% which is sign of damage. Results are confirmed from Seismostruct that there is damage between the 1<sup>st</sup> and the 2<sup>nd</sup> story as shown on Figure 5-14. Bending Moment and Rotation values for each spike time moment are marked with orange.

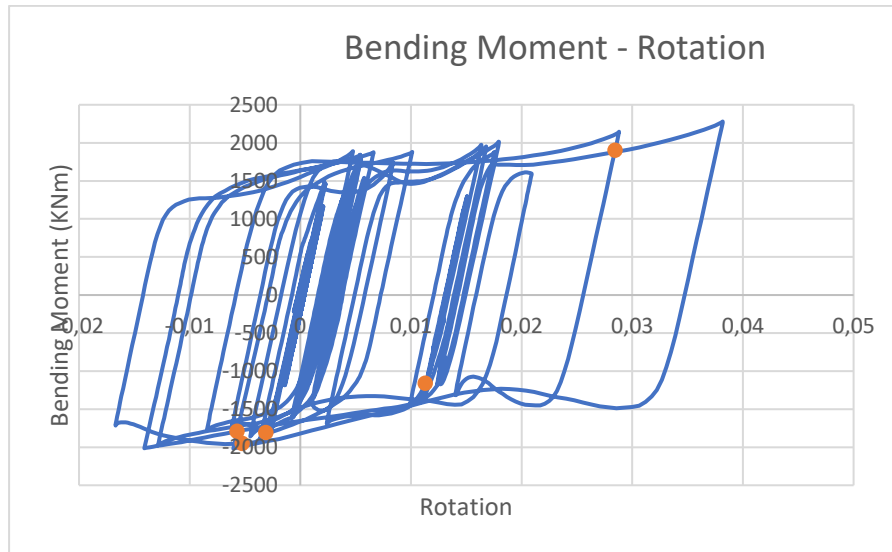


Figure 5-14: Bending Moment – Rotations diagram – 2<sup>nd</sup> story columns

#### 5.4 6 Story 3D Seismostruct model.

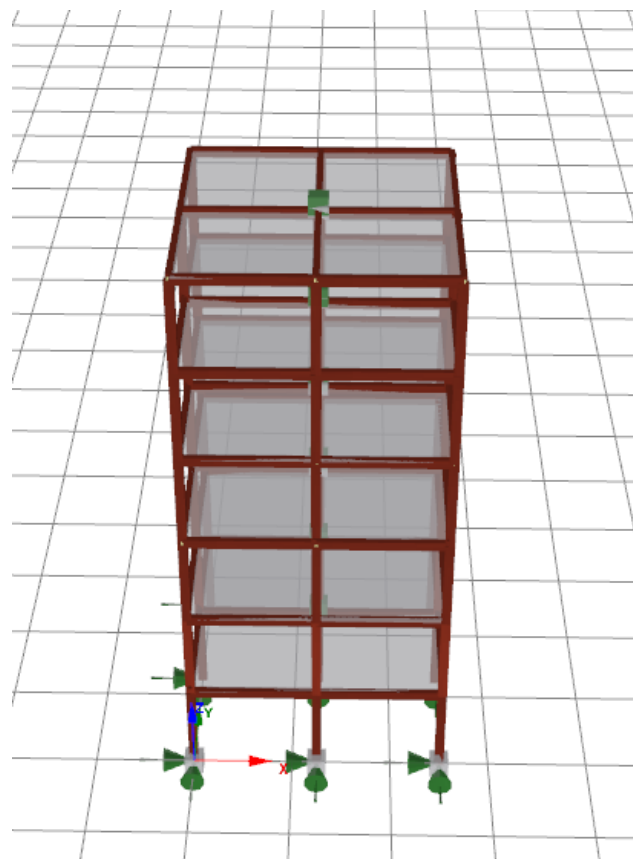


Figure 5-15: Seismostruct model

The present system was modelled as 10 Story 2D steel frame. The height of each story is 3m. Mass of 350MGr was concentrated on the middle of each beam. Moment of inertia  $3750\text{MGr}\cdot\text{m}^2$ . Columns and beams are  $0.3\times 0.2\text{m}$ . Elastic modulus of every column is  $1.5 \cdot 10^8 \text{KPa}$ . Elastic modulus of every beam



is  $2 * 10^{10} KPa$ . For this model all elements except the ones between the 1<sup>st</sup> and the 2<sup>nd</sup> story are always moving linearly. Yield stress of the columns between the 1<sup>st</sup> and the 2<sup>nd</sup> story is  $\sigma_y$  is 135Mpa. Steel is following the bilinear model. For X-Y axis the equivalent Kobe Earthquake excitation were used, both were adjusted with the same scaling factor  $\lambda$ .

First for  $\lambda$  scaling factor of 0.10 there is no damage on any of the elements.

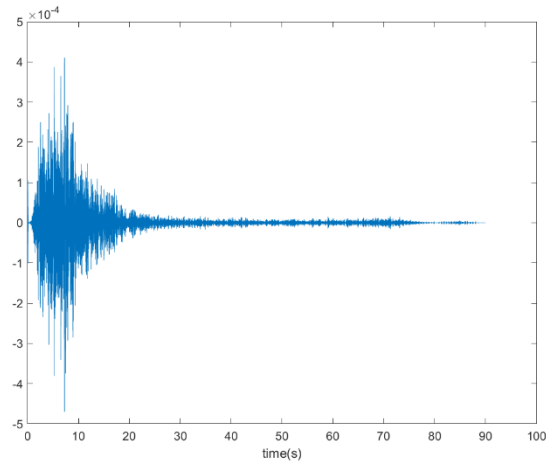


Figure 5-16: 1<sup>st</sup> level Details Diagram – X Axis

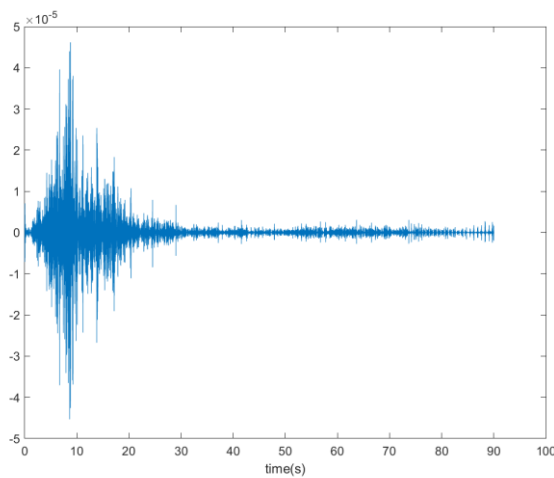


Figure 5-17: 1<sup>st</sup> level Details Diagram – Y Axis

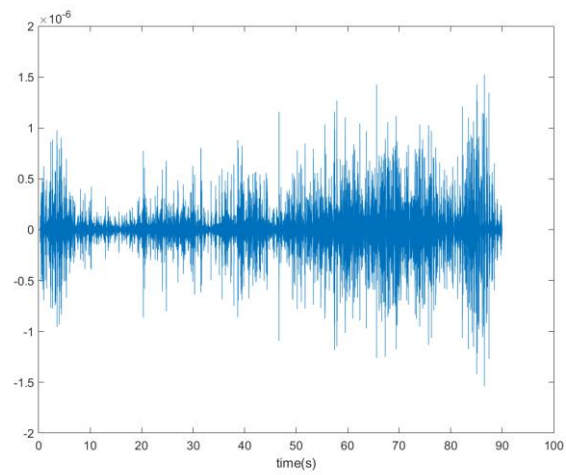
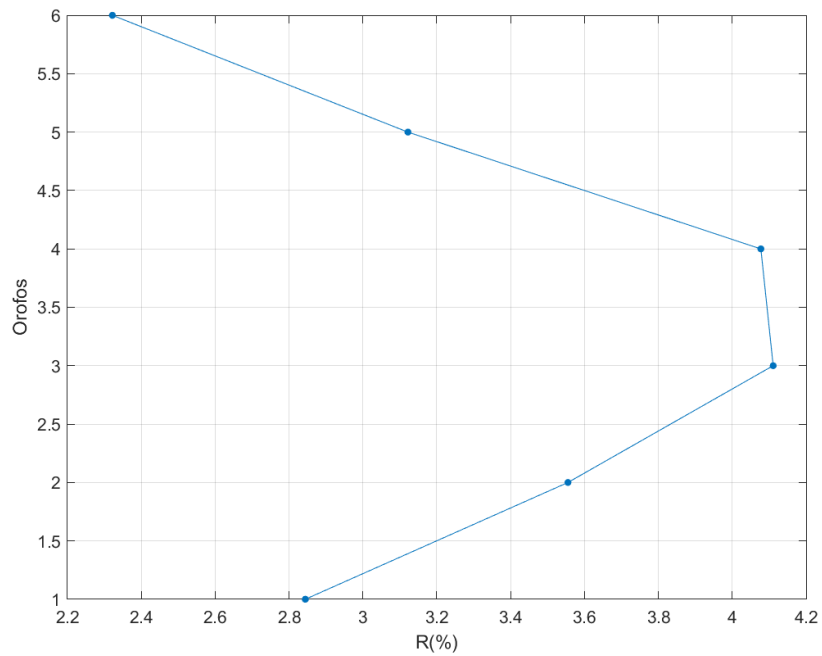
Figure 5-18: 1<sup>st</sup> level Details Diagram – RZ Axis

Figure 5-19: R values – X Axis

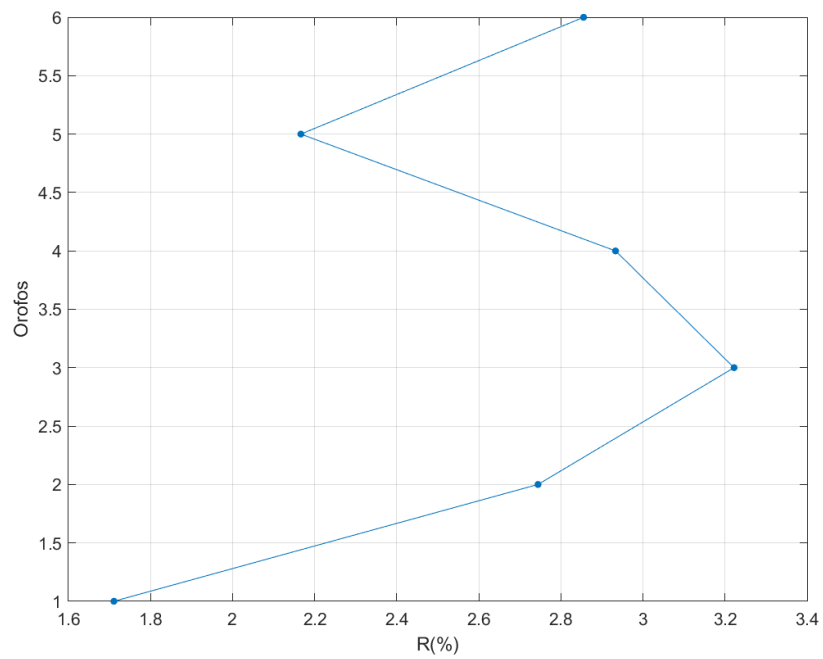


Figure 5-20: R values – Y Axis

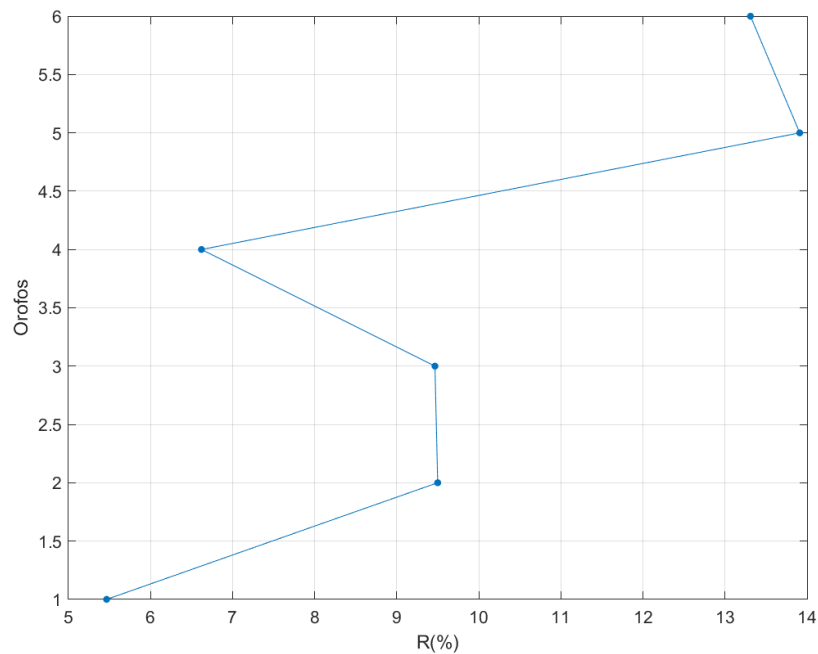
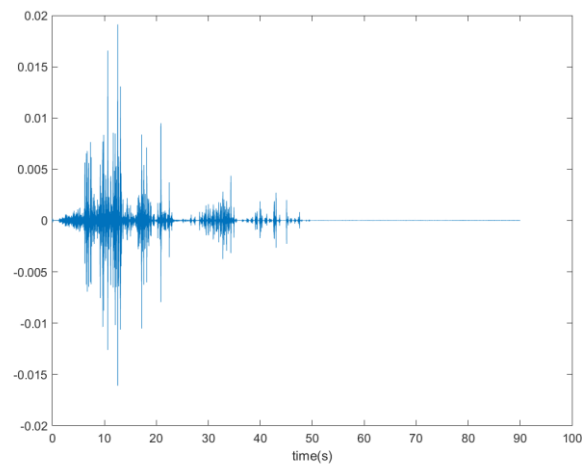
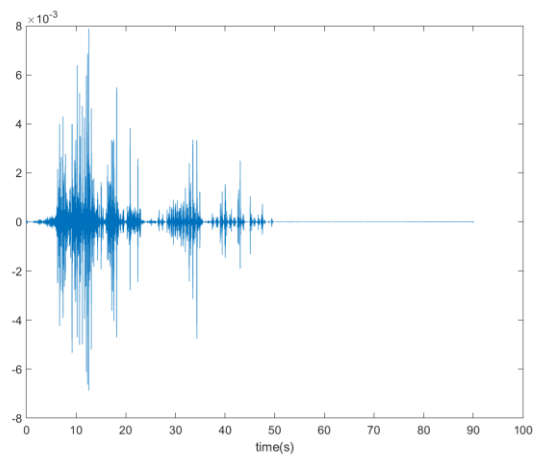
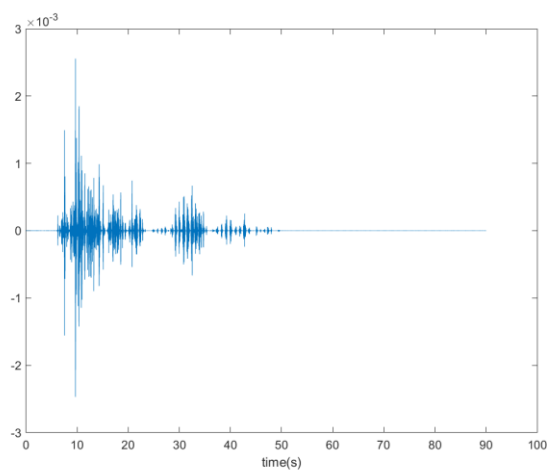


Figure 5-21: R Values – RZ Axis

The results are confirmed by the results from Seismostruct. There is no damage to the building.

For  $\lambda$  scaling factor 1.5 the columns between the first and the second story go past their yielding point.

Figure 5-22: 1<sup>st</sup> level Details Diagram – X AxisFigure 5-23: 1<sup>st</sup> level Details Diagram – Y AxisFigure 5-24: 1<sup>st</sup> level Details Diagram – RZ Axis

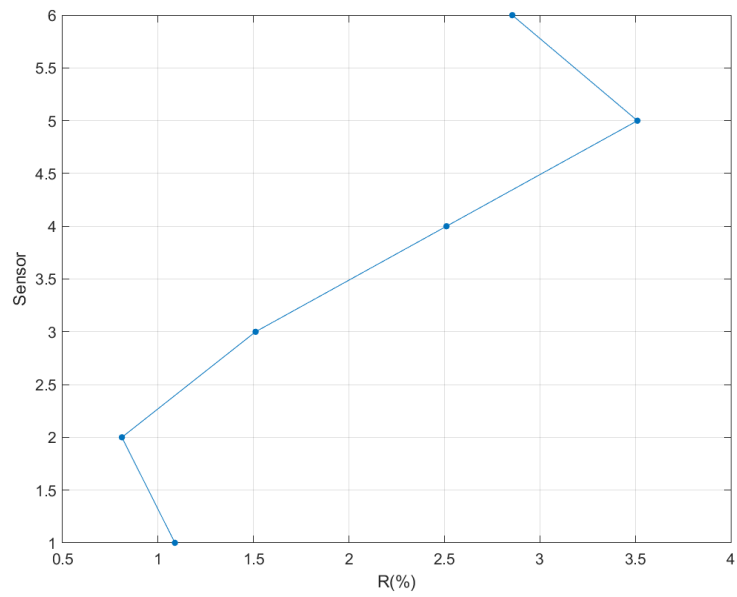


Figure 5-25: R Values – X Axis

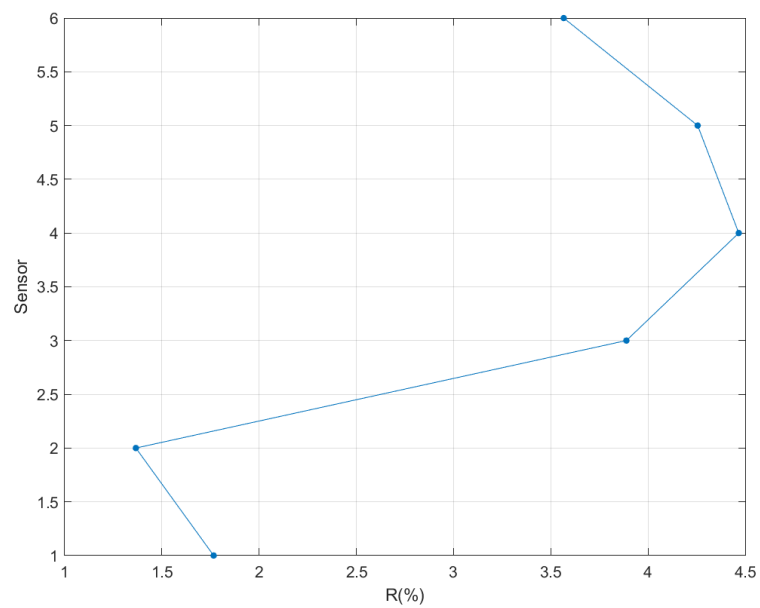


Figure 5-26: R values – Y Axis

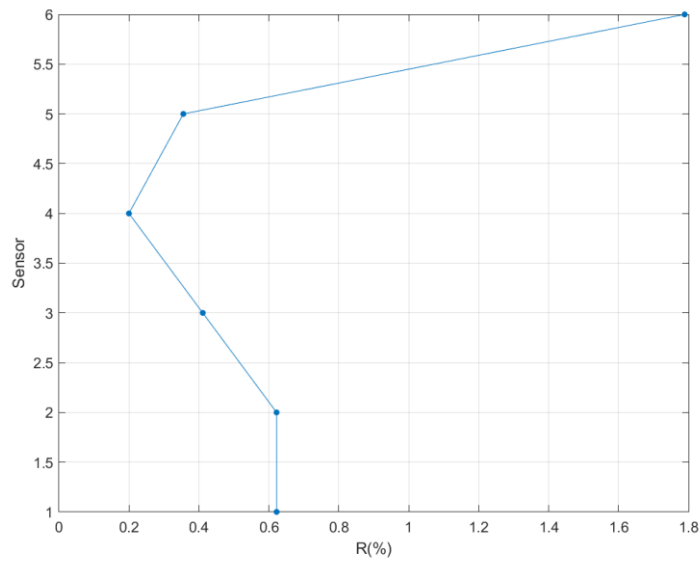
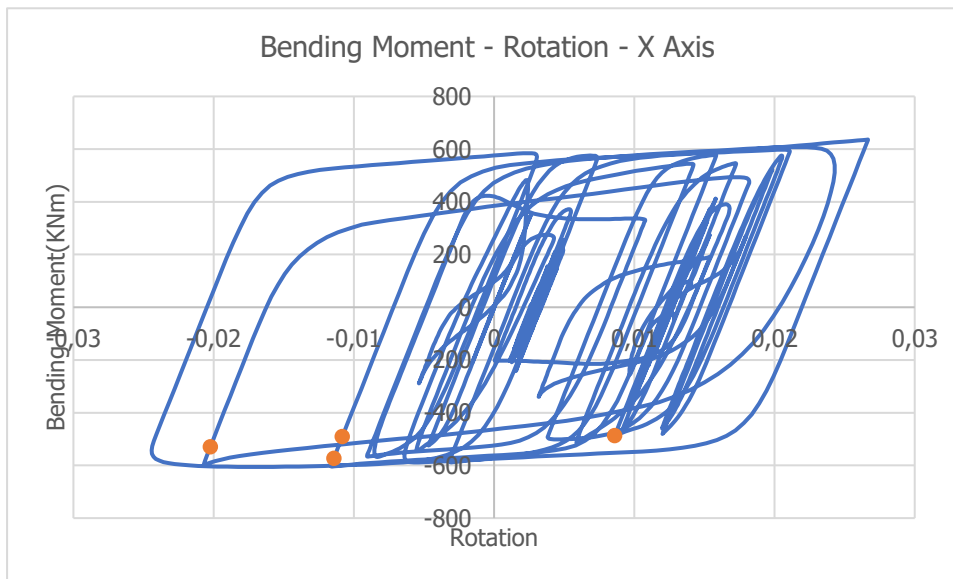


Figure 5-27: R Values – RZ Axis

R values on all 3 axis are close or lower than 1% which indicates that there are spikes in the details diagrams. Seismostruct results confirm that there is damage around the 1<sup>st</sup> and 2<sup>nd</sup> story. Bending Moment and Rotation values for each spike time moment are marked with orange.



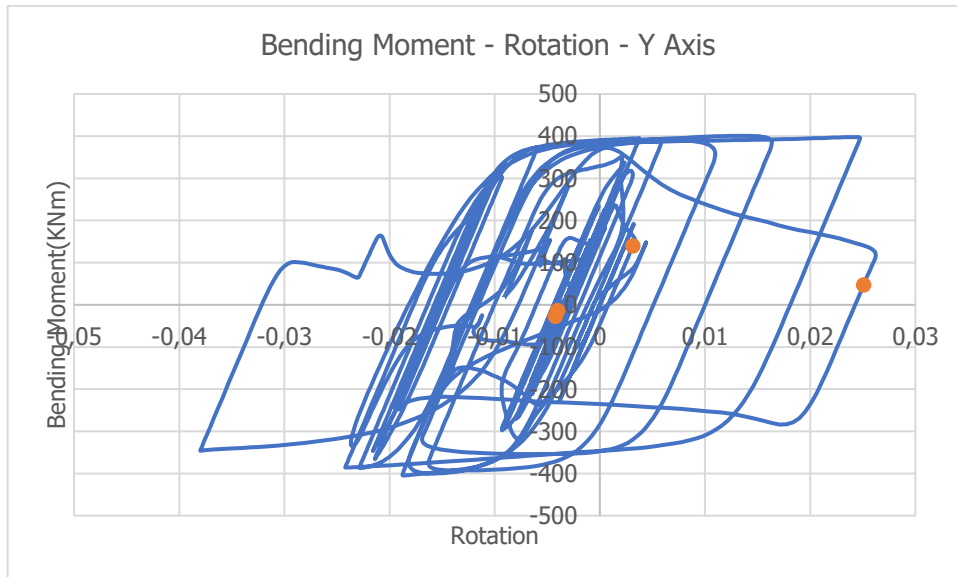


Figure 5-28: Bending Moment – Rotation Diagrams – 2<sup>nd</sup> story columns

Also, it's good to note that the weak axis is the one dictating when the spikes appear, in our case that's x axis.

### 5.5 10 Story 2D Seismostruct model using Menegotto – Pinto steel model

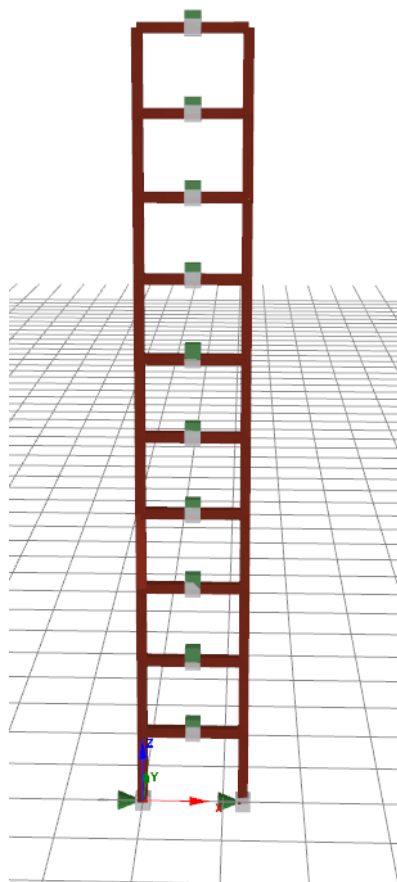


Figure 5-29: Seismostruct model

Menegotto – Pinto steel model is a single axis steel model based on a simple but effective formula proposed by Menegotto and Pinto in 1973 extended by Filippou et al. to include isotropic strain hardening effects (1983). Over 10 parameters can be changed to optimize the material behavior. [28]

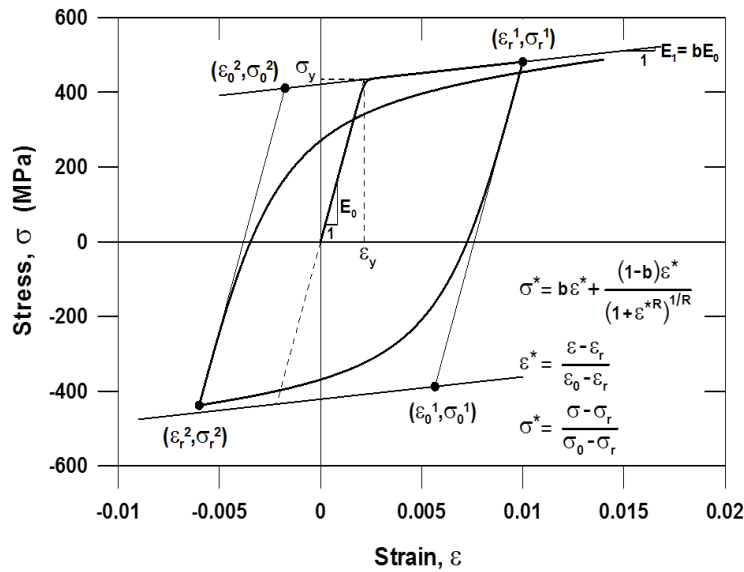


Figure 5-30: Menegotto – Pinto constitutive model for steel.

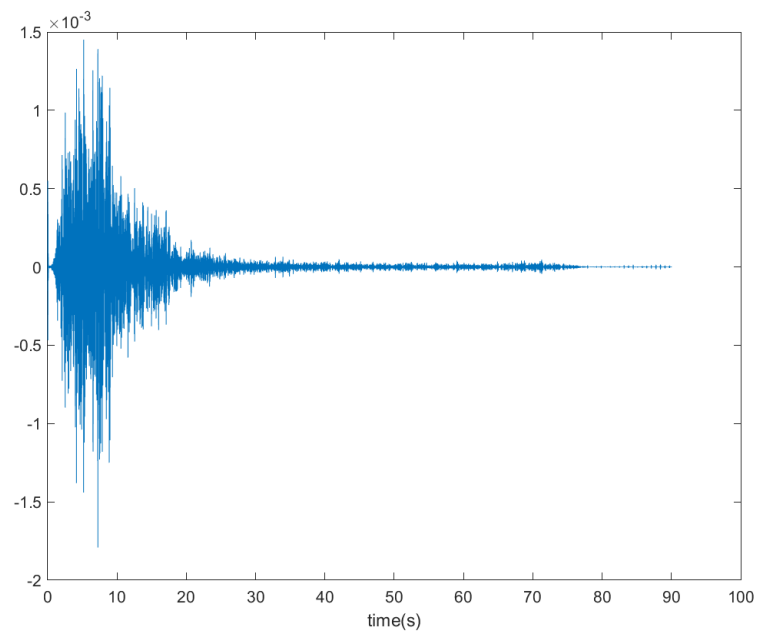
The present system was modelled as 10 Story 2D steel frame. The height of each story is 3m. Mass of 150MGr was concentrated on the middle of each beam. Columns and beams are 0.4x0.4m. Elastic modulus of each column is  $1.5 \cdot 10^8$ Kpa and the yield stress  $\sigma_y$  is 135Mpa. Elastic modulus of the beams is  $2 \cdot 10^{10}$ KPa. For this model all elements except the ones between the 1<sup>st</sup> and the 2<sup>nd</sup> story are always moving linearly.

Table 5-1: Menegotto – Pinto steel constitutional model parameters

<i>Material Properties</i>	<i>Value Chosen</i>
<i>Modulus of elasticity</i>	$1.5 \cdot 10^8$ (kPa)
<i>Yield strength</i>	135000(kPa)
<i>Strain hardening parameter - μ</i>	0.005
<i>Transition curve initial shape parameter - R0</i>	20
<i>Transition curve shape calibrating coefficient - A1</i>	18.5
<i>Transition curve shape calibrating coefficient - A2</i>	0.15
<i>Isotropic hardening calibrating coefficient - A3</i>	0
<i>Isotropic hardening calibrating coefficient - A4</i>	1
<i>Fracture/buckling strain</i>	0.1

First for λ scaling factor of 0.4 there is no damage on any of the elements.



Figure 5-31: 1<sup>st</sup> level Details diagram

All details diagrams follow the same pattern.

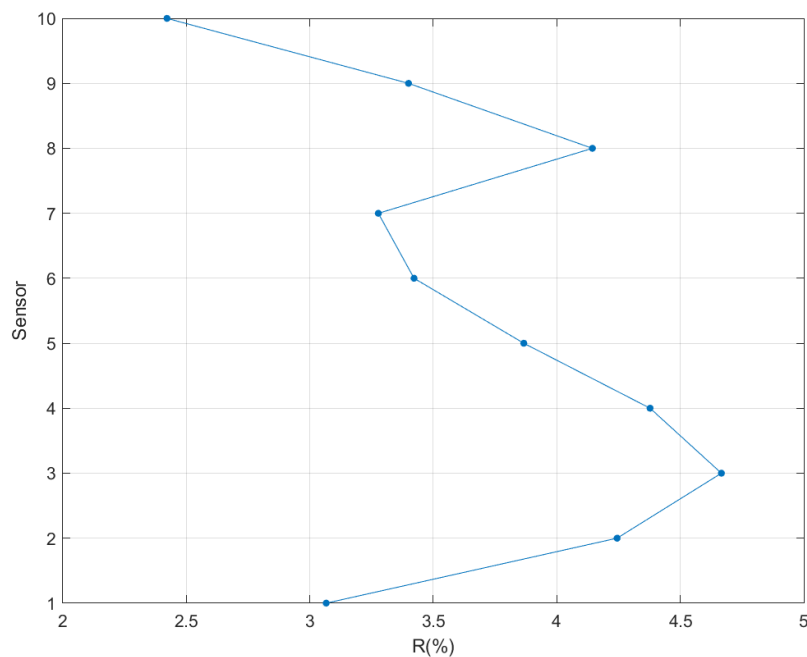


Figure 5-32: R Values for each story

From the R values calculated there is no damage indicated which is also confirmed from the results of the Seismostruct analysis.

For  $\lambda$  scaling factor of 1 the columns between the 1<sup>st</sup> and the 2<sup>nd</sup> story are past their yielding point.

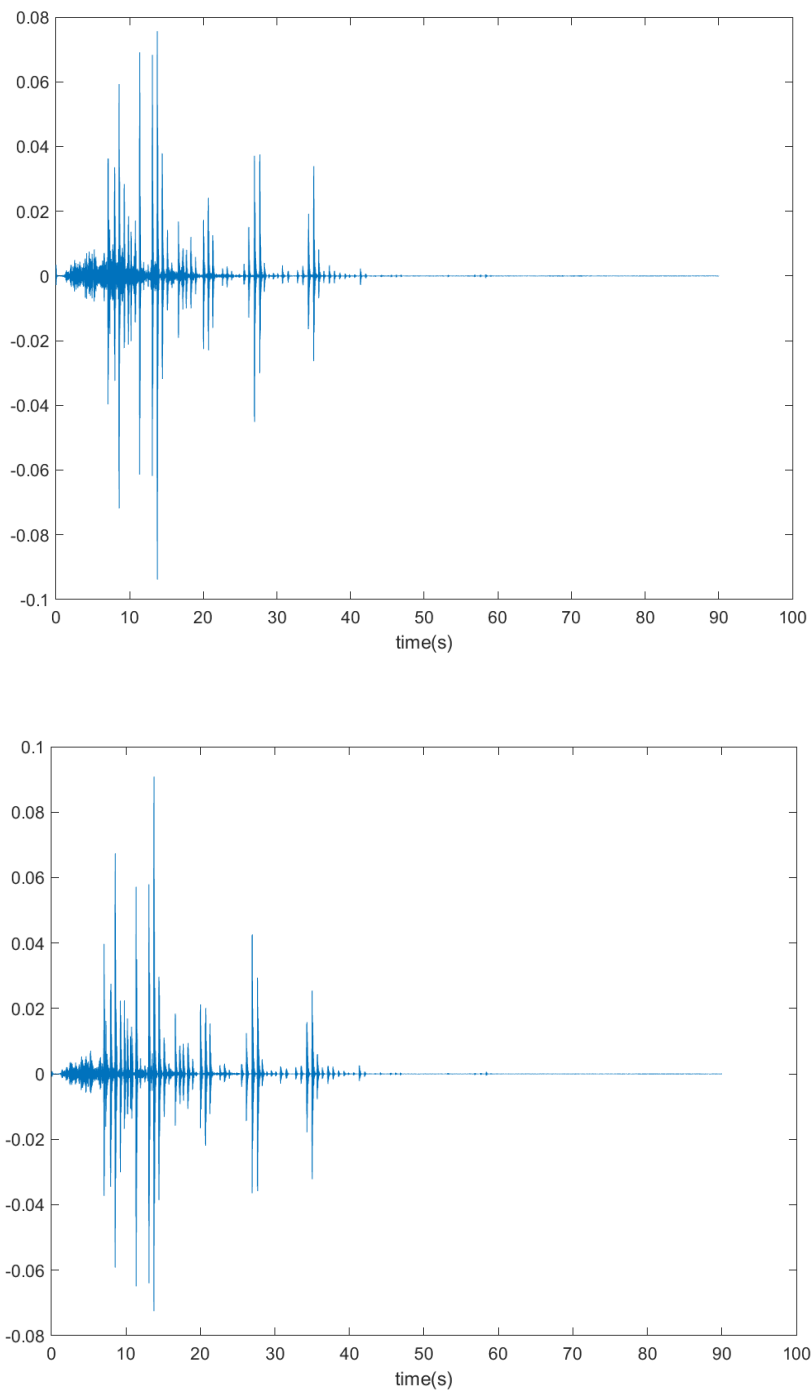


Figure 5-33: 1<sup>st</sup> level Details diagram of the accelerations of the first 2 floors.

There are obvious spikes which are also confirmed by the R values

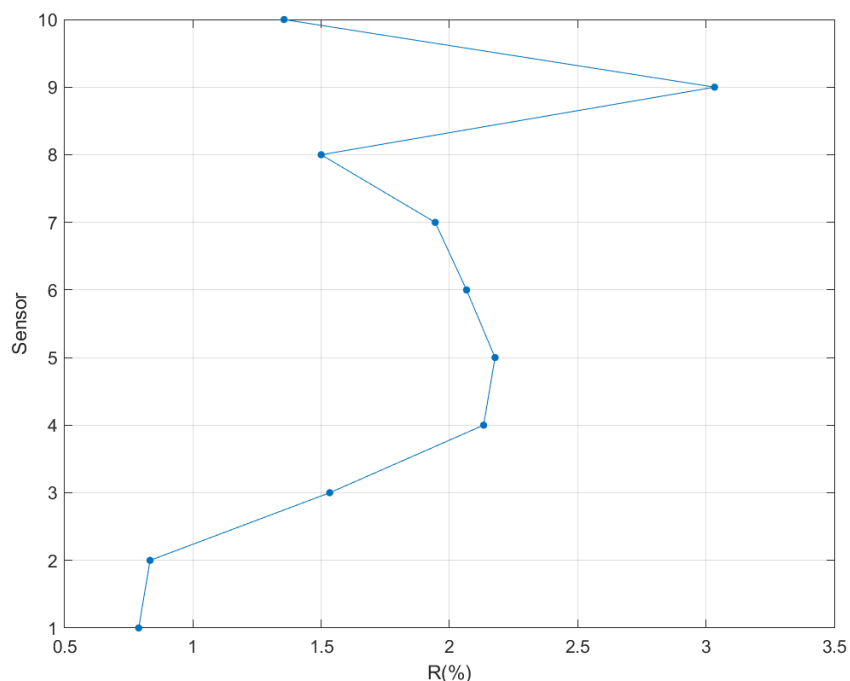
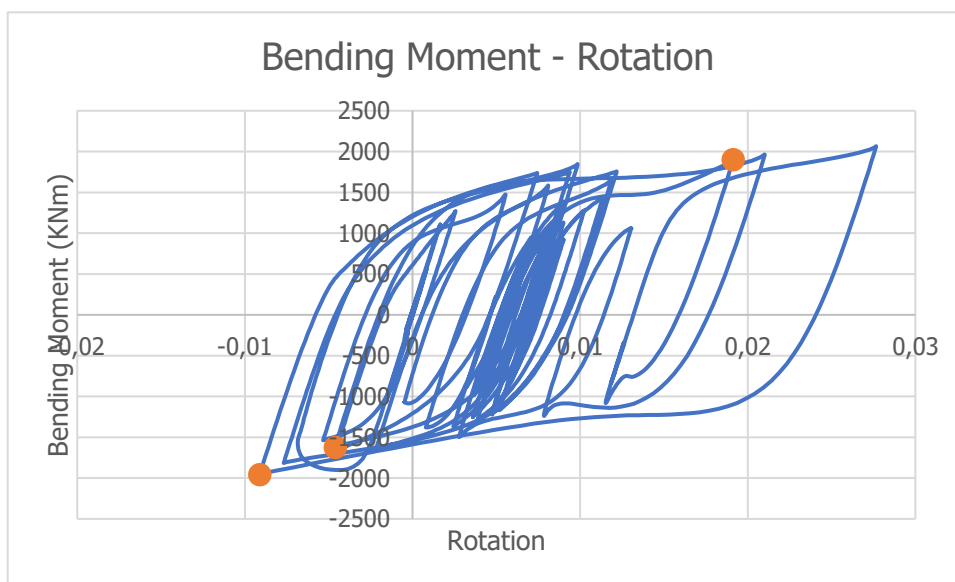


Figure 5-34: R Values

Close to the damage R values are significantly below 1% which is sign of damage. Results are confirmed from Seismostruct that there is damage between the 1<sup>st</sup> and the 2<sup>nd</sup> story as shown on Figure 5-14. Bending Moment and Rotation values for each spike time moment are marked with orange.

Figure 5-35: Bending Moment – Rotations diagram – 2<sup>nd</sup> story columns

## 5.6 Sherman Oaks – 13 Story commercial building.

Sherman Oaks is an office building designed in 1964 with 13 stories above and two floors below the ground. The vertical load carrying system consists of 4.5 inches thick one-way concrete slabs supported by concrete beams, girders and columns. The lateral load resisting system consists of moment resisting

concrete frames in the upper stories and concrete shear walls in the basements. The foundation system consists of concrete piles. Sensors were placed in different floors of the building.

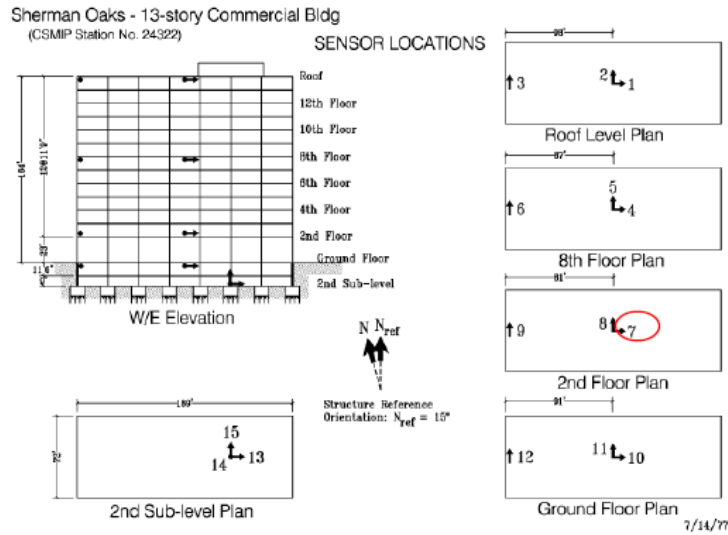


Figure 5-36: Sensor Locations

The building was moderately damaged during the 1994 Northridge earthquake while it sustained no damaged during the 1992 Landers Earthquake. Sensor 7 is the one closest to the damaged area.

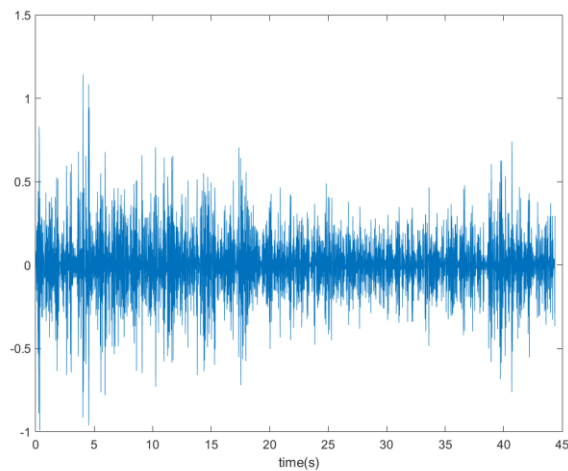


Figure 5-37: 1<sup>st</sup> level details of DWT applied on acceleration signal – 1992 – Sensor 7

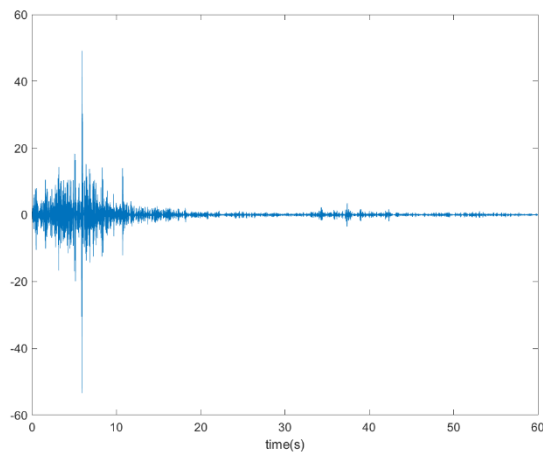


Figure 5-38: 1<sup>st</sup> level details of DWT applied on acceleration signal – 1994 – Sensor 7

There is a big spike on the details diagram from the 1994 recordings. This is indication of damage. This is also confirmed by the R values calculated for every sensor on both occasions.

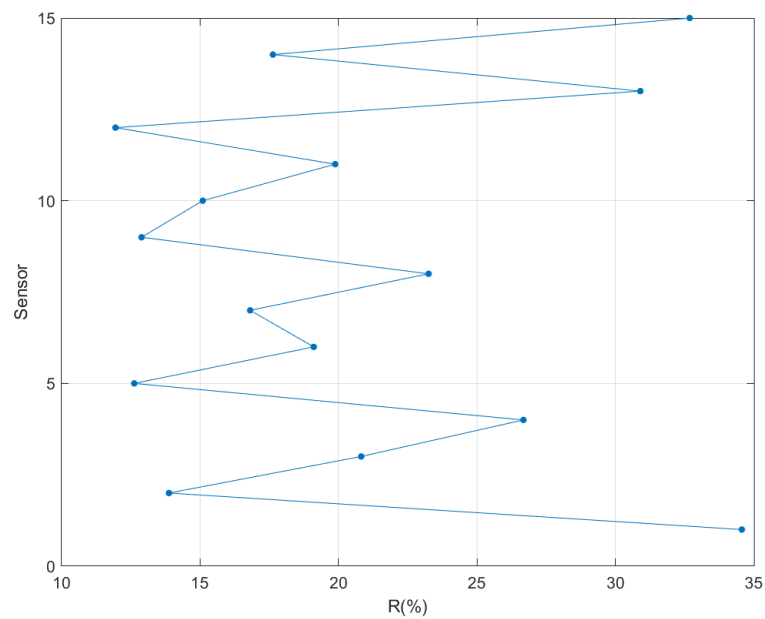


Figure 5-39: R Values - 1992

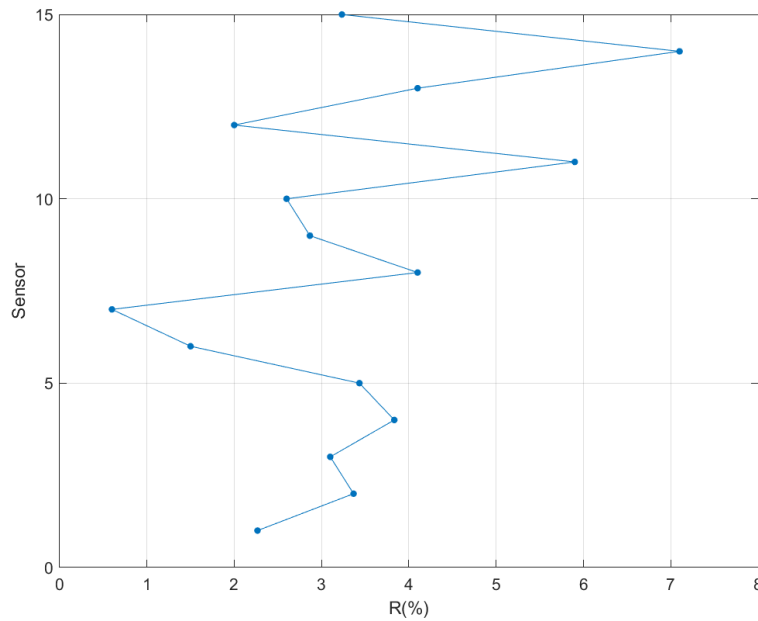


Figure 5-40: R Values – 1994

On the sensor closest to the damaged area R value is smaller than 1% which indicates that there are spikes on the details diagram. Results are in line with the performance analysis calculations for the building.

0.19W maximum base shear experienced by the building in the N-S direction is significantly larger than Uniform Building Code (UBS) analysis calculated strength design shear of 0.06W.

Table 5-2: Response Summary for Sherman Oaks 13-Story Commercial Building [8]

<i>Response Parameter</i>	<i>Direction</i>	<i>Time of Maxima (Seconds)</i>	<i>Maximum Value</i>
<i>Base Shear (% Total Weight)</i>	<i>N-S</i>	<i>5.14</i>	<i>18.70</i>
	<i>E-W</i>	<i>12.72</i>	<i>7.57</i>
	<i>Diff</i>	<i>3.24</i>	<i>6.69</i>
<i>Overturning Moment (% Total Weight x feet)</i>	<i>N-S</i>	<i>3.22</i>	<i>1304</i>
	<i>E-W</i>	<i>11.52</i>	<i>771</i>
	<i>Diff</i>	<i>3.22</i>	<i>615</i>
<i>Roof Lateral Displacement Relative to the Base (cm)</i>	<i>N-S</i>	<i>10.86</i>	<i>24.10 (0.0048) *</i>
	<i>E-W</i>	<i>37.98</i>	<i>33.42 (0.0067) *</i>
	<i>Diff</i>	<i>11.00</i>	<i>4.30 (0.0009) *</i>

\*Overall drift index values are shown in the brackets

## 6 CONTINUOUS WAVELET TRANSFORM (CWT) APPLICATIONS.

CWT is a tool that when applied to a signal, produces a time-frequency representation. By applying this transformation on the free response of a linear mechanical system it allows the estimation of the natural frequencies, viscous damping ratios and mode shapes. In case the free response is not available, then an approximation needs to be extracted from the signal using the Random Decrement (RD) method. Furthermore, difficulties appearing during the application of the method will be discussed along with ways to solve them.

Continuous wavelet transform was tested on 5 buildings

1. 1 Story 2D frame simulated with Seismostruct 2020
2. 10 Story 2d frame simulated with Seismostruct 2020
3. 6 Story 3d building simulated with Seismostruct 2020
4. 1 Story 3d building EUROPROTEAS
5. Sherman Oaks – 13 Story Commercial Building (recordings from StrongMotion.org)

### 6.1 Estimation of Damping Ratio and Mode shapes using wavelet transform.

A single degree of freedom system's equilibrium can be expressed as

$$m\ddot{x} + c\dot{x} + kx = f(t) \quad (6-1)$$

where  $m$  is the mass,  $c$  is the damping and  $k$  is the stiffness of the system. From the above equation the damped free vibration of an underdamped system can be expressed as

$$x(t) = A(t) * e^{\pm i\omega_n\sqrt{1-c^2}t} = A(t) * e^{i\varphi(t)} \quad (6-2)$$

or also as

$$A(t) = A_0 e^{-c\omega_n t} \quad (6-3)$$

where  $A(t)$  is the decaying envelope of the free vibration response,  $c$  the damping ratio and  $A_0$  the initial amplitude of the response.

Using the Morlet wavelet function, the modulus of CWT coefficients can be approximated as

$$|W(a, b)| \approx A(b) |G^*(a\hat{\varphi}(b))| \quad (6-4)$$

by using equation (6-2), (6-3), (6-4) and by knowing the initial amplitude  $A_0$

$$|W(a_0, b)| \approx A_0 e^{-c\omega_n b} \left| G^*(\pm a_0 i\omega_n \sqrt{1-c^2}) \right| \quad (6-5)$$

Applying logarithm to both sides

$$\ln(|W(a_0, b)|) \approx -c\omega_n b + \ln \left( \left| G^*(\pm a_0 i\omega_n \sqrt{1-c^2}) \right| \right) \quad (6-6)$$

solving this formula for  $c$ , the damping ratio of the system can be estimated from the slope of the straight line of the wavelet modulus cross using

$$c = \frac{1}{2\pi m} \ln \left| \frac{W(a_0, b)}{W(a_0, b + mT_0)} \right| \quad (6-7)$$

Wavelet coefficients between different Stories for a certain frequency have the same analogy as the mode shapes. So, mode shapes are estimated through the wavelet output response at point k and a reference point

$$\varphi_i^k = \frac{W^k(a_i, b)}{W^{ref}(a_i, b)} \quad (6-8)$$

## 6.2 Random Decrement (RD) Method

The Random decrement (RD) method is a method used to estimate the damping ratio of a structure. This method is using the ambient vibration measurement of the structure and is extracting a RD signature which represents the response equivalent to the damped free vibration response. This method is based on that the response of a dynamic system is composed of three response components. That is initial displacement, velocity and the force vibration response.

The intention of using the sampling technique is that averaging time segments of the ambient vibration measurement of a structure with a common triggering condition is to reduce the initial velocity response and the forced vibration response to zero. As number of segments increases the ensemble average of the forced vibration response tends to zero. If all segments in the average begin at the same threshold level and alternating positive and negative slope, then the response due to initial velocity is averaged out while the response due to initial displacement remains. Based on this explanation, the RD signature is equivalent to a damped free vibration response of a structure to an initial displacement equivalent to the selection amplitude. The RD signature  $\delta$  is expressed by

$$\delta_t = \frac{1}{N} \sum_{i=1}^N (x_{i,(t_i+r)}) \quad (6-9)$$

Where N is the number of segments used to evaluate the RD signature.

## 6.3 1 Story 2D Seismostruct model.

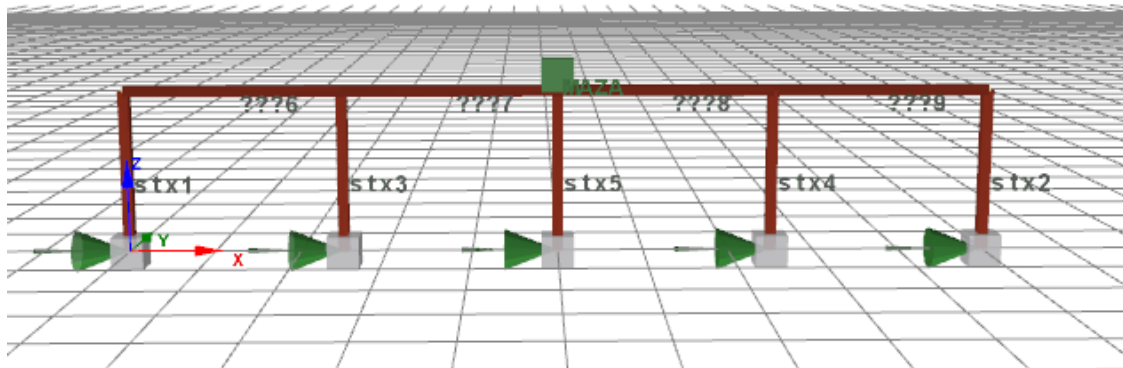


Figure 6-1: Seismostruct model.

The present system was modelled as 1 Story single degree of freedom 2D steel frame. The height of each story is 3m. Mass of 350MGr was concentrated on the middle of the beam. There are 5 columns with different



elastic modulus and yield strength of 270Mpa. The columns and the beam are 0.2x0.2m. The steel is following the bilinear model. Elastic Modulus of Column1 and Column2 is  $1.5 * 10^8$ Kpa. Elastic Modulus of Column 3 and Column4 is  $2 * 10^8$ Kpa. Elastic Modulus of Column 5 is  $4 * 10^8$ Kpa. Elastic Modulus of the beam is  $2 * 10^{10}$ Kpa and it is behaving only linear elastic. The acting load is Kobe's earthquake with 10 seconds of zero load added in the end so the free decaying response can be extracted without the use of any method. Newmark's method was used to solve the differential equation.

$\lambda$  scaling factor of 0.1 was applied to the excitation.

Through Seismostruct the natural frequency  $f_1$  is calculated to be 2.155HZ so  $T_1 = 0.464s$ . Damping ratio  $c$  is set to be 4%.

CWT is applied on last 10 seconds of the accelerations signal calculated through Seismostruct. This signal matches the 10 seconds time period of zero load added to the excitation. Morlet mother wavelet was used through MATLAB's wavelet toolbox.

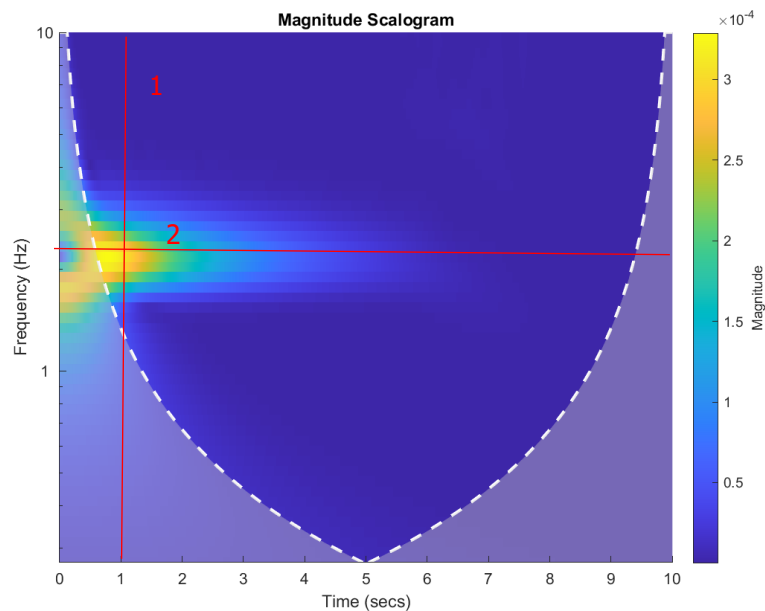


Figure 6-2: Magnitude Scalogram of the free decay accelerations signal.

After the time frequency resolution is calculated through CWT a window parallel to the frequency axis is extracted (Intersection 1).

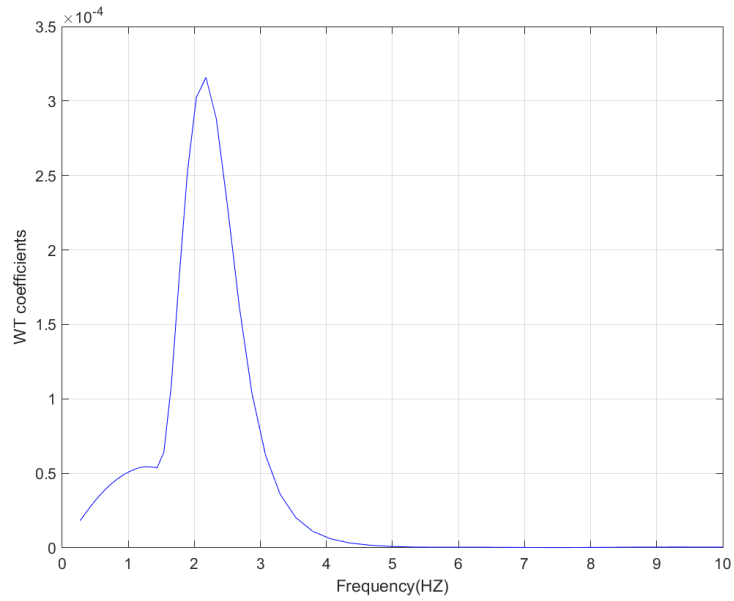


Figure 6-3: Extracted window parallel to frequency axis.[1]

The highest number of coefficients is at the frequency  $f_1 = 2.176\text{Hz} \rightarrow T_1 = 0.46\text{s}$ . Error is less than 1%. After  $f_1$  is calculated the parallel to frequency axis at the wavelet ridge is extracted.

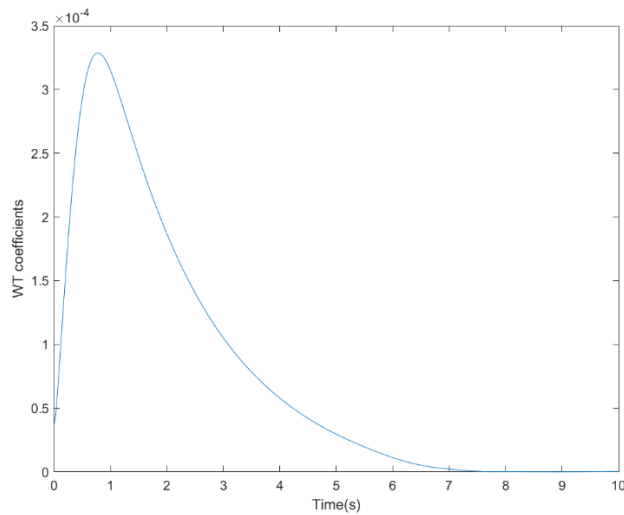


Figure 6-4 Extracted window parallel to frequency axis at the wavelet ridge [2]

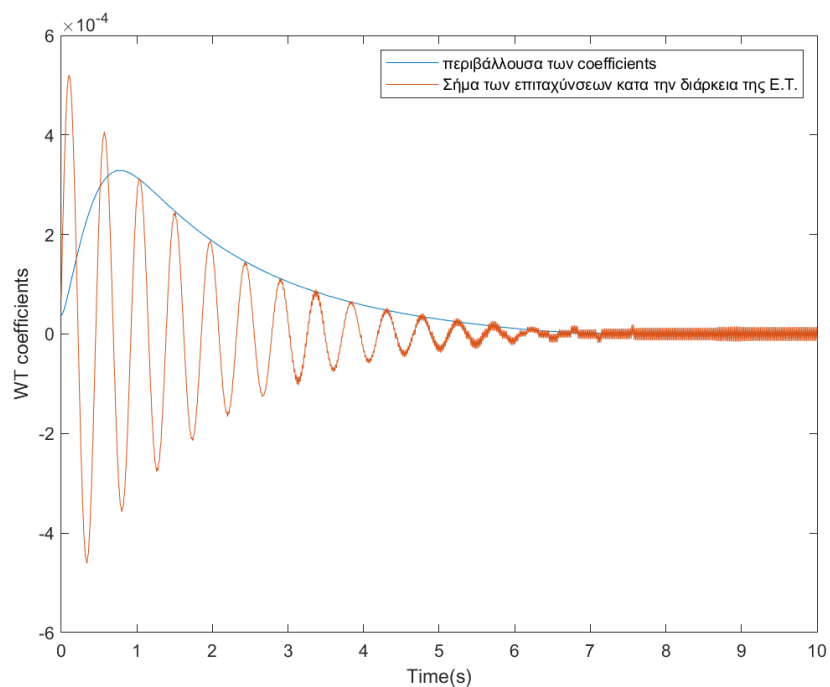


Figure 6-5: Comparison of free decay response and the extracted wavelet envelope [2]

After 6 seconds the response is so small that the diagram has no meaning.

From Equation (6-7), damping ratio can be calculated. In this case  $c = 0.0395$ . Error of 1.25%.

## 6.4 10 Story 2D Seismostruct model.

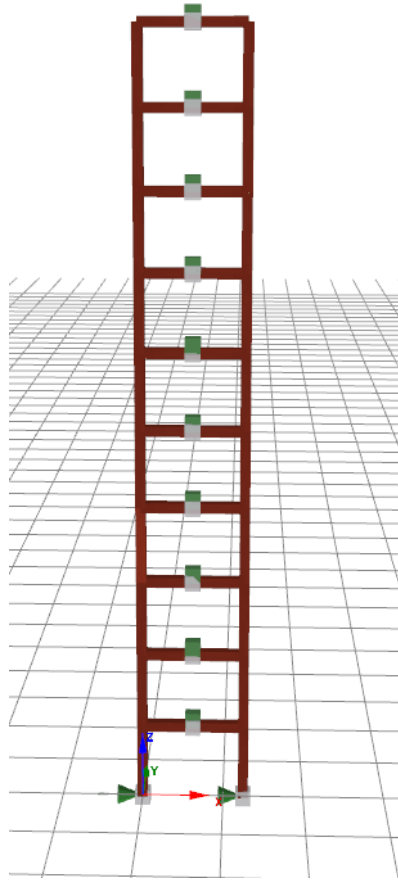


Figure 6-6: Seismostruct model

The present system was modelled as 10 Story 2D steel frame. The height of each story is 3m. Mass of 150MGr was concentrated on the middle of each beam. Columns and beams are 0.4x0.4m. Elastic modulus of each column is  $1.5 * 10^8$ KPa and the yield stress  $\sigma_y$  is 135Mpa. Elastic modulus of the beams is  $2 * 10^{10}$ KPa For this model all elements are always moving linearly. The acting load is Kobe's earthquake with 10 seconds of zero load added in the end so the free decaying response can be extracted without the use of any method. Newmark's method was used to solve the differential equation.

$\lambda$  scaling factor of 0.1 was applied to the excitation.

Through Seismostruct the natural frequencies and the mode shapes are calculated.

Table 6-1: Modal characteristics of the model

Frequencies	$\begin{bmatrix} f_1 \\ f_2 \\ f_3 \\ f_4 \\ f_5 \\ f_6 \\ f_7 \\ f_8 \\ f_9 \\ f_{10} \end{bmatrix} = \begin{bmatrix} 0,761 \\ 2,52 \\ 4,76 \\ 6,67 \\ 8,33 \\ 10 \\ 11,11 \\ 12,5 \\ 13,16 \\ 14,29 \end{bmatrix} \text{ Hz}$				
Damping Ratios	$\begin{bmatrix} \xi_1 \\ \xi_2 \\ \xi_3 \\ \xi_4 \\ \xi_5 \\ \xi_6 \\ \xi_7 \\ \xi_8 \\ \xi_9 \\ \xi_{10} \end{bmatrix} = \begin{bmatrix} 4\% \\ 6\% \\ - \\ - \\ - \\ - \\ - \\ - \\ - \\ - \end{bmatrix}$				
Modal Shapes	$\varphi_1 = \begin{bmatrix} 1 \\ 0,92 \\ 0,82 \\ 0,71 \\ 0,6 \\ 0,49 \\ 0,38 \\ 0,27 \\ 0,17 \\ 0,07 \end{bmatrix}, \varphi_2 = \begin{bmatrix} -0,98 \\ -0,64 \\ -0,21 \\ 0,22 \\ 0,61 \\ 0,88 \\ 1 \\ 0,95 \\ 0,73 \\ 0,4 \end{bmatrix}, \varphi_3 = \begin{bmatrix} 0,88 \\ 0,3 \\ -0,4 \\ -0,88 \\ -0,88 \\ -0,42 \\ 0,28 \\ 0,85 \\ 1 \\ 0,65 \end{bmatrix}, \varphi_4 = \begin{bmatrix} 0,88 \\ -0,13 \\ -0,98 \\ -0,86 \\ 0,12 \\ 1 \\ 0,91 \\ -0,05 \\ -0,96 \\ -0,93 \end{bmatrix}, \varphi_5 = \begin{bmatrix} 0,73 \\ -0,51 \\ -0,94 \\ 0,09 \\ 1 \\ 0,39 \\ -0,81 \\ -0,75 \\ 0,47 \\ 0,98 \end{bmatrix}$ $\begin{bmatrix} 10 \\ 9 \\ 8 \\ 7 \\ 6 \\ 5 \\ 4 \\ 3 \\ 2 \\ 1 \end{bmatrix}, \varphi_6 = \begin{bmatrix} -0,62 \\ 0,81 \\ 0,5 \\ -0,9 \\ -0,39 \\ 0,93 \\ 0,26 \\ -0,98 \\ -0,14 \\ 1 \end{bmatrix}, \varphi_7 = \begin{bmatrix} 0,52 \\ -0,98 \\ 0,20 \\ 0,85 \\ -0,80 \\ -0,27 \\ 1 \\ -0,44 \\ -0,67 \\ 0,95 \end{bmatrix}, \varphi_8 = \begin{bmatrix} 0,40 \\ -0,98 \\ 0,82 \\ -0,02 \\ -0,79 \\ 0,99 \\ -0,44 \\ -0,45 \\ 1 \\ -0,8 \end{bmatrix}, \varphi_9 = \begin{bmatrix} 0,27 \\ -0,77 \\ 1 \\ -0,87 \\ 0,44 \\ 0,15 \\ -0,69 \\ 0,98 \\ -0,92 \\ 0,56 \end{bmatrix}, \varphi_{10} = \begin{bmatrix} -0,14 \\ 0,43 \\ -0,68 \\ 0,87 \\ -0,98 \\ 1 \\ -0,92 \\ 0,78 \\ -0,55 \\ 0,28 \end{bmatrix}$				

CWT is applied on last 10 seconds of the accelerations signal for each floor calculated through Seismostruct. This signal matches the 10 seconds time period of zero load added to the excitation. Morlet mother wavelet was used through MATLAB's wavelet toolbox.

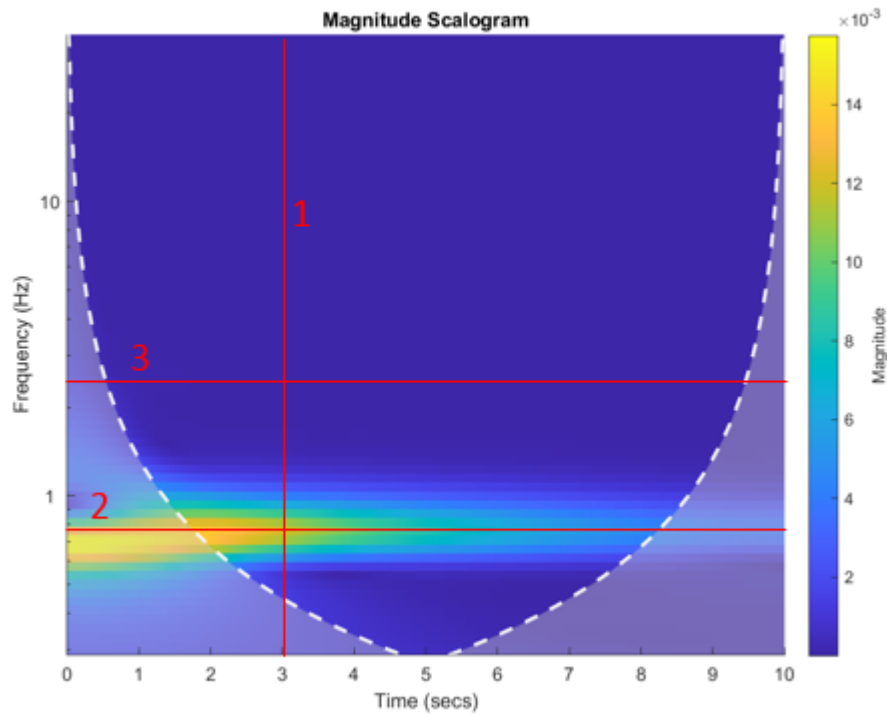


Figure 6-7: Magnitude Scalogram of the free decay accelerations signal – 10<sup>th</sup> story.

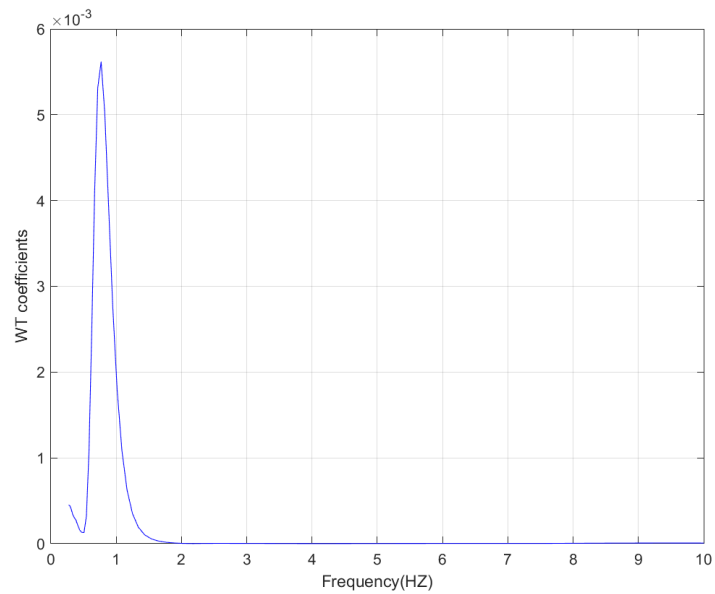


Figure 6-8: Extracted window parallel to frequency axis. [1]

The highest number of coefficients is at frequency  $f_1 = 0.759\text{Hz} \rightarrow T_1 = 1.317\text{s}$ , error of 0.25%

To calculate the damping ratio, after  $f_1$  is calculated the parallel to frequency axis at the wavelet ridge is extracted.

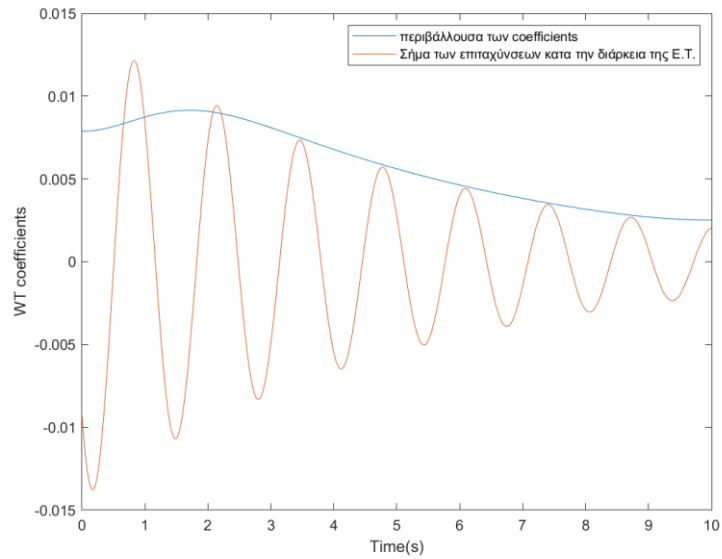


Figure 6-9: Comparison of free decay response and the extracted wavelet envelope. [2]

Damping ratio is calculated 3,96%

For  $T_2$  because excitation is weak, the response is fading too fast for CWT to see. For this reason, CWT is applied to the signal between 70 and 80 seconds. Following the same procedure  $f_2 = 2.46\text{Hz} \rightarrow T_2 = 0.4\text{s}$

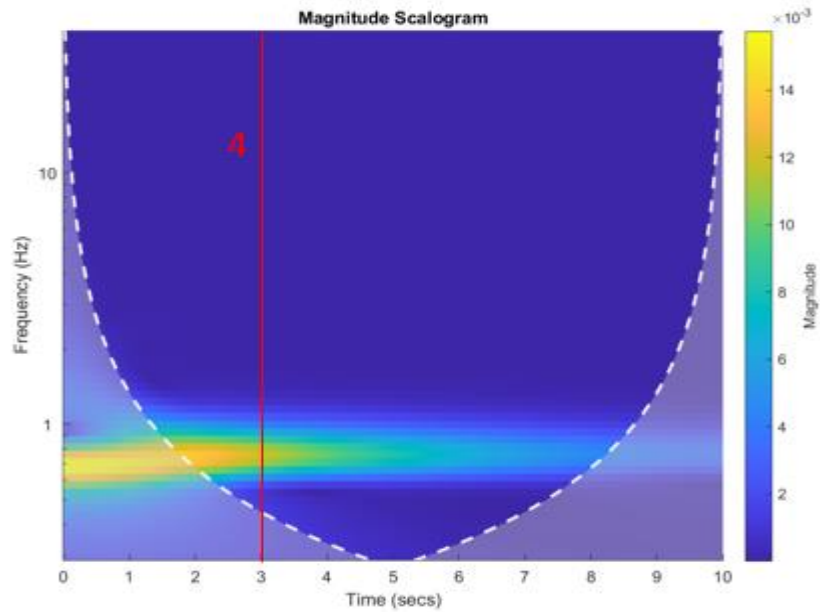


Figure 6-10: Magnitude Scalogram – Accelerations signal 10<sup>th</sup> floor.

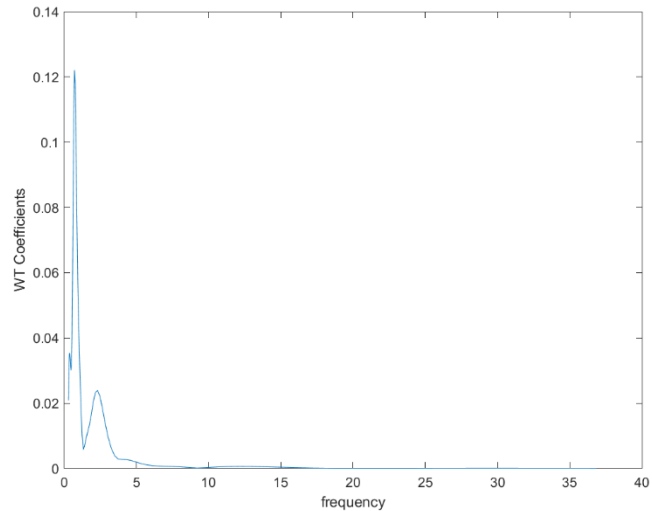


Figure 6-11: Extracted window parallel to frequency axis. [4]

To calculate the damping ratio, after  $f_2$  is calculated the parallel to frequency axis at the wavelet ridge is extracted from the CWT transform of the **free decaying signal (80-90 seconds)**.

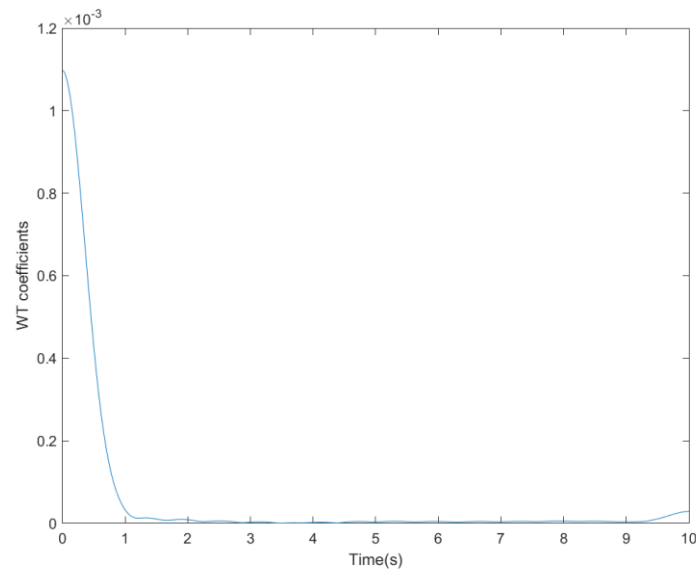


Figure 6-12: Extracted wavelet envelope parallel to the frequency at the wavelet ridge. [3]

Damping ratio is calculated 6.21%. 3.4% error

This procedure is applied to every signal acquired for every floor. Through the analogy of the coefficients on a fixed time moment, mode shapes are calculated.



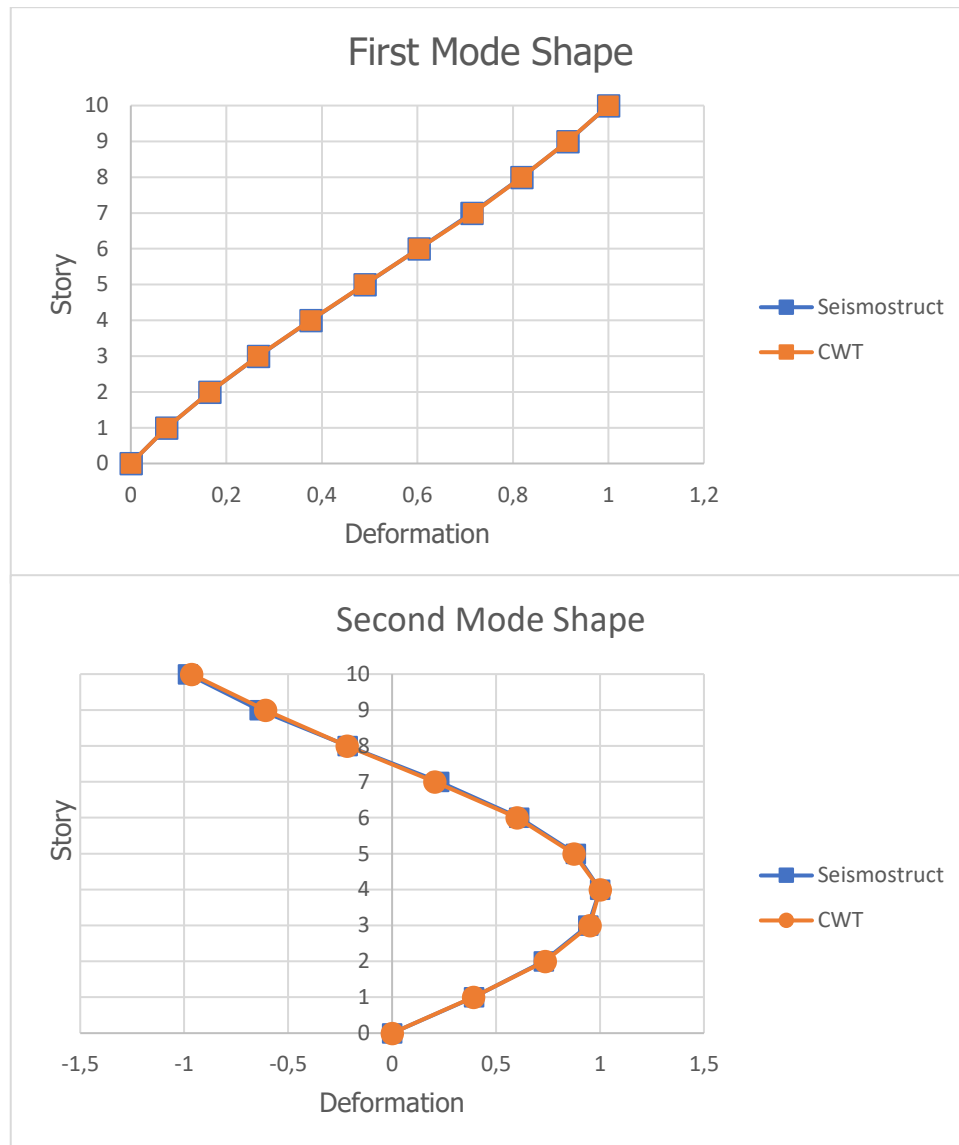


Figure 6-13: Figure: First 2 mode shapes as calculated by Seismostruct (blue) and CWT (orange).

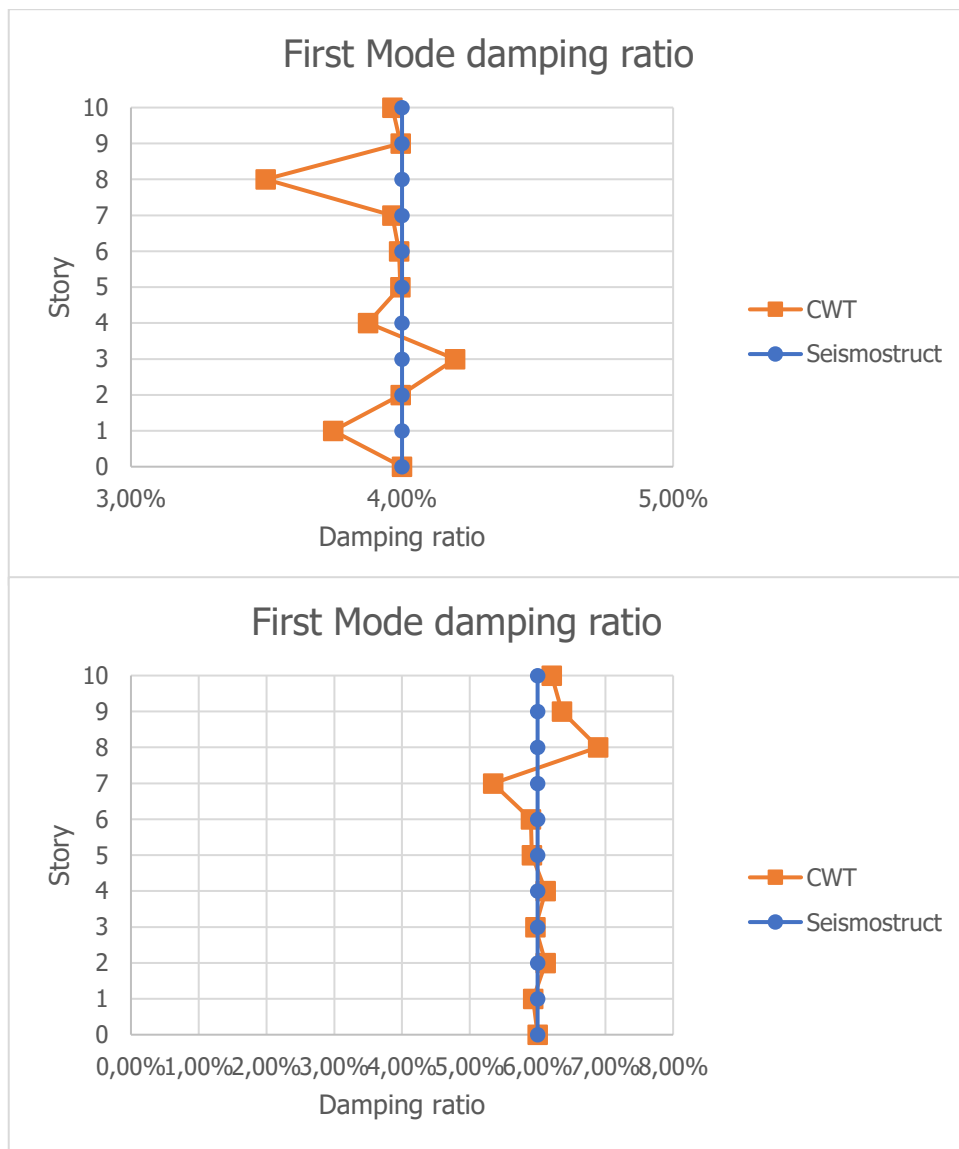


Figure 6-14: Figure: First 2 mode damping ratio as calculated by Seismostruct (blue) and CWT (orange).

## 6.5 6 Story 3D Seismostruct model.

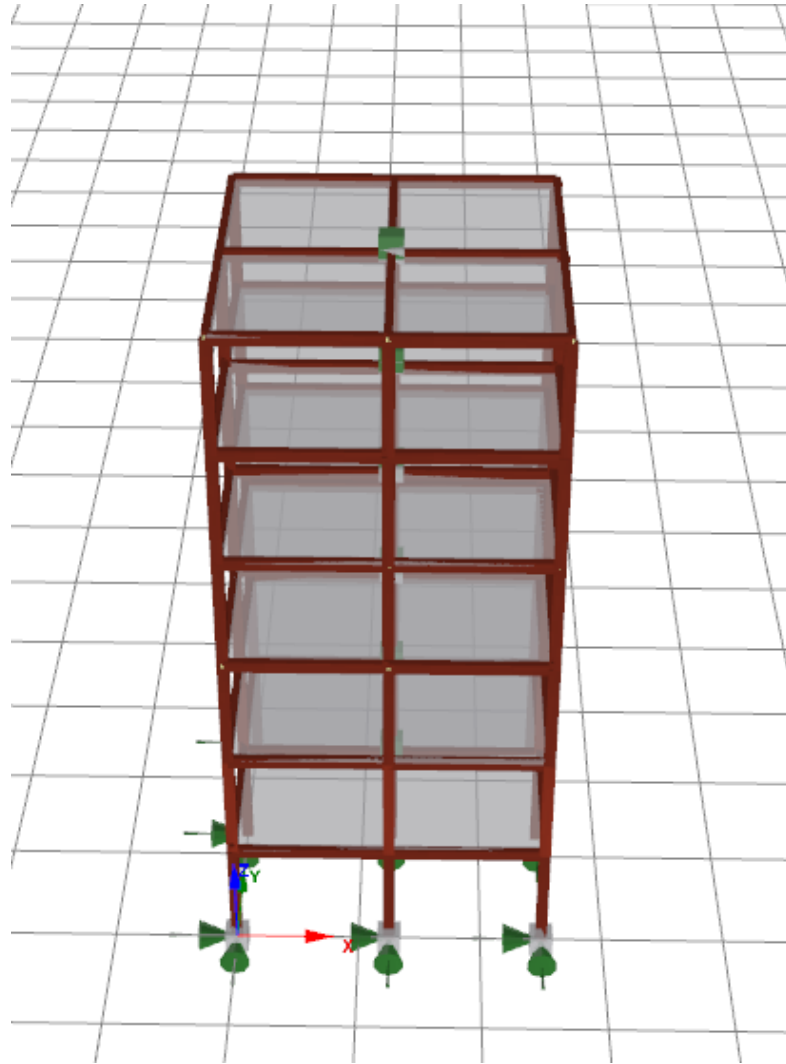


Figure 6-15: Seismostruct model

The present system was modelled as 10 Story 2D steel frame. The height of each story is 3m. Mass of 350MGr was concentrated on the middle of each beam. Moment of inertia  $3750\text{MGr}\cdot\text{m}^2$ . Columns and beams are  $0.2\times 0.3\text{m}$ . Elastic modulus of every column is  $1.5 * 10^8\text{KPa}$ . Elastic modulus of every beam is  $2 * 10^{10}\text{KPa}$ . For this model all elements are always moving linearly. For X-Y axis the equivalent Kobe Earthquake excitation were used, both were adjusted with the same scaling factor  $\lambda$ .

$\lambda$  scaling factor is equal to 0.10

Through SeismoStruct the natural frequencies and the mode shapes are calculated. Only the first 5 Mode shapes are listed.

Table 6-2: Structure Characteristics as calculated on SeismoStruct

<i>Frequencies</i>	$\begin{bmatrix} f_1 \\ f_2 \\ f_3 \\ f_4 \\ f_5 \\ f_6 \\ f_7 \\ f_8 \\ f_9 \\ f_{10} \end{bmatrix} = \begin{bmatrix} 0.7 \\ 1.02 \\ 1.28 \\ 2.06 \\ 3.03 \\ 3.33 \\ 3.70 \\ 4.34 \\ 5 \\ 5.26 \end{bmatrix} \text{ Hz} \quad \begin{bmatrix} f_{11} \\ f_{12} \\ f_{13} \\ f_{14} \\ f_{15} \\ f_{16} \\ f_{17} \\ f_{18} \end{bmatrix} = \begin{bmatrix} 5.7 \\ 6.06 \\ 6.57 \\ 7.8 \\ 8 \\ 8.62 \\ 9.43 \\ 10.4 \end{bmatrix} \text{ Hz}$
<i>Damping Ratios</i>	$\begin{bmatrix} \xi_1 \\ \xi_2 \\ \xi_3 \\ \xi_4 \\ \xi_5 \\ \xi_6 \\ \xi_7 \\ \xi_8 \\ \xi_9 \\ \xi_{10} \end{bmatrix} = \begin{bmatrix} 4\% \\ 6\% \\ - \\ - \\ - \\ - \\ - \\ - \\ - \\ - \end{bmatrix}$
<i>Modal Shapes</i>  <i>Story</i> $\begin{bmatrix} 6 \\ 5 \\ 4 \\ 3 \\ 2 \\ 1 \end{bmatrix}$	$\varphi_1 = \begin{bmatrix} 0 \\ 0 \\ 0 \\ 0 \\ 0 \\ 0 \end{bmatrix} [X], \begin{bmatrix} 1 \\ 0.94 \\ 0.82 \\ 0.66 \\ 0.46 \\ 0.23 \end{bmatrix} [Y], \begin{bmatrix} 0 \\ 0 \\ 0 \\ 0 \\ 0 \\ 0 \end{bmatrix} [Rz] \quad \varphi_2 = \begin{bmatrix} 1 \\ 0.93 \\ 0.80 \\ 0.64 \\ 0.44 \\ 0.22 \end{bmatrix} [X], \begin{bmatrix} 0 \\ 0 \\ 0 \\ 0 \\ 0 \\ 0 \end{bmatrix} [Y], \begin{bmatrix} 0 \\ 0 \\ 0 \\ 0 \\ 0 \\ 0 \end{bmatrix} [Rz]$ $\varphi_3 = \begin{bmatrix} 0 \\ 0 \\ 0 \\ 0 \\ 0 \\ 0 \end{bmatrix} [X], \begin{bmatrix} 0 \\ 0 \\ 0 \\ 0 \\ 0 \\ 0 \end{bmatrix} [Y], \begin{bmatrix} 1 \\ 0.94 \\ 0.83 \\ 0.67 \\ 0.47 \\ 0.24 \end{bmatrix} [Rz] \quad \varphi_4 = \begin{bmatrix} 0 \\ 0 \\ 0 \\ 0 \\ 0 \\ 0 \end{bmatrix} [X], \begin{bmatrix} -0.94 \\ -0.45 \\ 0.26 \\ 0.84 \\ 1 \\ 0.66 \end{bmatrix} [Y], \begin{bmatrix} 0 \\ 0 \\ 0 \\ 0 \\ 0 \\ 0 \end{bmatrix} [Rz]$ $\varphi_5 = \begin{bmatrix} -0.94 \\ -0.44 \\ 0.27 \\ 0.85 \\ 1 \\ 0.66 \end{bmatrix} [X], \begin{bmatrix} 0 \\ 0 \\ 0 \\ 0 \\ 0 \\ 0 \end{bmatrix} [Y], \begin{bmatrix} 0 \\ 0 \\ 0 \\ 0 \\ 0 \\ 0 \end{bmatrix} [Rz]$

First on X axis, CWT transform is applied on the free decay accelerations signal of every story. The same procedure is applied.  $f_2, f_5$  and  $\xi_2$  are calculated.  $f_2 = 1.019\text{Hz} \rightarrow T_2 = 0.98\text{s}$   $f_5 = 3.037\text{Hz} \rightarrow T_5 = 0.329\text{s}$   $\xi_2 = 6,09\%$ . Error of 0.41% ,0.3% and 1.48% respectively. This is calculated for every floor to calculate the mode shapes.

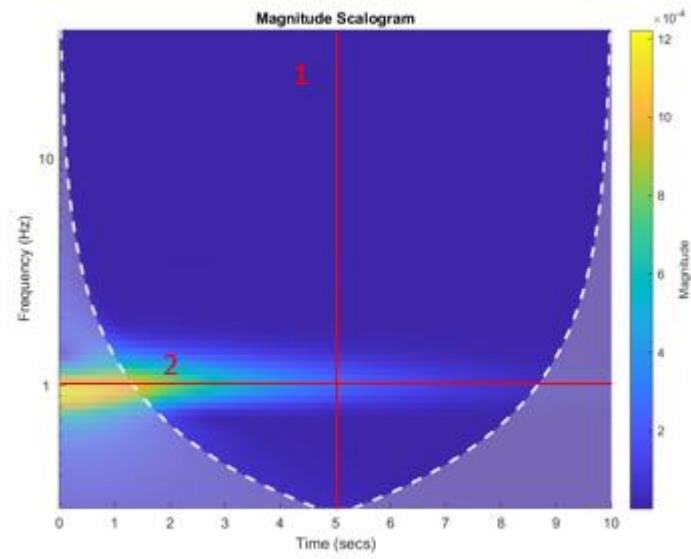


Figure 6-16: Magnitude Scalogram – Accelerations signal 6<sup>th</sup> floor.

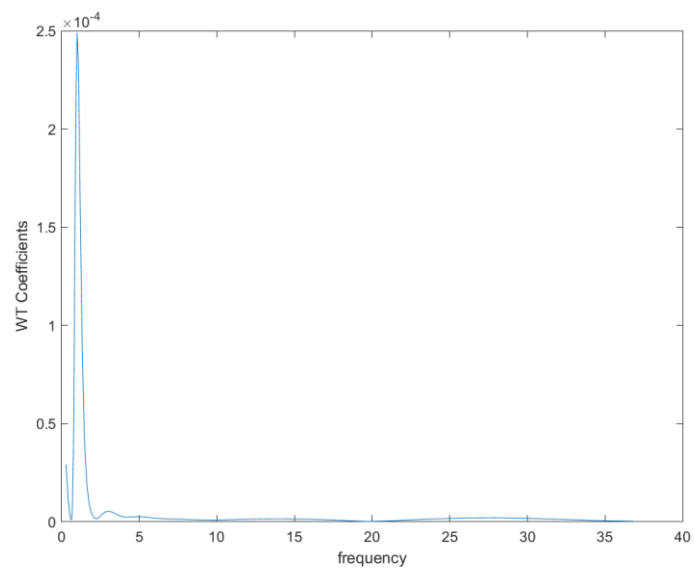


Figure 6-17: Extracted window parallel to frequency axis. [1]

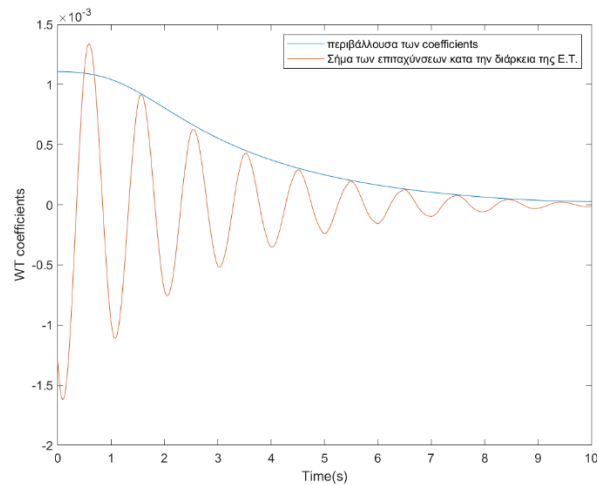


Figure 6-18: Comparison of free decay response and the extracted wavelet envelope. [2]

On Y Axis following again the same procedure  $f_1$ ,  $f_4$  and  $\xi_1$  are calculated. Because  $f_4$  is not visible from the CWT transform of the last 10 seconds, CWT transform is also applied to seconds 70 to 80. From this 2,  $f_1 = 0.708\text{Hz} \rightarrow T_1 = 1.41\text{s}$   $f_4 = 1.896\text{Hz} \rightarrow T_4 = 0.52\text{s}$   $\xi_1 = 3.9\%$ . Error of 1.6% ,6.5% and 2.5% respectively.

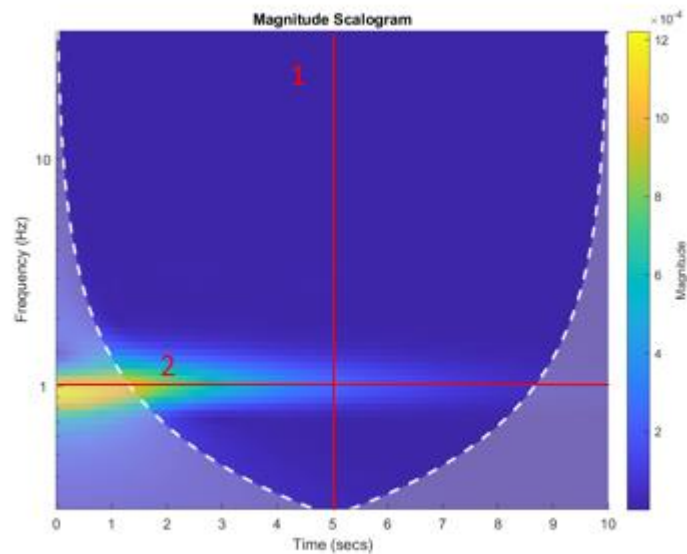


Figure 6-19: Magnitude Scalogram – Accelerations signal 6<sup>th</sup> floor – 80 to 90s

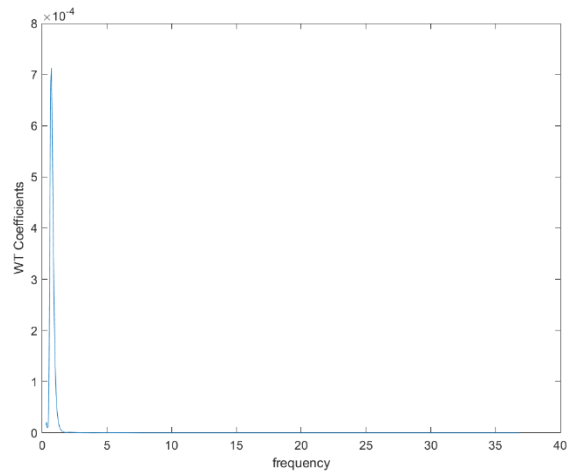


Figure 6-20: Extracted window parallel to frequency axis. [1]

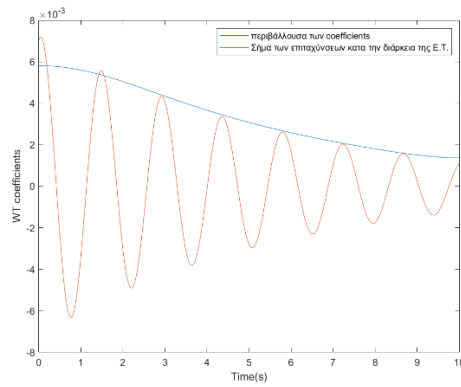
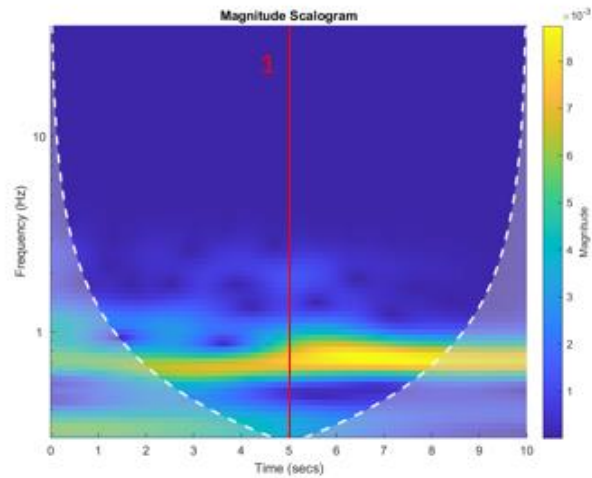


Figure 6-21: Comparison of free decay response and the extracted wavelet envelope. [2]

Figure 6-22: Magnitude Scalogram – Accelerations signal 6<sup>th</sup> floor – 70 to 80

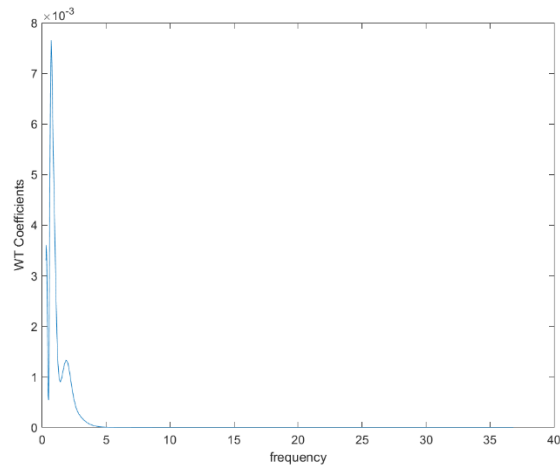


Figure 6-23: Extracted window parallel to frequency axis. [1]

On Rz Axis following again the same procedure  $f_3$ , is calculated.  $f_3 = 1.322\text{Hz} \rightarrow T_1 = 0.756\text{s}$ . Error of 3.3%

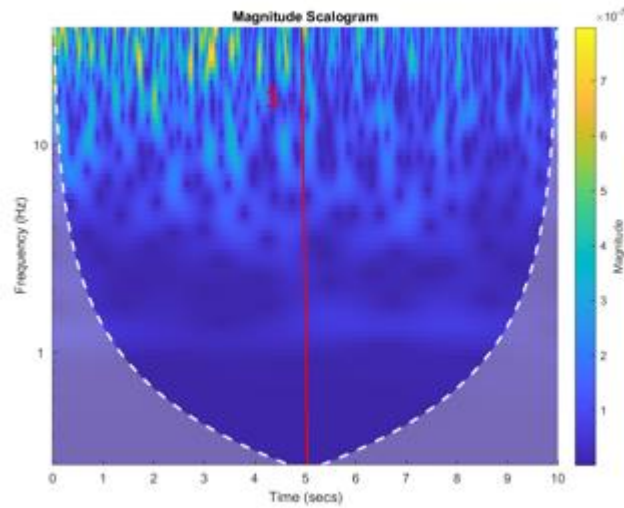


Figure 6-24: Magnitude Scalogram – Accelerations signal 6<sup>th</sup> floor

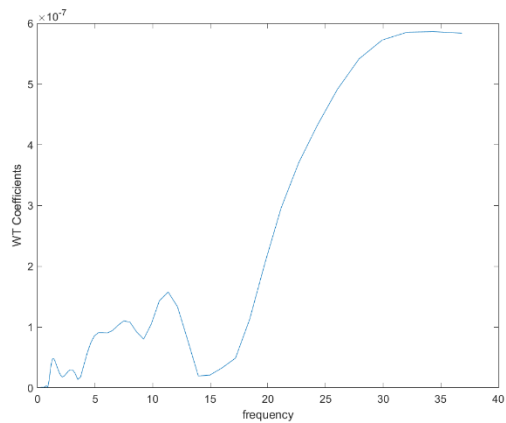
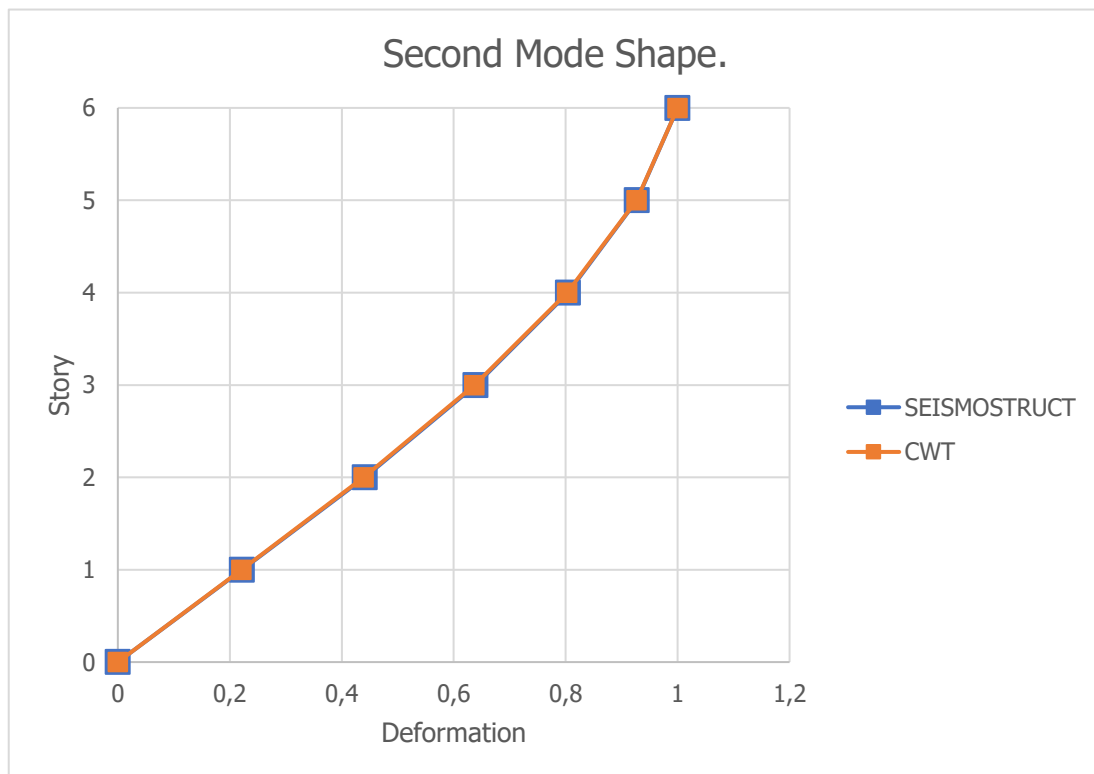
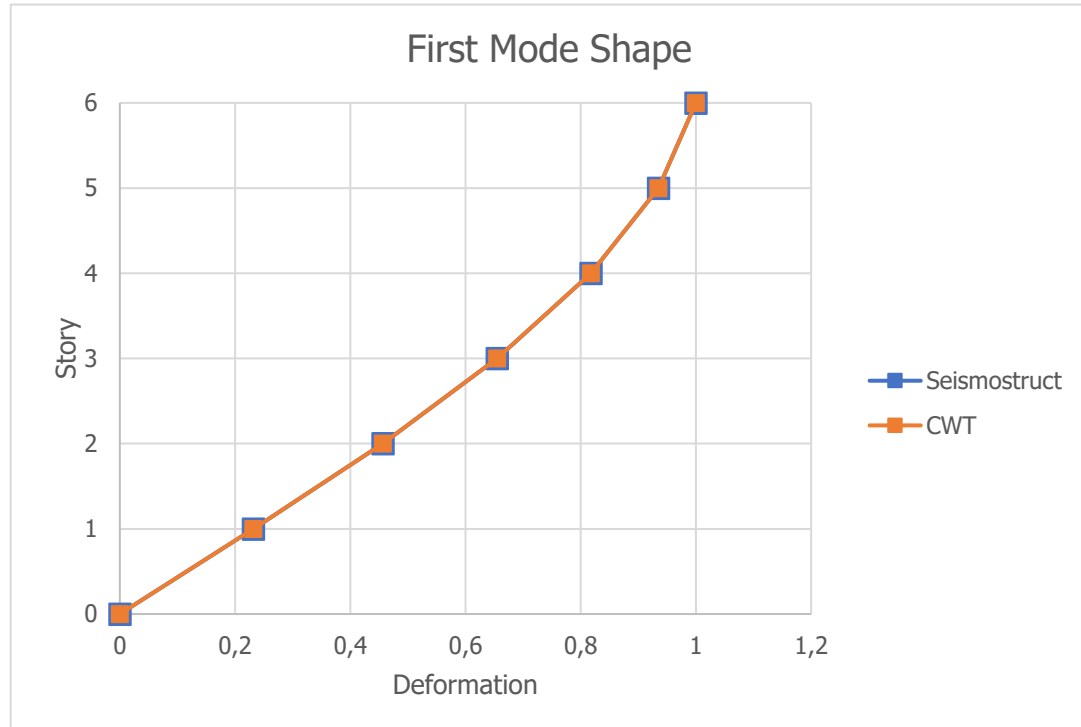
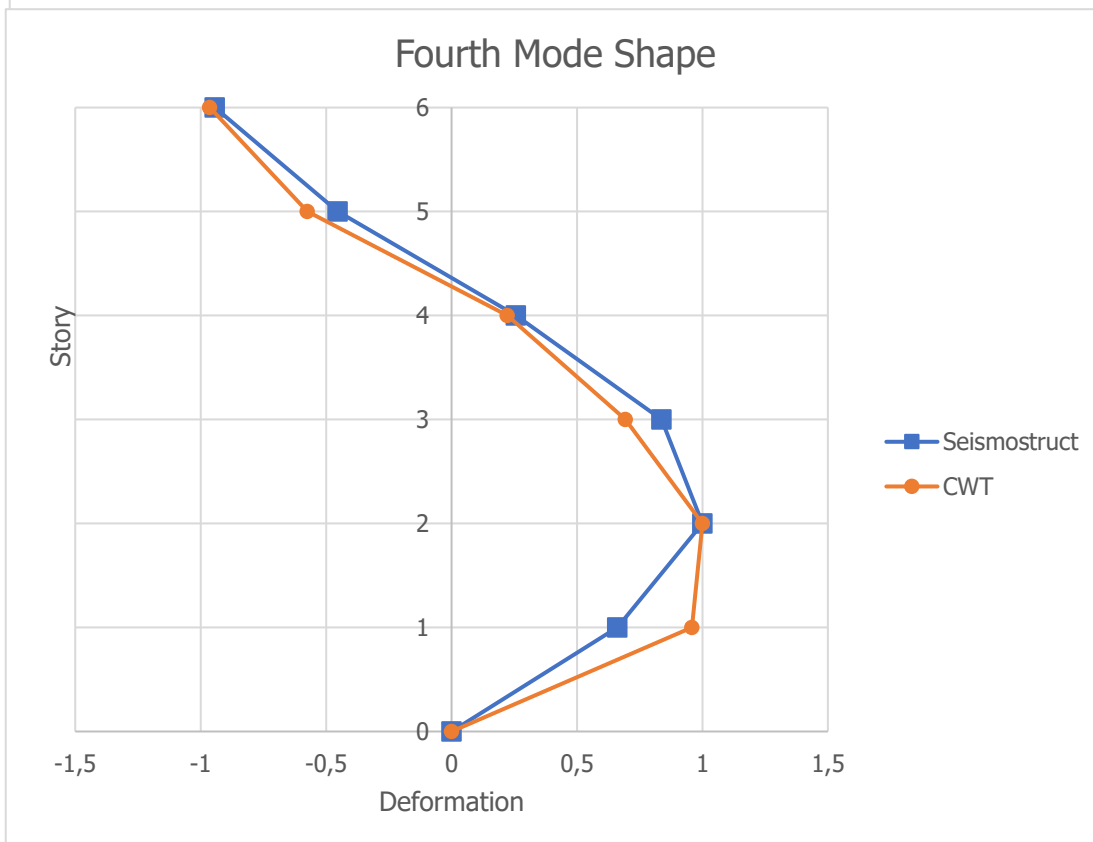
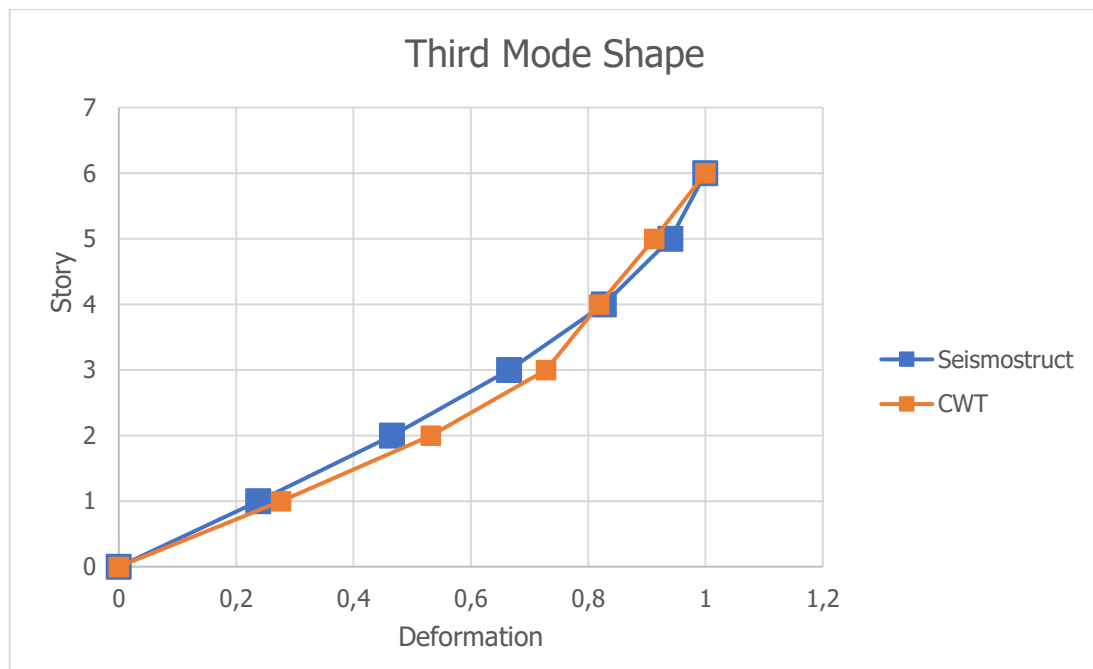


Figure 6-25: Extracted window parallel to frequency axis. [1]



After applying CWT to the acceleration signals from every floor, mode shapes are calculated.





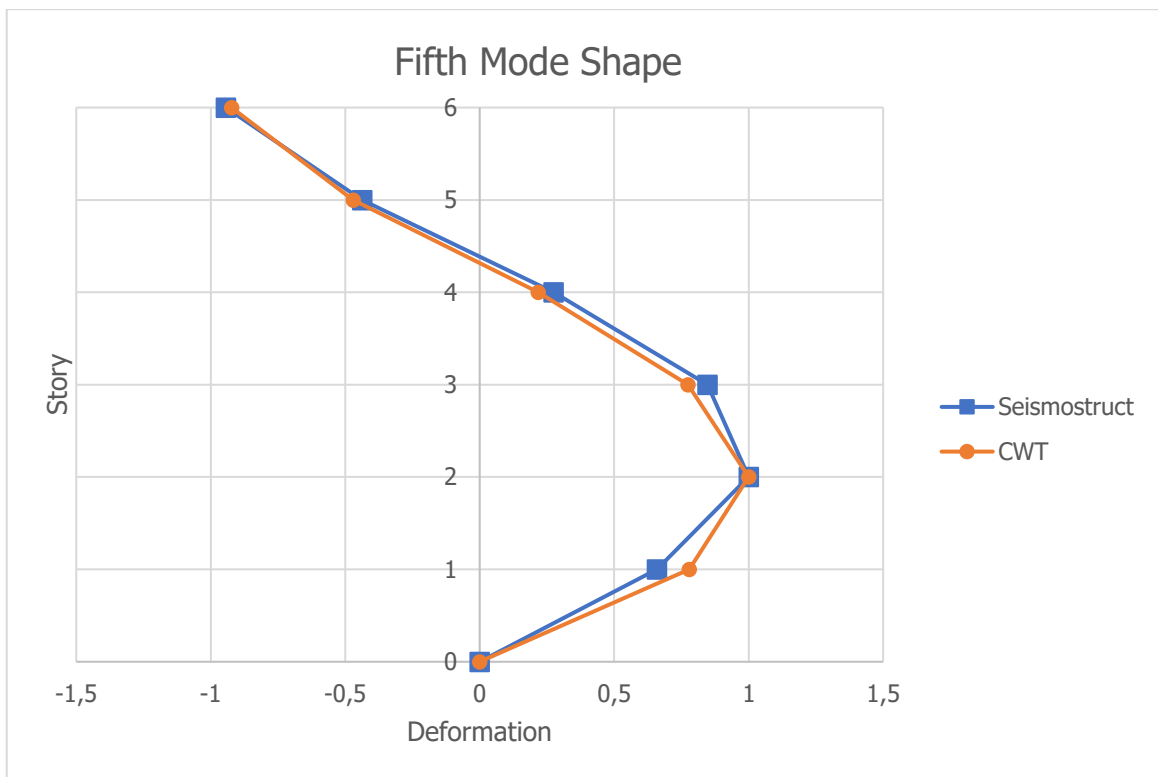


Figure 6-26: Figure: First 5 mode shapes as calculated by Seismostruct (blue) and CWT (orange).

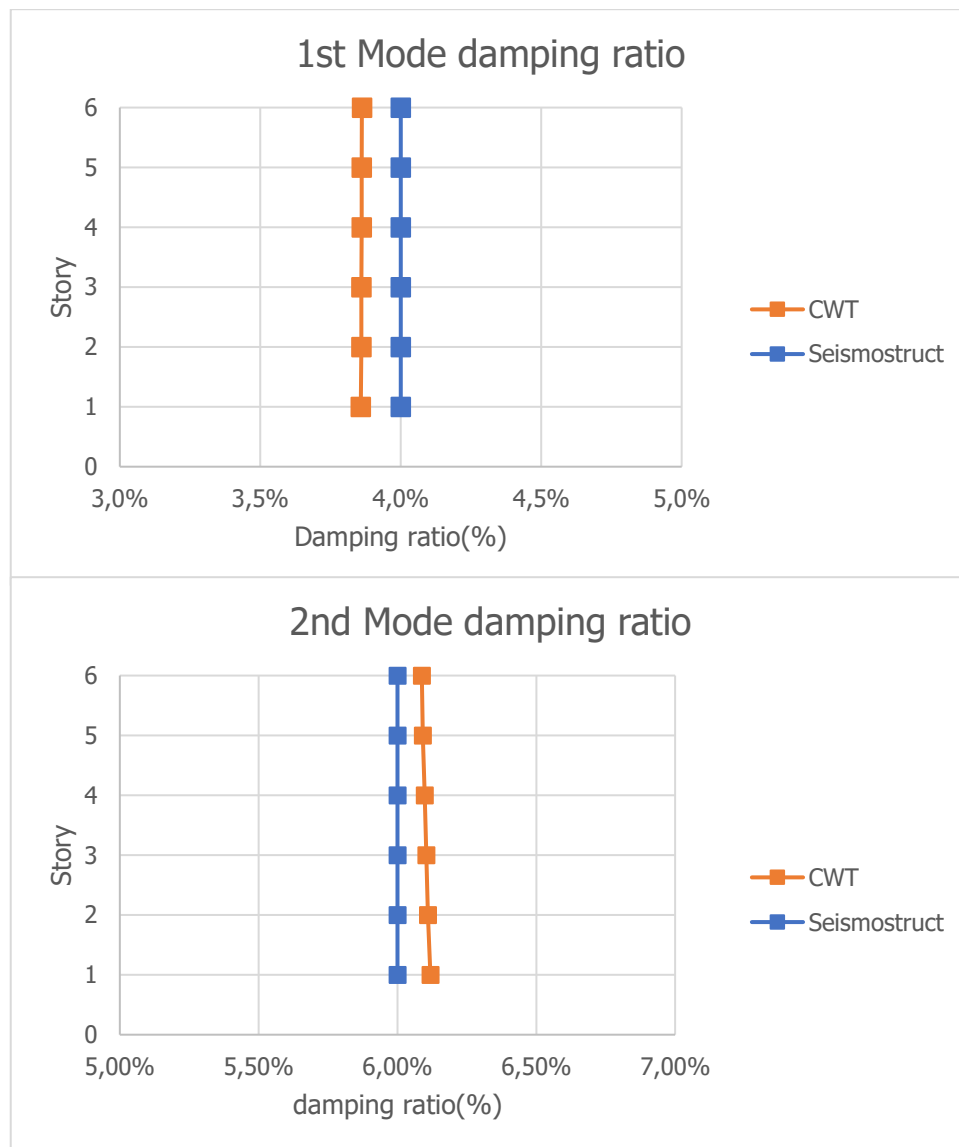


Figure 6-27: First 2 mode damping ratio as calculated by Seismostruct (blue) and CWT (orange).

## 6.6 Modal Assurance Distribution (MAD)

As seen from the previous applications, the values of the wavelet components related to a given time instant and a given frequency subband of each recording channel can be interpreted as the elements of a structural mode near the resonance peak of the frequency response spectrum. This means that near the natural frequencies of the building the analogy between the values of the wavelet components are very similar. This provides another way to monitor a building. By forming a matrix that compares that analogy for every given time and comparing it to neighbouring subbands it is possible to follow the frequencies that a building is oscillating. Through Equation (6-8) mode shapes can be calculated and after  $m_k[t]$  matrix can be calculated

$$m_k[t] = \frac{|\varphi_k^T[t]\varphi_{k+1}[t]|^2}{(\varphi_k^T[t]\varphi_k[t])(\varphi_{k+1}^T[t]\varphi_{k+1}[t])} \quad (6-10)$$

where  $\varphi_k[t]$  is the mode shape for the kth subband. This matrix will be filled with values from 0 to 1, subbands where persistent high values will appear in the time-frequency areas where modal responses are present.

There are though problems arising because random similarities between noise-frequencies will give rise to beta-distributed noise so without proper signal processing this matrix is very hard to apply. Table  $m_k$  was calculated for the previous studied 10story 2d frame. As it can be seen from the graph, for  $f = 0.759Hz$  there is consistent values close to 1, with only few time moments out of 1000 that are a slightly lower than 1. For  $f_2 = 2.5Hz$  there is bigger fluctuations but  $m_k$  values are again steadily near 1.

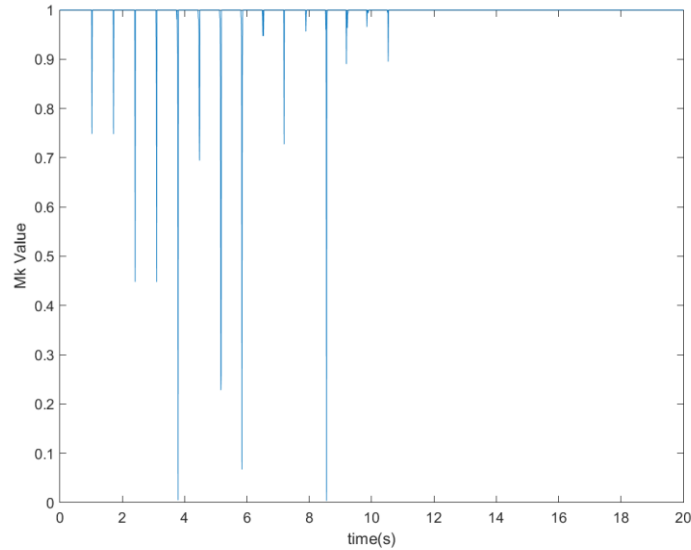


Figure 6-28: Mk Values for F1=0.759Hz

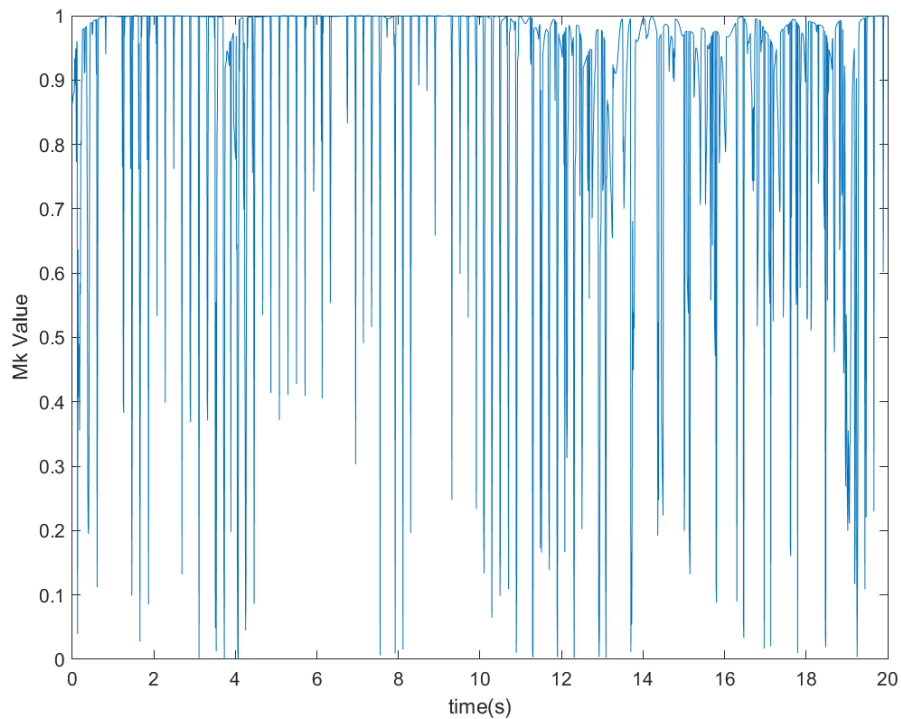


Figure 6-29: Mk Values for F2=2.5Hz

## 6.7 Europroteas

EuroProteas is a real-scale simplified model structure built in Euroseistest site in the framework of the European project "Seismic Engineering Research Infrastructures for European Synergies, Series". It is a project conducted by Dimitris Pitilakis et al, aiming to identify the soil-foundation system interaction. The structure consists of a steel frame on a reinforced concrete (RC) of 0.40m thickness. Two similar RC slabs of 9Mg are placed on top of the frame. It is instrumented with more than 80 instruments (accelerometers, seismometers, MEM sensors). The whole model is customizable with possibility to change stiffness, damping ratio and the type of the excitation (Forced-vibration, free-vibration and ambient noise). Resonant frequency is varying between 2.9Hz and 11.8Hz depending on the configuration. The thesis results are based on a total of 277sec recordings on 6 accelerometers with a sampling rate of 0.005sec.

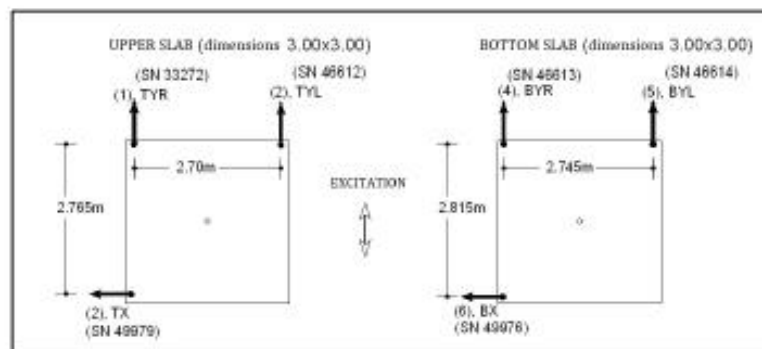


Figure 6-30: The structure and the 6 accelerometers layout used in this example.

The structure's modal characteristics were identified by the MACEC software using 2 other methods of modal analysis (SSI\_COV and FDD)

Table 6-3: Europroteas modal characteristics

	<i>Peak picking</i>		<i>FDD</i>		<i>SSI</i>	
<i>Mode</i>	<i>Frequency (Hz)</i>	<i>Shape</i>	<i>Frequency (Hz)</i>	<i>Shape</i>	<i>Frequency (Hz)</i>	<i>Shape</i>
1	4.102	Transverse	4.102	Transverse	4.107	Transverse
2	4.199	Transverse	4.297	Transverse	4.286	Transverse
3	9.668	Torsional	9.668	Torsional	9.603	Torsional
4	21.191	Coupled	21.191	Coupled	21.131	Coupled
5	22.363	Coupled	22.363	Coupled	22.419	Coupled

CWT Transform using MATLAB's toolbox is applied to the accelerations signal for each sensor. Free decay response is not available so the CWT is applied to the response during the excitation of the structure with an ambient vibration. For this reason, damping ratio cannot be calculated as well.

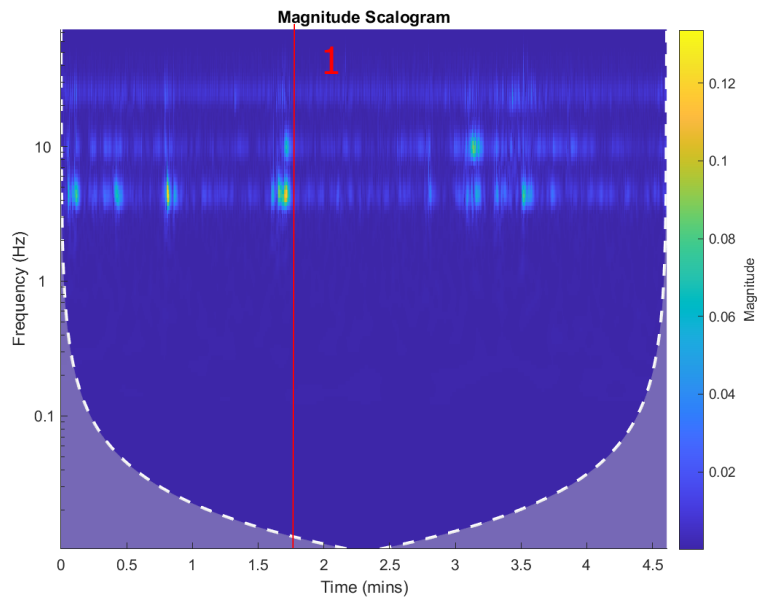


Figure 6-31: Magnitude Scalogram – Sensor 1

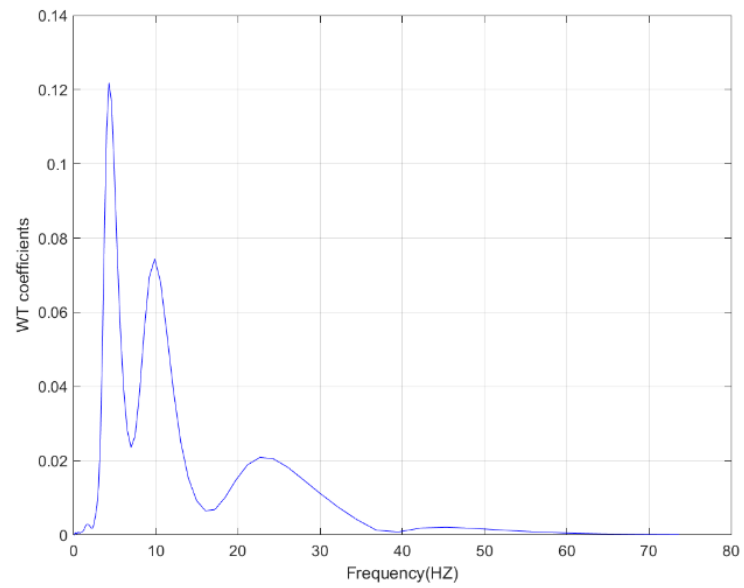


Figure 6-32: Window Parallel to the frequency axis for  $t=1.7$ minutes – Sensor 1 [1]

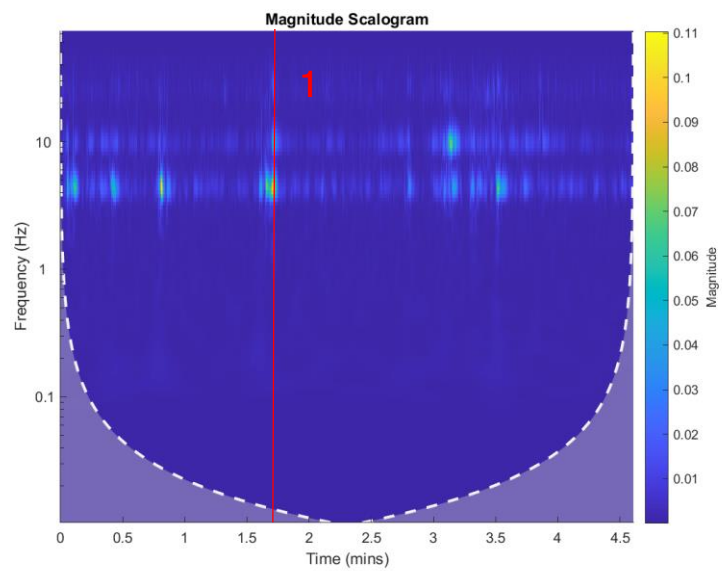


Figure 6-33: Magnitude Scalogram – Sensor 2



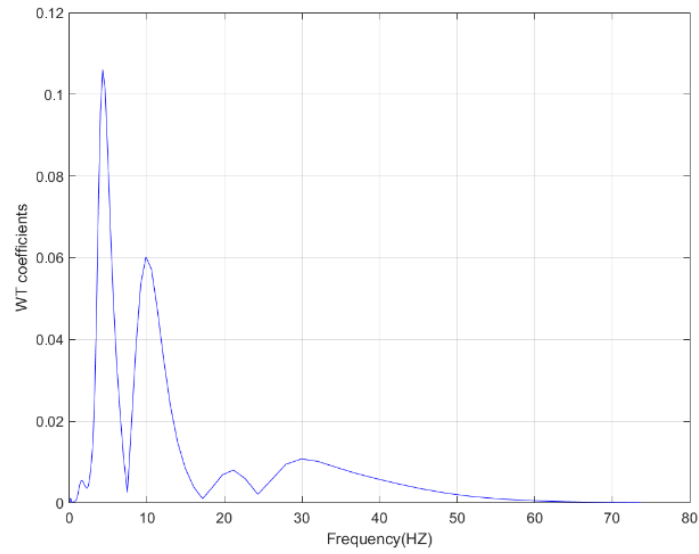


Figure 6-34: Window Parallel to the frequency axis for  $t=1.7$ minutes – Sensor 2 [1]

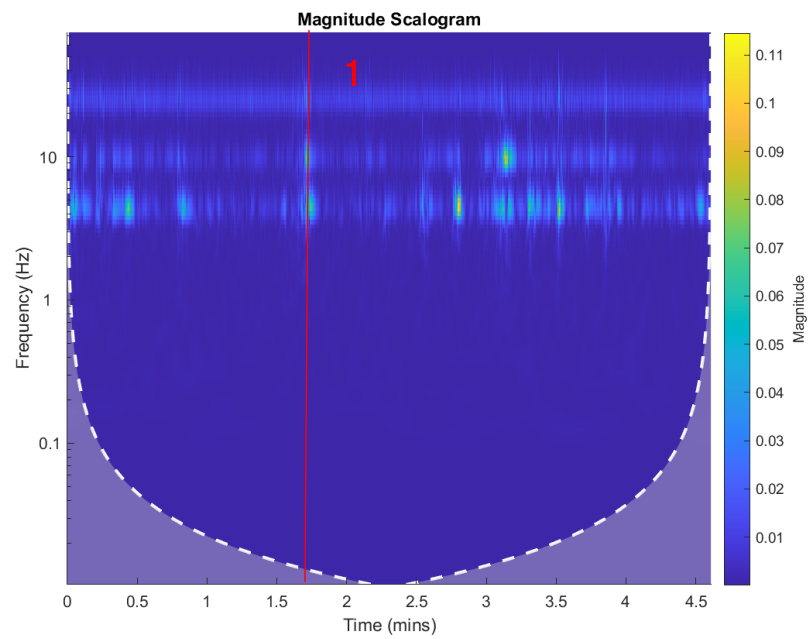


Figure 6-35: Magnitude Scalogram – Sensor 3

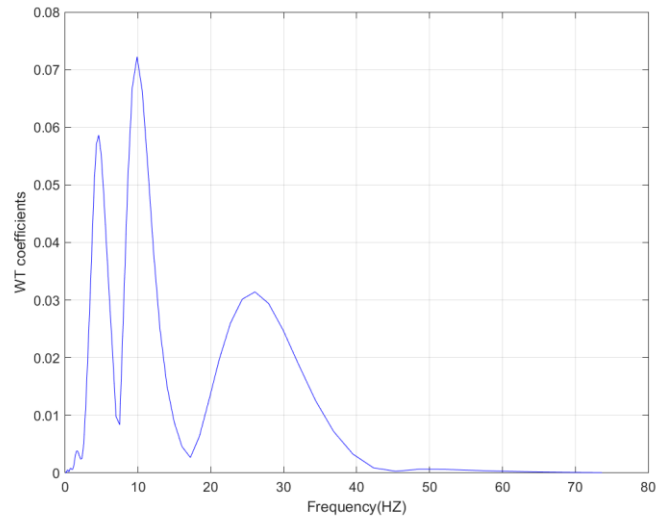


Figure 6-36: Window Parallel to the frequency axis for  $t=1.7$  minutes – Sensor 3 [1]

From the diagrams above modal characteristics are calculated.

Table 6-4: Modal characteristics calculated through MATLAB's CWT – Error compared to FDD Method

<i>Mode Shape</i>	<i>Frequency</i>	<i>Error</i>	<i>Shape</i>
1	4.295	4.5%	Transverse
2	4.603	6.65%	Transverse
3	9.867	2.01%	Torsional
4	21.1522	0.18%	Coupled
5	26.0414	14.12%	Coupled

To calculate the mode shapes the following formulas were used to calculate the deformation at the center of mass of the floor using the recordings from the 3 sensors.

$A_1, A_2$  and  $A_3$  are the values of coefficients calculated through MATLAB's CWT for each of the resonant frequencies.  $d_1, d_2, d_3$  are the distance from the center of mass of each sensor respectively. The response of the center of mass in the  $x, y, rz$  directions are related to  $A_1, A_2$  and  $A_3$  with the following equations in matrix form.

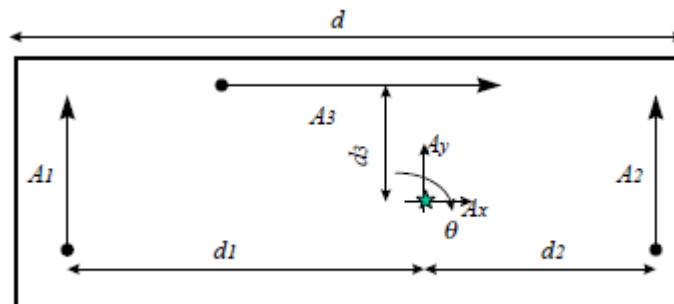


Figure 6-37: Formulas to calculate center of mass displacements [8]

$$\begin{Bmatrix} A_1 \\ A_2 \\ A_3 \end{Bmatrix} = \begin{bmatrix} 0 & 1 & d_1/d \\ 0 & 1 & -d_1/d \\ 1 & 0 & d_3/d \end{bmatrix} \begin{Bmatrix} A_x \\ A_y \\ A_{rz} \end{Bmatrix} \rightarrow \begin{Bmatrix} A_x \\ A_y \\ A_{rz} \end{Bmatrix} = \begin{bmatrix} 0 & 1 & d_1/d \\ 0 & 1 & -d_1/d \\ 1 & 0 & d_3/d \end{bmatrix}^{-1} \begin{Bmatrix} A_1 \\ A_2 \\ A_3 \end{Bmatrix} \quad (6-11)$$

Table 6-5: Mode Shapes of Europroteas as Calculated through MATLAB's CWT

<b>Mode Shapes</b> $\begin{bmatrix} X \\ Y \\ R_z \end{bmatrix}$	$\varphi_1 = \begin{bmatrix} -0,57 \\ 1 \\ 0,15 \end{bmatrix}, \varphi_2 = \begin{bmatrix} -0,61 \\ 1 \\ 0,16 \end{bmatrix}, \varphi_3 = \begin{bmatrix} -0,02 \\ 0,05 \\ 1 \end{bmatrix},$ $\varphi_4 = \begin{bmatrix} 1 \\ 0,94 \\ 0,85 \end{bmatrix}, \varphi_5 = \begin{bmatrix} 0,72 \\ 0,24 \\ 1 \end{bmatrix}$
---------------------------------------------------------------------	---------------------------------------------------------------------------------------------------------------------------------------------------------------------------------------------------------------------------------------------------------------------------------------------------------------------------

First issue appearing is the inability to calculate the damping ratio. For this, Random Decrement method needs to be used to calculate an approximation of the free decay. Second issue is that there is decent amount of error. This is because of couple of reasons. First of all, the excitation is influencing the results. If the analyzed signal is not free decay, which means excitation is zero, the excitation is changing the results, especially if it's a signal with periodic components like most in Earthquake Engineering. Second of all modes 1 and 2, 4 and 5 are very close to each other. To decouple those frequencies some parameters of the CWT analysis need to be changed. Last but not least like mentioned on chapter (3.5) MATLAB's toolbox is calculating an approximation of the CWT to save time and computing power. These issues need to be addressed to be able to reduce the error and acquire better results.

To tackle these issues a more advanced toolbox than MATLABs was used. This tool allows us to change different wavelet properties like  $c_f, c_t$  and  $Q$ . Also it has built in Random Decrement extraction tool that allows us to calculate also the Damping Ratio.  $c_f, c_t$  are both chosen to be equal to 5.

First, FFT transform is applied to the signal for an estimation of  $\omega_j$  for each Mode.

Table 6-6: Choosing Q Value for CWT analysis

$\omega_j$	$d\omega_j$	$c_f \frac{\omega_j}{2d\omega_j} \leq Q \leq L \frac{\omega_j}{2c_t}$	<i>Q Chosen</i>
27,1	27,1	$2.5 \leq Q \leq 270.80$	50
27,33	0,3	$271.875 \leq Q \leq 273.3$	272
60,9	33,6	$4.53271 \leq Q \leq 609,5$	50
143,89	82,9	$4.33 \leq Q \leq 1438.8$	50
157,2	13,3	$29.5 \leq Q \leq 1572.1$	50

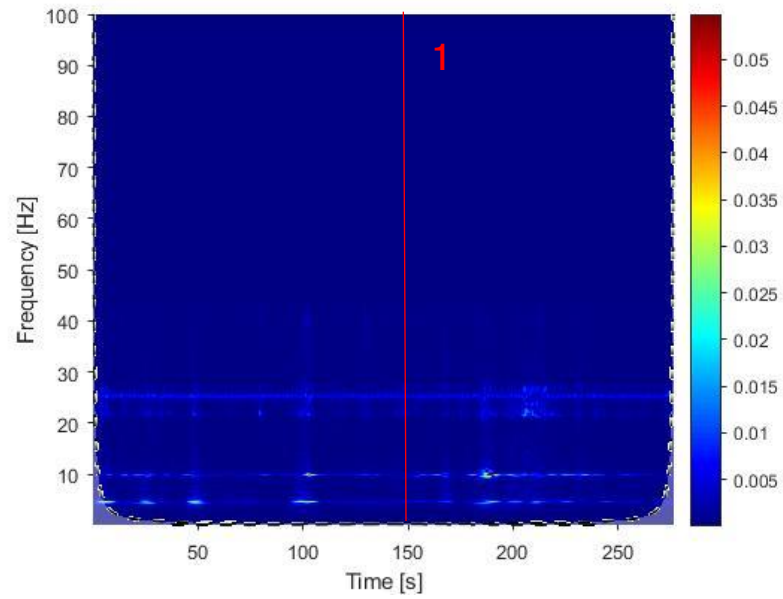


Figure 6-38: Scalogram – Sensor 1 – Q=50

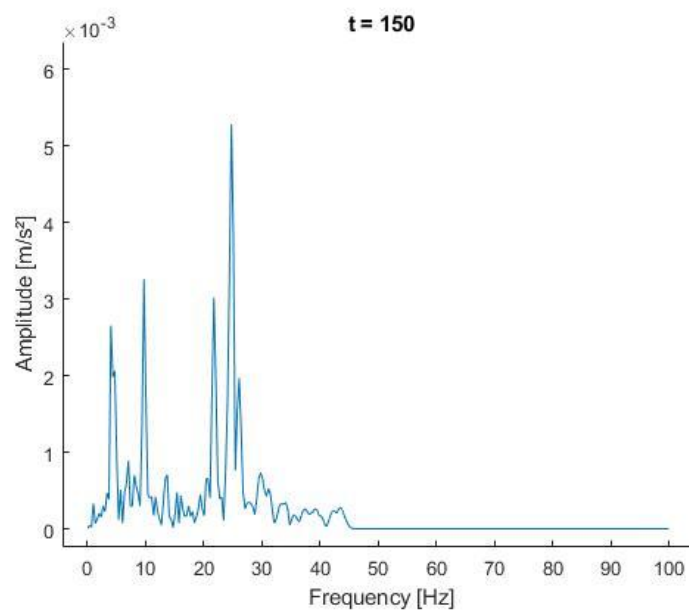


Figure 6-39: Extracted Window Parallel to Frequency Axis [1]

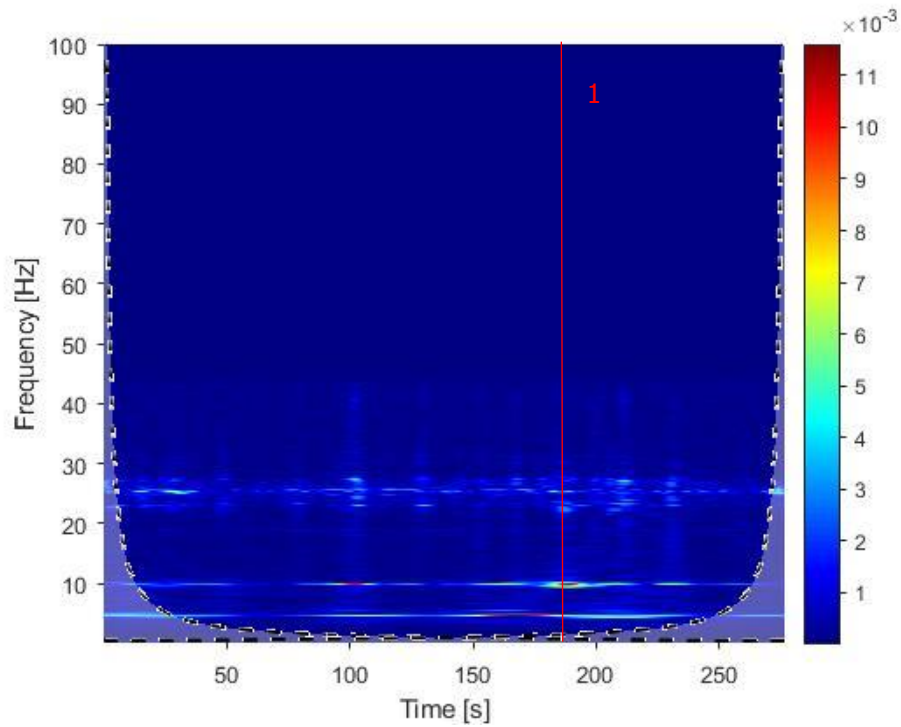
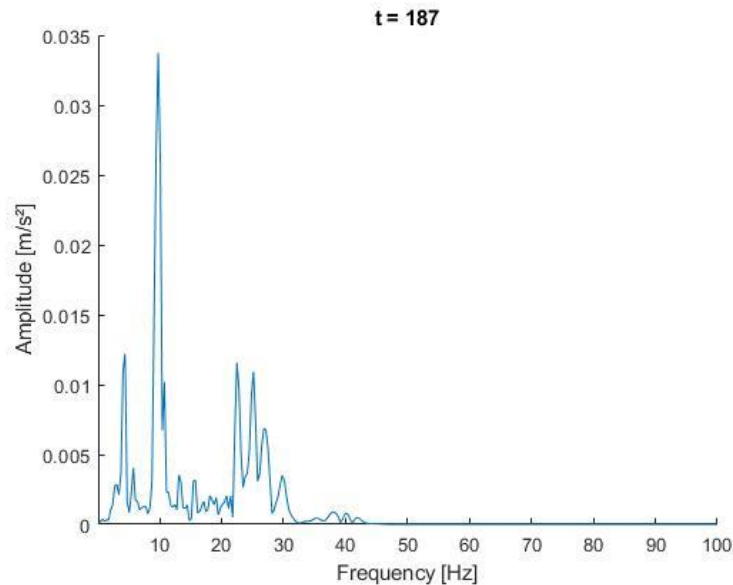
Figure 6-40: Scalogram – Sensor 3 –  $Q=273$ 

Figure 6-41: Extracted Window Parallel to Frequency Axis [1]

After all natural frequencies are calculated through this analysis, RD method is used to extract an approximation for the free decay to be able to estimate the damping ratio. Depending on  $Q$ , length of the free decay approximation needs to be big enough so the maximum  $Q$  value is not too small. For  $Q = 50 \rightarrow L = 20s$  and for  $Q = 273 \rightarrow L = 100s$ . After free decay is extracted, CWT is applied with same settings as before and for every natural frequency calculated, the window parallel to time axis is extracted. Comparing the coefficients and the free decay approximation, area is found where the ratio coefficients are decreased is matching the response.

Table 6-7: Calculated modal characteristics – Error Compared to FDD Method

<i>Mode</i>	<i>Frequency (Hz)</i>	<i>Error</i>	<i>Damping Ratio</i>	<i>Error</i>
1	4.109	0.17%	2.9%	4.6%
2	4.443	3.29%	3.3%	3.5%
3	9.79	1.25%	0.75%	6.25%
4	21.82	2.88%	1.5%	10%
5	22.48	0.52%	0.85%	11.76

We see that the error decreased by a big margin for the frequencies compared to MATLAB's toolbox and an estimation for the damping ratio is now available. There is some error but it is possible to decrease it further with experimentation with the RD variables like triggering point or length of the approximation.

### 6.8 Sherman Oaks – 13 Story commercial building.

Sherman Oaks is an office building designed in 1964 with 13 stories above and two floors below the ground. The vertical load carrying system consists of 4.5 inches thick one-way concrete slabs supported by concrete beams, girders and columns. The lateral load resisting system consists of moment resisting concrete frames in the upper stories and concrete shear walls in the basements. The foundation system consists of concrete piles. Sensors were placed on different floors of the building.

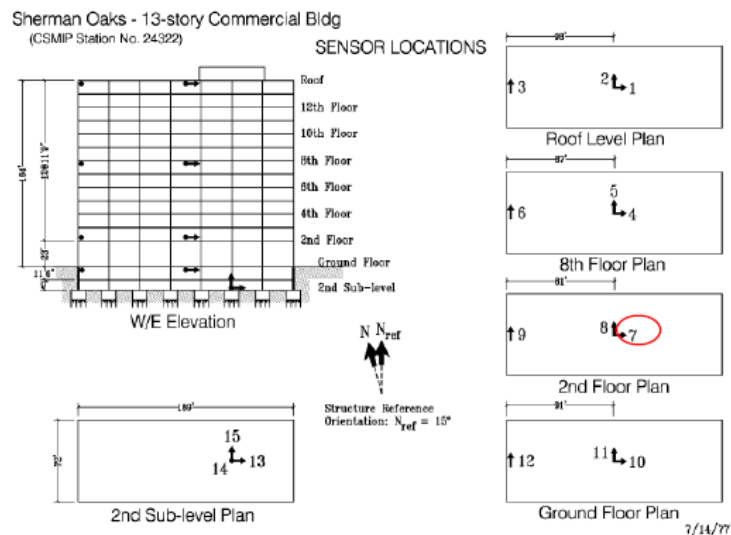


Figure 6-42: Sensor Locations

The building was moderately damaged during the 1994 Northridge earthquake while it sustained no damaged during the 1992 Landers Earthquake. Sensor 7 is the one closest to the damaged area.

On Chapter 5. DWT transform was used to determine if and where the building sustained any damage. On this chapter a different approach will be used. Through CWT on different points in time, natural frequencies will be calculated. If the building sustained damage, there should be decrease of the natural frequencies because of the softening that is result of the damage on the reinforced concrete.

First using MATLAB's toolbox while trying to find parts of the signal through the scalogram that are not influenced too much from the excitation.

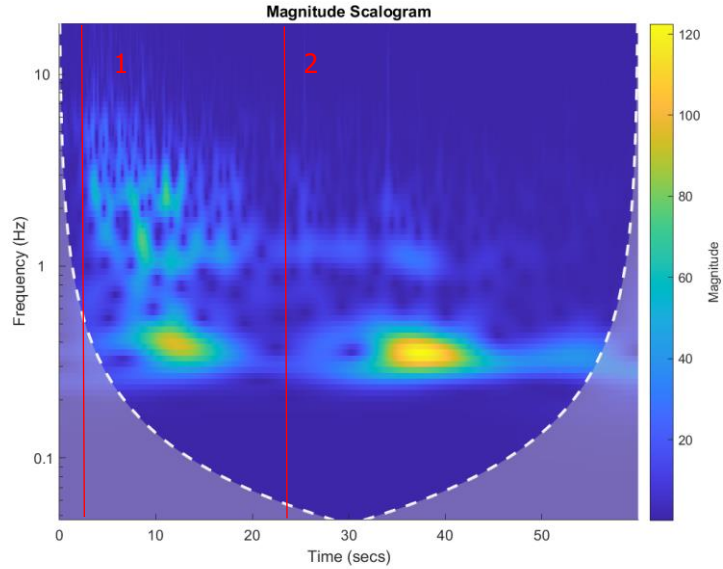


Figure 6-43: Magnitude Scalogram – Sensor1 - 1994

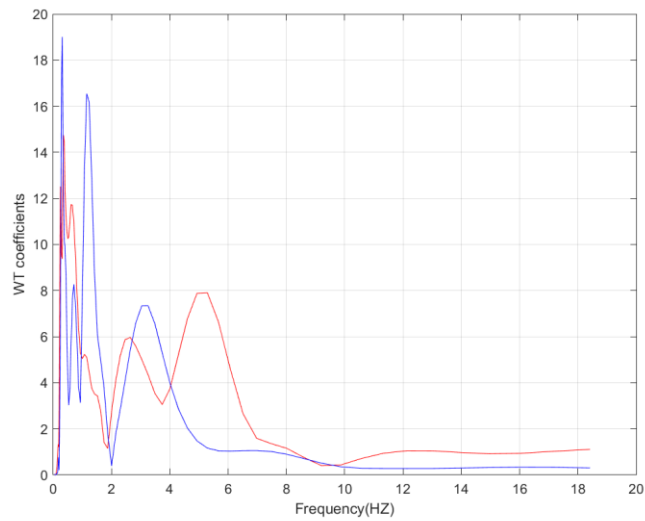


Figure 6-44: Window parallel to frequency axis for  $t_1 = 2s$  (red) and  $t_2 = 24s$  (blue) – Sensor1

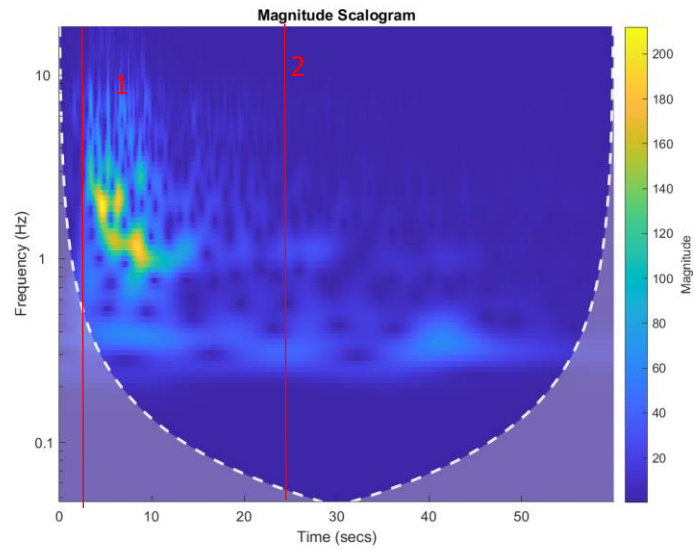
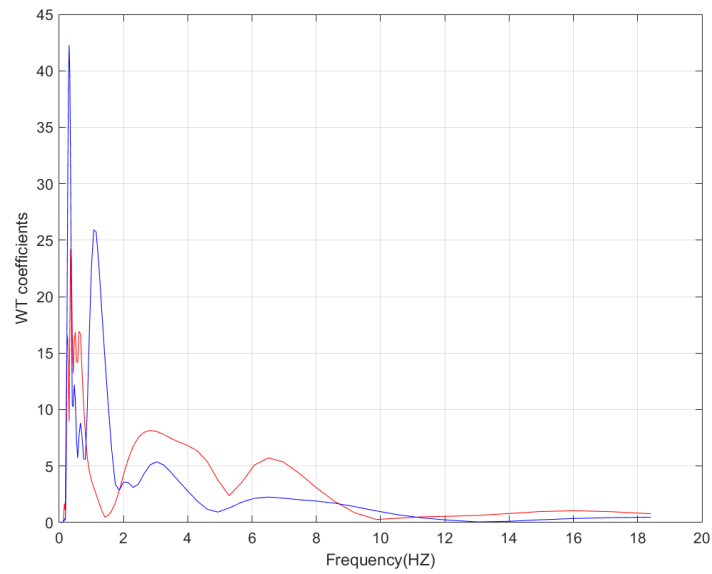


Figure 6-45: Magnitude Scalogram – Sensor2 – 1994

Figure 6-46: Window parallel to frequency axis for  $t_1 = 2s$  (red) and  $t_2 = 24s$  (blue) – Sensor 2



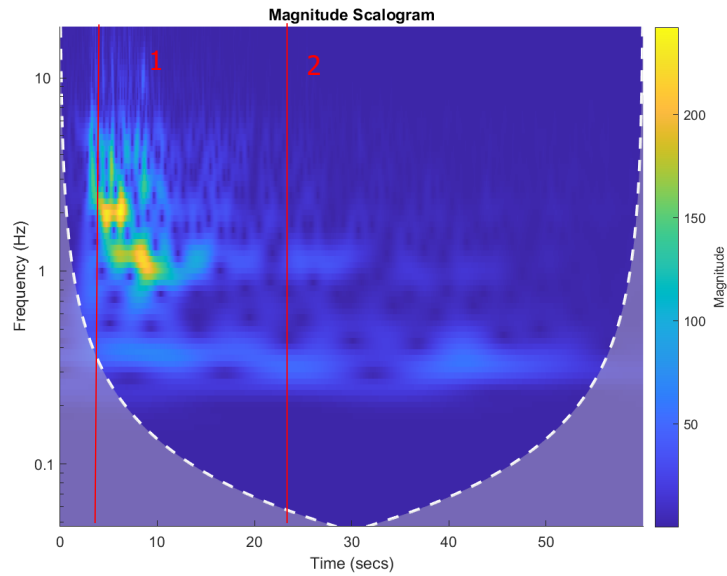
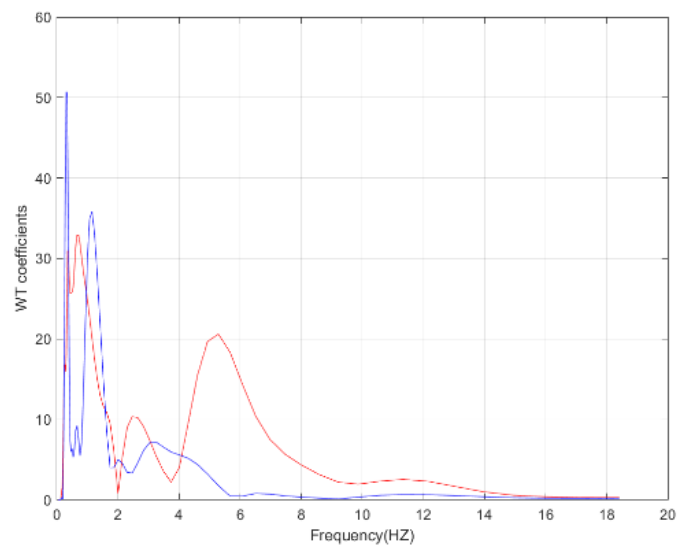


Figure 6-47: Magnitude Scalogram – Sensor2 – 1994

Figure 6-48: Window parallel to frequency axis for  $t_1 = 2s$  (red) and  $t_2 = 24s$  (blue) – Sensor 2

From all the sensors appears to be a decrease on the natural frequencies but because of the way MATLAB is calculating CWT and the nature of the excitation which is periodic since it's an actual earthquake and not some ambient vibration the results are influenced and they need to be confirmed using more sophisticated ways.

For this the other toolbox will be used. Mother wavelet will be Morlet. Because of the limited signal length  $L=60s$  available, we are choosing  $c_f = 1$  and  $c_t = 2$ . FFT transform is used to sensor 1,2 and 3 signals from 1994. The following frequencies are appearing.

Table 6-8: Choosing Q Value

<i>Frequency (Hz)</i>	$\omega_j$	$d\omega_j$	$c_f \frac{\omega_j}{2d\omega_j} \leq Q \leq L \frac{\omega_j}{2c_t}$	<i>Q Chosen</i>
0.26	1.63	1.63	$0.5 \leq Q \leq 24.5$	20
0.31	1.95	0.31	$3.1 \leq Q \leq 29.22$	20
0.33	2.07	0.125	$8.25 \leq Q \leq 31.1$	20
0.37	2.3	0.23	$5.08 \leq Q \leq 34.5$	20
0.38	2.39	0.09	$13.6 \leq Q \leq 35.8$	20
0.4	2.5	0.12	$10.5 \leq Q \leq 37.6$	20

CWT is applied with the above settings to the accelerations signal of sensors 1,2 and 3.

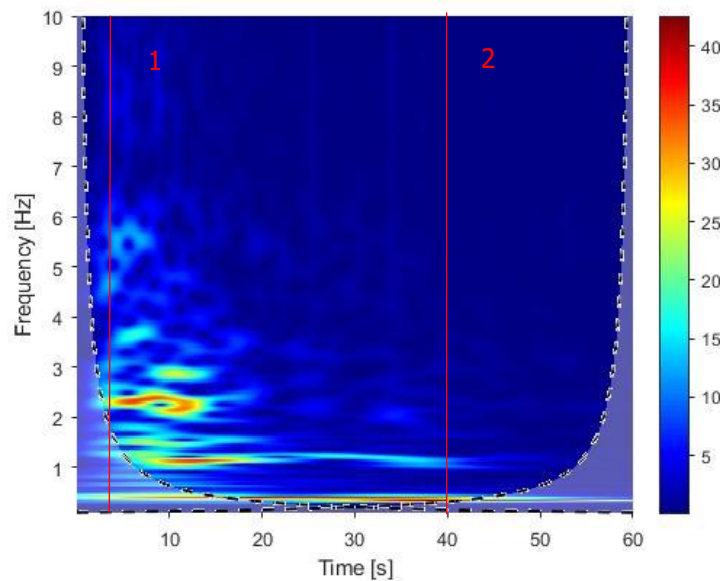
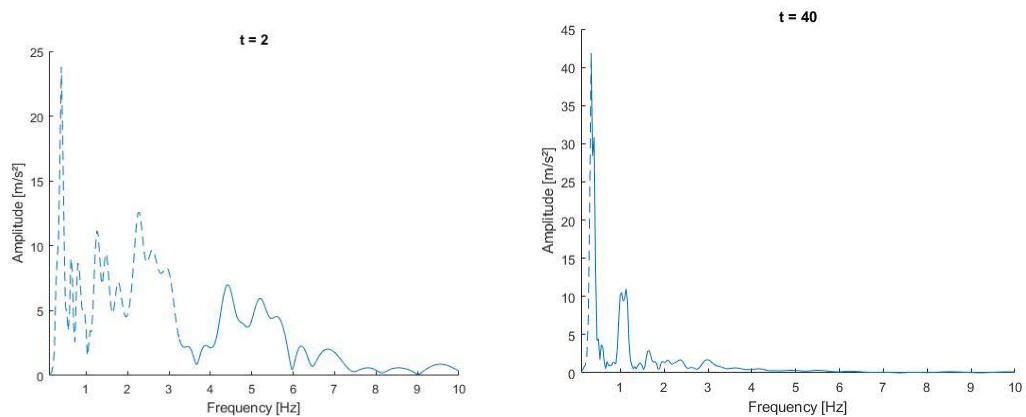


Figure 6-49: Magnitude Scalogram – Sensor1 – 1994

Figure 6-50: Window parallel to frequency axis for  $t_1 = 2s$  (left) and  $t_2 = 40s$  (right) – Sensor 1

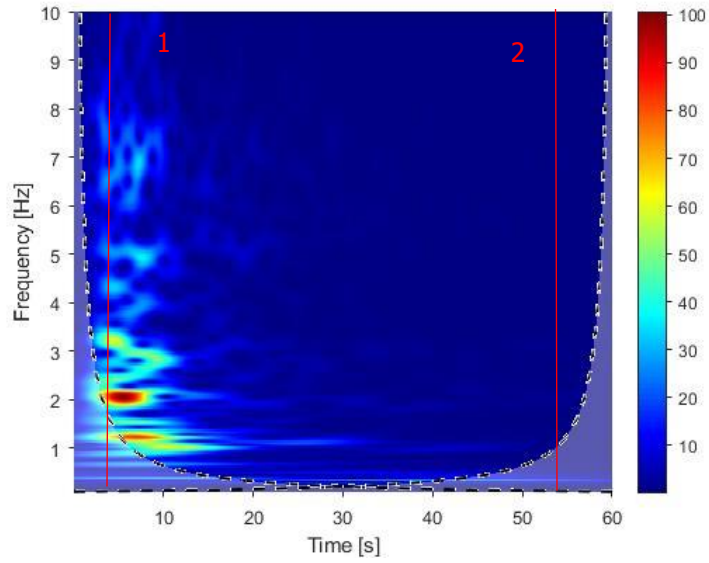


Figure 6-51: Magnitude Scalogram – Sensor2 – 1994

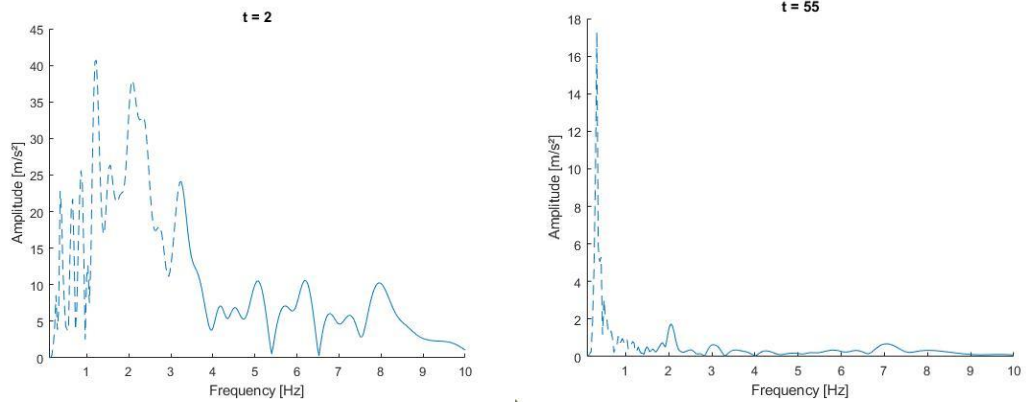


Figure 6-52: Window parallel to frequency axis for  $t_1 = 2s$  (left) and  $t_2 = 55s$  (right) – Sensor 2

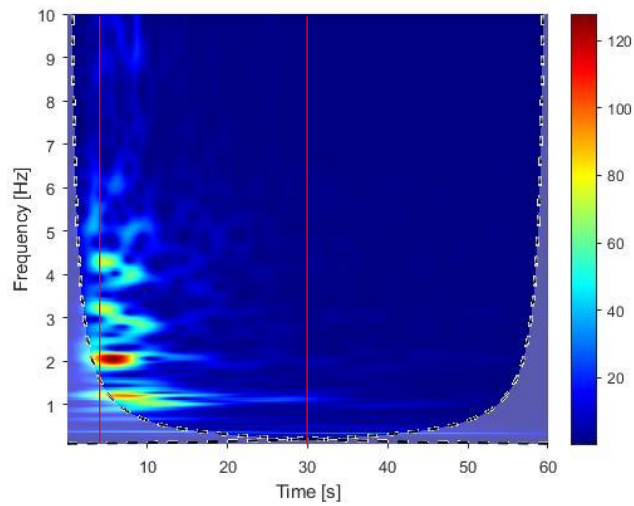


Figure 6-53: Magnitude Scalogram – Sensor 3 – 1994

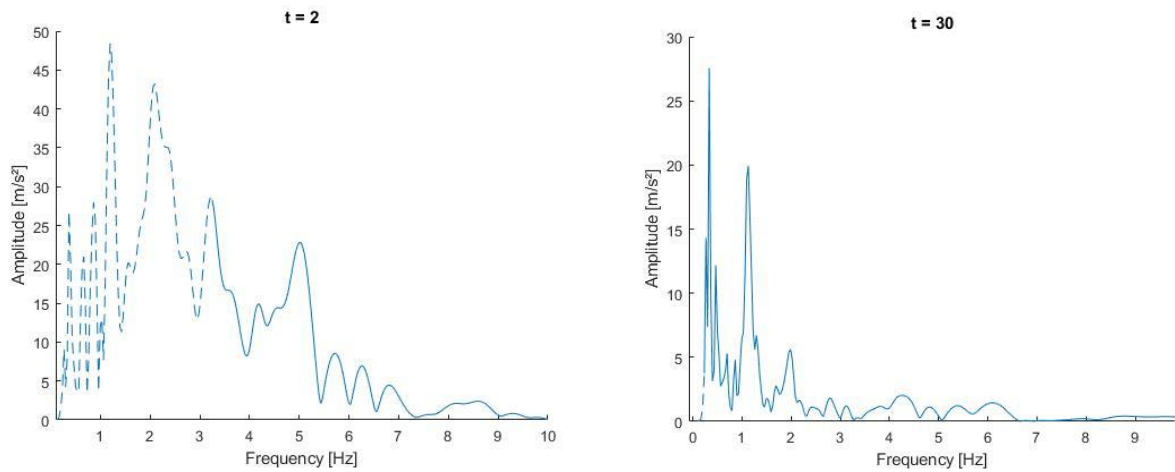


Figure 6-54: Window parallel to frequency axis for  $t_1 = 2s$  (left) and  $t_2 = 30s$  (right) – Sensor 2

Results are confirming what we were expecting, there is a decrease in natural frequency from  $f_1 = 0.397 \rightarrow T_1 = 2.52s$  to  $f_1 = 0.331 \rightarrow T_1 = 3.02s$ . The results are in line with [8] where an increase from 2.6 to 2.9 is calculated.

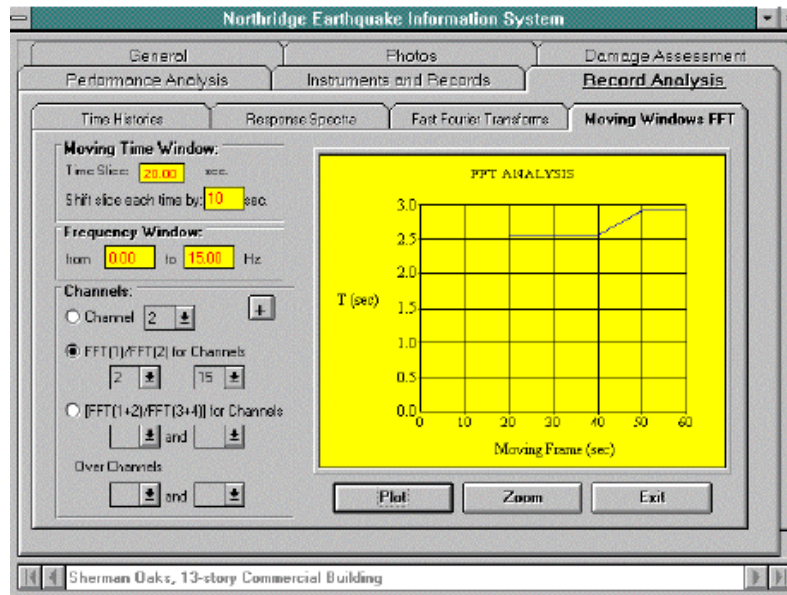


Figure 6-55: Moving windows FFT analysis [8]

## 7 CONCLUSIONS

Operational Modal Analysis with the use of Wavelets appears to be a very efficient tool for estimating the actual modal characteristics of a building and live structural health monitoring. Requirements on equipment are minimal. 3 accelerometers per story if there's interest in mode shapes, otherwise 3 accelerometers every 2 to 3 floors so both DWT and CWT can be applied. There's also no need to evacuate the building or make any other preparations except applying some signal denoising technics when needed.

DWT is the easiest method to apply, through few simple calculations in a generic calculation program (MATLAB), you can have a quick first estimation if and where damage occurred. The method seems to be very efficient in both simulations and real case buildings like Sherman Oaks without almost any optimization other than choosing a proper mother wavelet.

CWT on the other hand is a very optimization and excitation sensitive method. It works best when you have the free decay available, without the need to use the random decrement method to extract it, so you remove the excitation from the results. Furthermore, it is very important to calculate correctly the FFT of the signal. This way  $\omega_j$  can be estimated in order proper values of  $c_f$  and  $c_t$  to be decided, resulting to the range of the accepted  $Q$  values. Choosing the correct  $Q$  value is very important so close natural frequencies are decoupled. If everything is done correctly it is possible to get very good estimations of the Natural frequencies, mode shapes, damping ratios and detect "softening" of the building caused by damage.

Both methods offer accurate results. DWT though only gives answer to if damage exists and partially to where. CWT on the other hand gives a variety of information regarding the building but they might be harder to obtain. Ideally for better results both methods should be applied.

Further work on this subject should be aimed towards ways to

- further decrease the error when the free decay is not available.
- remove noise so Modal Assurance Distribution (MAD) can be applied to detect changes in mode shapes and natural frequencies as a result of structural damage.
- find the most efficient combination of sensor type and placement to collect signals without noise and big sampling rate without spending too much on equipment.
- test other available wavelets to see if they increase the quality of the results.
- locate where the damage is with bigger accuracy
- estimate damage severity
- find how different levels of noise change DWT results and ways to improve that.
- recognize false alarm spikes in DWT analysis.



## 8 REFERENCES

[1]	Nikos Pnevmatikos and George Hatzigeorgiou, "Damage detection of framed structures subjected to earthquake excitation using discrete wavelet analysis", Bulletin of Earthquake Engineering, January 2017.
[2]	Thien-Phu Le and Pierre Argoul, "Continuous wavelet transform for modal identification using free decay response", Journal of Sound and Vibration, Vol. 277, pp. 73-100, 2004.
[3]	Kushan Wijesundara, Evelyne Foerster and Caterina Negulescu, "Estimation of Modal Properties of Low-Rise Buildings Using Ambient Excitation Measurements, Shock and Vibration, September 2015
[4]	Farzad Naeim, Scott Hagie, Arzhang Alimorad and Eduardo Miranda, "Automated post-earthquake damage assessment and safety evaluation of instrumented buildings", John A. Martin & Associates, inc., Report number 2005-10639, 2005.
[5]	Z. Hou, M. Noori and R. St. Amand, "Wavelet-Based Approach for Structural Damage Detection"
[6]	Carlos A. Gaviria and Luis A. Montejo, "Optimal Wavelet Parameters for System Identification of Civil Engineering Structures, 2016
[7]	S. R. Ibrahim, "Random Decrement Technique for Modal Identification of Structures", J. Spacecraft, Vol. 14, No. 11, pp 696-700, 1977
[8]	Farzad Naeim, "Performance of Extensively Instrumented Buildings during the January 17, 1994 Northridge Earthquake", John A. Martin & Associates, inc., Report number 97-7530.68, February 1997.
[9]	Luis Aguiar-Conraria and Maria Joana Soares, "The Continuous Wavelet Transform: A Primer", NIPE WP 23, 2010
[10]	Said Quqa, Luca Landi and Pier Paolo Diotallevi, "Seismic structural health monitoring using the modal assurance distribution", Earthquake Engng Struct Dyn., 2021
[11]	Carlos E. Ventura, Rune Brincker, "Introduction to Operational Modal Analysis, Chichester: John Wiley & Sons Ltd, 2015
[12]	Steven W. Smith, "The Scientist and Engineer's Guide to Digital Signal Processing", San Diego: California Technical Publishing, 1999.
[13]	<a href="https://en.wikipedia.org/wiki/Discrete_Fourier_transform">https://en.wikipedia.org/wiki/Discrete_Fourier_transform</a>
[14]	<a href="https://www.thefouriertransform.com/pairs/sinusoids.php">https://www.thefouriertransform.com/pairs/sinusoids.php</a>
[15]	<a href="https://en.wikipedia.org/wiki/Short-time_Fourier_transform">https://en.wikipedia.org/wiki/Short-time_Fourier_transform</a>
[16]	Stylianakis Stavros, Operational Modal Analysis, March 2020
[17]	<a href="https://en.wikipedia.org/wiki/Morlet_wavelet">https://en.wikipedia.org/wiki/Morlet_wavelet</a>
[18]	Rima Alaifari, Francesca Bartolucci and Matthias Wellershoff, "Phase retrieval of bandlimited functions for the wavelet transform, September 2020

[19]	<a href="https://en.wikipedia.org/wiki/Harmonic_wavelet_transform">https://en.wikipedia.org/wiki/Harmonic_wavelet_transform</a>
[20]	<a href="https://ww2.mathworks.cn/matlabcentral/fileexchange/37272-harmonic-wavelet-for-wavelet-transform?s_tid=FX_rc2_behav">https://ww2.mathworks.cn/matlabcentral/fileexchange/37272-harmonic-wavelet-for-wavelet-transform?s_tid=FX_rc2_behav</a>
[21]	<a href="https://ngawest2.berkeley.edu/">https://ngawest2.berkeley.edu/</a>
[22]	<a href="https://en.wikipedia.org/wiki/Great_Hanshin_earthquake">https://en.wikipedia.org/wiki/Great_Hanshin_earthquake</a>
[23]	M. Fragiadakis, M. Georgioudakis and P. Georgakis (2021), SeismoLEE: An online tool for ground motion record processing, Laboratory of Earthquake Engineering, School of Civil Engineering, National Technical University of Athens (NTUA), url: <a href="http://www.seismolee.eu">www.seismolee.eu</a> .
[24]	K. Gram-Hansen, K. Dorizze, "On the choice of parameters for time-frequency analysis, in: Y.Meyer (Ed.), Wavelets and Applications, Proceedings of the International Conference, Masson, Paris, 1991, pp. 86-92.
[25]	H. Zhivomirov, "On the Development of STFT-analysis and ISTFT-synthesis Routines and their Practical Implementation", TEM Journal, ISSN: 2217-8309, DOI: 10.18421/TEM81-07, Vol. 8, No. 1, pp.56-64, Feb.2019. ( <a href="http://www.temjournal.com/content/81/TEMJournalFebruary2019_56_64.pdf">http://www.temjournal.com/content/81/TEMJournalFebruary2019_56_64.pdf</a> )
[26]	Hristo Zhivomirov, "Short-Time Fourier Transform (STFT) with Matlab" ( <a href="https://www.mathworks.com/matlabcentral/fileexchange/45197-short-time-fourier-transform-stft-with-matlab">https://www.mathworks.com/matlabcentral/fileexchange/45197-short-time-fourier-transform-stft-with-matlab</a> ), MATLAB Central File Exchange. Retrieved August 28, 2021.
[27]	<a href="https://learn.lboro.ac.uk/archive/olmp/olmp_resources/pages/workbooks_1_50_jan2008/Workbook24/24_2_properties_fourier_trnsform.pdf">https://learn.lboro.ac.uk/archive/olmp/olmp_resources/pages/workbooks_1_50_jan2008/Workbook24/24_2_properties_fourier_trnsform.pdf</a>
[28]	<a href="https://seismosoft.com/wp-content/uploads/prods/lib/SeismoStruct-2021-%CE%95%CE%B3%CF%87%CE%B5%CE%B9%CF%81%CE%AF%CE%B4%CE%B9%CE%BF-%CE%A7%CF%81%CE%AE%CF%83%CE%B7%CF%82_GRE.pdf">https://seismosoft.com/wp-content/uploads/prods/lib/SeismoStruct-2021-%CE%95%CE%B3%CF%87%CE%B5%CE%B9%CF%81%CE%AF%CE%B4%CE%B9%CE%BF-%CE%A7%CF%81%CE%AE%CF%83%CE%B7%CF%82_GRE.pdf</a>
[29]	<a href="https://opensees.berkeley.edu/wiki/index.php/SteelMPF_-_Menegotto_and_Pinto_(1973)_Model_Extended_by_Filippou_et_al._(1983)">https://opensees.berkeley.edu/wiki/index.php/SteelMPF_-_Menegotto_and_Pinto_(1973)_Model_Extended_by_Filippou_et_al._(1983)</a>